Interaction Notes

Note 445

June 1985

HEMP-Induced Transients in Transmission and Distribution (T&D) Lines

N. Engheta
K.S.H. Lee
F.C. Yang
R. Aguero

Dikewood

Division of Kaman Sciences Corporation

Santa Monica, California 90405

ABSTRACT

The corona effects on the early-time induced transients on the transmission and distribution (T&D) lines are calculated based on two differnet corona models; namely, the Townsend model and the conductivity model. Three different sources of excitation of the lines are considered, which include a HEMP plane wave, a localized voltage source, and a current injected at a point on the wire. The induced current and charge are calculated and compared with some available experimental data and with the results of Baum's model. The results illustrate that the corona generally reduces the peak value of the induced current as much as 30% of the value and decreases the rate of rise by about 40%.

The HEMP-induced stresses across dielectric insulators in some typical electric power systems are also calculated. The insulators that are considered are line supports in T&D line poles, and transmformer bushings in distribution and power transformers. Different elevation and azimuthal angles of HEMP incidence with two different values of ground conductivity are considered. The HEMP-induced "potential difference" across the line support and air gap in the transmission lines and the HEMP-induced open-circuit voltage across transformer bushings are calculated. The "potential difference" across the line support and across the air gap can be as high as 7 MV. The rise time of the "Potential difference" is about 110 ns, and the fall time is about 2-3 μs. The open-circuit voltage across transfomer bushings can be as large as few tens of MVs and the rise time is in the order of 100 ns and the fall time 800 ns

FORWARD

The Division of Electric Energy Systems (EES) of the United States Department of Enegy (DOE) has formulated a program for the research and development of technologies and systems for the assessment, operation, and control of electric power systems when subjected to electromagnetic pulse (EMP). The DOE/EES EMP program plan is documented in a DOE report entitled Program Plan for Research and Development of Technologies and Systems for Electric Power Systems Under the Influence of Nuclear Electromagnetic Pulses, DOE/NBB-003, May 1983. The research documented in the Oak Ridge National Laboratory (ORNL) report was conducted under program plan elements E1, "EMP Surge Characterization and Effects."

Research for this report was sponsored by the Division of Electrical Energy Systems, United States Department of Energy under contract No. DE-AC05-840R21400 with Martin Marietta Energy Systems, Inc. as operator of the Oak Ridge National Laboratory. The work was performed by Dikewood, a division of Kaman Sciences Corporation, for Zaininger Engineering Company under Subcontract 85X-73986C with Martin Marietta Energy Systems, Inc.

The research documented in this report considers two issues associated with High-Altitude Electromagnetic Pulse (HEMP) interaction with T&D lines. The first issue is the impact of corona on the HEMP-induced transients with emphasis on the early-time responses. The second issue is the determination of the HEMP-induced stresses on insulators. The results of this work will be used to assess HEMP effects on T&D systems.

ACKNOWLEDGEMENT

The authors would like to thank P. R. Barnes, B. W. McConnell of ORNL, and C. E. Baum of AFWL for helpful discussions and suggestions.

TABLE OF CONTENTS

1. INTRODUCTION

1.1 BACKGROUND AND CONTENT

The high-altitude electromagnetic pulse (HEMP) has a fast rise and a large amplitude. The peak value of its electric field is in order of 40 to 80 kV/m. When a large network of conductors, e.g., a power grid, is exposed to such a field, large and fast transients can be induced on the network. Since these induced transients rise very quickly to a large amplitude, the induced electric field on the conductors may exceed, in the first few tens of nanoseconds, the breakdown field of the surrounding air, consequently causing such nonlinear phenomena as corona and flashover to occur.[1]

Section 2 of this report is devoted to a study of corona effects on early time induced transients on transmission and distribution (T&D) lines. The problem is formulated for two different corona models, i.e., Townsend's model and the conductivity model. Three different sources are considered for the excitation of a long wire in air. They are a HEMP plane wave, a localized voltage source, and a current injected on a point of the wire. The nonlinear differential equations that result from the formulation are solved by the method of characteristics. The induced current and charge are calculated and compared with some experimental data[2,3] and with the results of Baum's model.[4]

The HEMP-induced transients on the T&D lines may damage the dielectric insulators in power systems. The insulators that are considered in this report are line supports in transmission and distribution line poles, and transformer bushings in distribution and power transformers. The HEMP-induced stresses across these insulators must be calculated. Section 3 deals with the problem of HEMP-induced stresses across the line support and air gap (Fig. 3.1) in a typical 230-kV, H-frame transmission line. Different elevation and azimuthal angles of incidence with two different values of ground conductivity are considered. The "potential difference," which is defined to be line integral of the induced electric fields across the air gap or the line

support, is calculated. Section 4 treats the HEMP-induced stresses across transformer bushings. The open-circuit voltage is derived for the HEMP-induced stress. A knowledge of the open-circuit voltage together with the source or input impedance of the Thévenin equivalent circuit will aid in designing appropriate pulsers for testing the susceptibility of the transformer bushings. Section 5 summarizes the important results of the report and an appendix is reserved for a compilation of more analytical results.

2. CORONA EFFECTS ON INDUCED TRANSIENTS ON T&D LINES

2.1 AN OVERVIEW

The analysis of the corona effects on overhead transmission and distribution power lines is a challenging theoretical problem. The first step in analyzing such a problem is to study the basic physics of the phenomenon involved and to understand the role of parameters contained in the phenomenon. This study will lead one to a set of equations concerning the parameters involved, along with a set of boundary and initial conditions. The second step is to substitute for the physical parameters models that simplify the equations. The corona problem is a time-dependent one, and the equations are, in general, nonlinear partial differential equations. The third step in the study is to compare analytical results with available experimental data and other corona models.

2.2 FORMULATION OF THE PROBLEM

To formulate the problem mathematically, consider a very long, straight wire of radius a made out of perfectly conducting material. It is momentarily assumed that the wire is not near the ground. Now, introduce a cartesian coordinate system (x,y,z) and a cylindrical coordinate system (ρ,ϕ,z) where the z-axis is along the axis of wire and $x=\rho\cos\phi$, $y=\rho\sin\phi$. A pulse of electromagnetic plane wave with given time history is incident on the wire. The electric field vector and the wave vector $\vec{k}$ of this pulse are assumed to be in the x-z plane and the wave vector $\vec{k}$ makes the angle θ with the positive z-axis (Fig. 2.1).

Physically speaking, when this pulse falls on the wire, the electric current is induced in the wire and the radial component of the electric field is generated. If the radial component of the electric field on the surface of the wire exceeds the corona onset voltage gradient, E_c, the corona discharge will take place and charged particles will be moving around the wire. This phenomenon affects the propagation of the pulse and

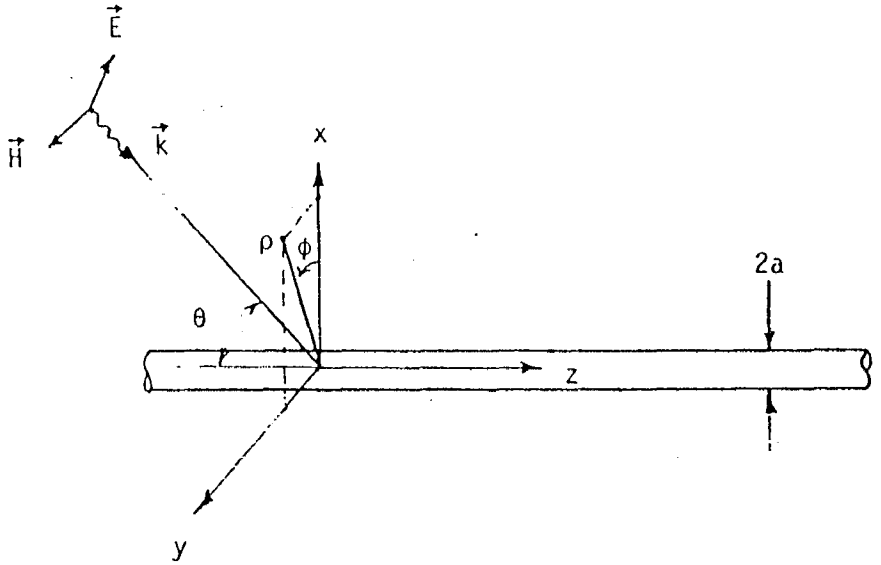

Fig. 2.1. Geometry of the problem.

consequently the induced current in the wire. The objective of this section is to quantitatively understand these effects.

To quantify these effects, one starts with the Maxwell field equations for the fields around the wire, i.e.,

$$\nabla \times \vec{E} = - \mu_o \frac{\partial \vec{H}}{\partial t} \tag{2.1}$$

$$\nabla \times \vec{H} = \vec{J} + \varepsilon_o \frac{\partial \vec{E}}{\partial t} \tag{2.2}$$

where $\vec{E}$ and $\vec{H}$ are total electric and total magnetic field vectors, μ_o and ε_o are the permeability and dielectric constant of free-space, respectively, and $\vec{J}$ is a current density due to the motion of the ionized charged particles in the vicinity of the wire. The above equations can be written in terms of the field components; that is,

$$\frac{\partial E_\rho}{\partial z} - \frac{\partial E_z}{\partial \rho} = - \mu_o \frac{\partial H_\phi}{\partial t} \tag{2.3}$$

$$- \frac{\partial H_\phi}{\partial z} = J_\rho + \varepsilon_o \frac{\partial E_\rho}{\partial t} \tag{2.4}$$

In writing the Maxwell equations, in terms of the field components, it is assumed that the field components and J_ρ are independent of the coordinate ϕ. Integrating Eqs. (2.3) and (2.4) over the circumference of the wire at $\rho = a$, one can obtain on the surface of the wire

$$\frac{1}{\varepsilon_o} \frac{\partial Q}{\partial z} + \mu_o \frac{\partial I}{\partial t} = 2 \pi a \frac{\partial E_z}{\partial \rho} \tag{2.5}$$

$$\frac{\partial Q}{\partial t} + \frac{\partial I}{\partial z} = - 2 \pi a J_\rho \tag{2.6}$$

where $Q = 2 \pi a \varepsilon_o E_\rho$ is the charge per unit length in the wire and $I = 2 \pi a H_\phi$ is the total current in the wire. As was mentioned earlier

J_ρ is the current density resulting from the ionized charged particles from corona discharge and can generally be a nonlinear function of Q or the electric field around the wire. Therefore, one must look into the methods of solving nonlinear partial differential equations. One of such methods is the method of characteristics.[5] In using the method, Eqs. (2.5) and (2.6) are multiplied by two constants α_1 and α_2, respectively, and then are added. Thus, one gets the following expression:

$$\alpha_1\left(\frac{1}{\epsilon_o}\frac{\partial Q}{\partial z} + \mu_o\frac{\partial I}{\partial t}\right) + \alpha_2\left(\frac{\partial Q}{\partial t} + \frac{\partial I}{\partial z}\right) = 2\,\pi a\alpha_1\frac{\partial E_z}{\partial \rho} - 2\,\pi a\alpha_2 J_\rho \qquad (2.7)$$

The above equation can be rearranged as follows:

$$\alpha_2\left(\frac{\partial Q}{\partial t} + \frac{\alpha_1}{\alpha_2\epsilon_o}\frac{\partial Q}{\partial z}\right) + \alpha_1\mu_o\left(\frac{\partial I}{\partial t} + \frac{\alpha_2}{\alpha_1\mu_o}\frac{\partial I}{\partial z}\right) = 2\,\pi a\alpha_1\frac{\partial E_z}{\partial \rho} - 2\,\pi a\alpha_2 J_\rho \qquad (2.8)$$

To have Eq. (2.8) in the characteristic form, the characteristic velocity v_c must be

$$v_c = \frac{dz}{dt} = \frac{\alpha_1}{\alpha_2\epsilon_o} = \frac{\alpha_2}{\alpha_1\mu_o} \qquad (2.9)$$

Accordingly, Eq. (2.8) can be written in the following form

$$\alpha_2\left(\frac{dQ}{dt} + \frac{\alpha_1\mu_o}{\alpha_2}\frac{dI}{dt}\right) = 2\,\pi a\alpha_1\frac{\partial E_z}{\partial \rho} - 2\,\pi a\alpha_2 J_\rho \qquad (2.10)$$

along the characteristic line $v_c = \frac{dz}{dt}$

The constants α_1 and α_2 can be obtained from the following set of equations

$$\begin{cases} \alpha_1 - \varepsilon_o v_c \alpha_2 = 0 & (2.11) \\ \mu_o v_c \alpha_1 - \alpha_2 = 0 & (2.12) \end{cases}$$

To have nonzero solutions for α_1 and α_2, the determinant of this set must be zero. Hence,

$$v_c^2 = \frac{1}{\mu_o \varepsilon_o} = c^2 \qquad (c = \text{vacuum velocity of light}) \qquad (2.13)$$

There are two sets of solutions for v_c, α_1 and α_2, that is

$$v_c = c : \qquad \alpha_2 = 1 \qquad \alpha_1 = +\sqrt{\frac{\varepsilon_o}{\mu_o}} \qquad (2.14)$$

$$v_c = -c : \qquad \alpha_2 = 1 \qquad \alpha_1 = -\sqrt{\frac{\varepsilon_o}{\mu_o}} \qquad (2.15)$$

Substituting (2.14) and (2.15) into Eq. (2.10), one obtains the following set of ordinary differential equations in the characteristic form, i.e.,

$$\begin{cases} \frac{d}{dt}\left(Q + \frac{I}{c}\right) = 2\pi a \sqrt{\frac{\varepsilon_o}{\mu_o}} \frac{\partial E_z}{\partial \rho} - 2\pi a J_\rho & \text{along } \frac{dz}{dt} = c \qquad (2.16) \\ \frac{d}{dt}\left(Q - \frac{I}{c}\right) = -2\pi a \sqrt{\frac{\varepsilon_o}{\mu_o}} \frac{\partial E_z}{\partial \rho} - 2\pi a J_\rho & \text{along } \frac{dz}{dt} = -c \qquad (2.17) \end{cases}$$

Using the method of characteristics, one can find I and Q from Eqs. (2.16) and (2.17) provided that $\frac{\partial E_z}{\partial \rho}$ and J_ρ are given on the wire surface.

A choice for $\frac{\partial E_z}{\partial \rho}$ can be obtained from the assumption that the given set of nonlinear equations, i.e., Eqs. (2.5) and (2.6) must be reduced to the linear equations when the corona effects are absent, i.e., when $J_\rho = 0$

for all z. Therefore, putting J_ρ equal to zero in Eq. (2.6), one can get a second order differential equation for I, that is

$$\frac{\partial^2 I}{\partial z^2} - \frac{1}{c^2}\frac{\partial^2 I}{\partial t^2} = -2\pi a\varepsilon_o \frac{\partial^2 E_z}{\partial t\, \partial \rho} \tag{2.18}$$

On the other hand, a differential equation for the current induced in a straight wire exposed to an incident field can be obtained via a different method, viz.,[6,1]

$$\frac{\partial^2 I}{\partial z^2} - \frac{1}{c^2}\frac{\partial^2 I}{\partial t^2} = -\frac{4\pi}{\Omega}\varepsilon_o \frac{\partial E_t^i}{\partial t} \tag{2.19}$$

where $E_t^i = E_z^i$ is the tangential component of the incident electric field along the wire, and $\Omega = 2\ell n\left[2(ct - z\cos\theta + a\sin\theta)/(\Gamma a\sin\theta)\right]$ for $ct - z\cos\theta + a\sin\theta > 0$, θ is the elevation angle, and Γ is the exponential of Euler's constant 1.7810... Comparing Eqs. (2.18) and (2.19), one can get $\frac{\partial E_z}{\partial \rho}$ in terms of the incident electric field, i.e.,

$$\frac{\partial E_z}{\partial \rho} = \frac{2}{a\,\Omega} E_z^i\,(z,t) \tag{2.20}$$

along the wire.

For J_ρ one may try different functional forms; this is where different models for corona can be introduced. In this study, two different models are introduced. In the next subsection, these two different corona models will be discussed in detail.

2.3 CORONA MODELS

As was mentioned before, J_ρ is the current density due to corona discharge at the surface of the wire. The problem has been formulated in such a way that a knowledge of J_ρ at $\rho = a$ is required for obtaining the Q

and I in the wire. There are different corona models based on how J_ρ is expressed in terms of the normal component of the electric field at the surface of the wire or equivalently in terms of the charge per unit length Q. In this report, two different corona models are studied. These models are called Townsend's model and the conductivity model. It must be noted that the effect of space charge in these two models is not incorporated. As a result, the effects of corona in these two models are overemphasized.

2.3.1 TOWNSEND'S MODEL

This is a model of fully developed corona with the corona current i per unit length of the wire related to the voltage V of the wire by a parabolic form:

$$i = \kappa V(|V| - V_c)\, U\,(|V| - V_c) \tag{2.21}$$

where κ is a constant, V_c is the corona onset voltage, U( ) is the unit-step function. The exact voltage-current characteristics of this model has a more complicated form.[7,8] But, the above parabolic form will suffice. At the surface of the wire, i and J_ρ are related by

$$i = 2\pi a J_\rho \tag{2.22}$$

Since i can be written in terms of J_ρ and voltage V can be written in terms of the charge Q per unit length of wire, there exists a relationship between J_ρ and Q; that is

$$J_\rho = \alpha_j Q \left(\frac{|Q|}{2\pi a \varepsilon_o} - E_c \right) U\left(|Q| - 2\pi a \varepsilon_o E_c \right) \tag{2.23}$$

where α_j is

$$\alpha_j = \frac{\gamma K_+}{2\pi a^2}\, \alpha_{jc} \tag{2.24}$$

with

γ = dimensionless constant $\approx 2.17 \times 10^{-3}$

K_+ = ion mobility $\approx 2 \times 10^{-4}$ $m^2 volt^{-1} sec^{-1}$

a = wire radius in meter

E_c = critical voltage gradient in volt m^{-1}

α_{jc} = dimensionless parameter

In Townsend's original model α_{jc} is unity. Since the present problem deals with transient responses, α_{jc} is not necessarily unity. The proper value of α_{jc} can be estimated by comparing the results obtained from this model with the experimental data or with the results of other models.

2.3.2 CONDUCTIVITY MODEL

In this model, the corona current density J_ρ at $\rho = a$ is related to the radial component of the electric field E_ρ at $\rho = a$ through a conductivity parameter σ. Since corona current is the result of the air ionization, E_ρ must be greater than E_c. Consequently, the relationship between J_ρ and E_ρ must include a unit-step function. Hence, one obtains,

$$J_\rho = \sigma E_\rho U(|E_\rho| - E_c) \qquad \text{at } \rho = a \tag{2.25}$$

Writing E_ρ at $\rho = a$ in terms of Q, one gets

$$J_\rho = \sigma \frac{Q}{2\pi a \varepsilon_0} U\left(\frac{|Q|}{2\pi a \varepsilon_0} - E_c\right) \qquad \text{at } \rho = a \tag{2.26}$$

This is a parametric relationship between J_ρ and Q, where σ is a parameter. The proper value of σ can be found from a comparison of the obtained results using this model with the experimental results or the results from other models.

2.4 DIFFERENT EXCITATIONS OF THE WIRE

Three different sources of excitation of the wire are considered:

2.4.1 HEMP PLANE WAVE EXCITATION

In this case a high-altitude electromagnetic pulse (HEMP) illuminates the wire. As was shown in Fig. 2.1, the wave vector $\vec{k}$ and the wire lie in the x-z plane, and the electric field vector is vertically polarized, i.e., the electric vector is also in the x-z plane. The elevation angle is θ. The pulse as a function of time is the double exponential function:

$$w = E_0 \left[\exp(-\alpha t) - \exp(-\beta t)\right] \tag{2.27}$$

where E_0, α and β have the typical values,

$E_0 = 52.5$ kV/m

$\alpha = 4 \times 10^6$ sec^{-1}

$\beta = 4.78 \times 10^8$ sec^{-1}

2.4.2 LOCALIZED VOLTAGE SURGE

In this case, a finite length of the wire is excited by a voltage source whose electric field is tangent to the wire and varies with time as a double-exponential function. Therefore, the electric field of this localized voltage source is

$$E = E_0\left[\exp(-\alpha t) - \exp(-\beta t)\right], \text{ for } z_0 - \frac{\Delta \ell}{2} < z < z_0 + \frac{\Delta \ell}{2} \tag{2.28}$$

where

z_0 = a point on the wire

$\Delta \ell$ = source region

$$\alpha = 4 \times 10^6 \text{ sec}^{-1}$$

$$\beta = 4.78 \times 10^8 \text{ sec}^{-1}$$

$$E_o = \frac{V_o}{\Delta \ell} = 200 \text{ kV/m} \quad (V_o \text{ is the potential difference of the source})$$

One reason to consider such an excitation is that voltage surges on power lines due to switching may be described by a localized voltage source. Another reason to consider this type of excitation is the fact that it is possible to set up experiments using voltage sources to obtain experimental data on corona.

2.4.3 CURRENT INJECTION TO A POINT ON THE WIRE

Current injection to a point of the wire can be a source of wire excitation. Lightning attachment to a wire can be considered as current injection. The current is taken to be a double-exponential function of time. Therefore, I(t) can be written as follows:

$$I(t) = I_o \left[\exp(-\alpha t) - \exp(-\beta t) \right] \tag{2.29}$$

where I_o, α, and β are the typical values of severe lightning strikes, i.e.,

$$I_o = 100 \text{ kA}$$

$$\alpha = 1.43 \times 10^4 \text{ sec}^{-1}$$

$$\beta = 4 \times 10^6 \text{ sec}^{-1}$$

2.5 ANALYTICAL RESULTS

So far, two different corona models along with three types of sources have been studied. Using characteristic method, computer codes were generated and induced current and charges were calculated. The induced

currents as function of time are plotted and presented in the following order:

2.5.1 HEMP PLANE WAVE EXCITATION

The induced current in an infinitely long, straight wire of radius a is calculated due to HEMP excitation. Townsend's and the conductivity models are used. Figures 2.2 and 2.3 present the induced currents in the wire using Townsend's and conductivity models, respectively. In these two figures, α_j and σ are the parameters. Figures 2.4 and 2.5 present the same induced current when θ is the parameter. Figures 2.6 through 2.9 illustrate the induced current in the wires in the presence of the perfectly conducting ground, for different values of α_j and σ and different elevation angles. Additional curves are given in an appendix.

2.5.2 LOCALIZED VOLTAGE SOURCE

A localized voltage source feeds a very long, straight wire of radius a. Townsend's and the conductivity models are used. Induced current at the different observation points have been calculated and plotted. Figures 2.10 and 2.11 show the results for Townsend's and the conductivity models. Additional curves for different values of α_j and σ are presented in the Appendix.

2.5.3 CURRENT INJECTION TO A POINT ON THE WIRE

A current source injects current at a point of the very long wire of radius a. Townsend's and the conductivity models are used. The induced currents at the different observation points have been calculated and plotted. Figures 2.12 and 2.13 present the results for these two models. More plots for different values of α_j and σ are given in the appendix.

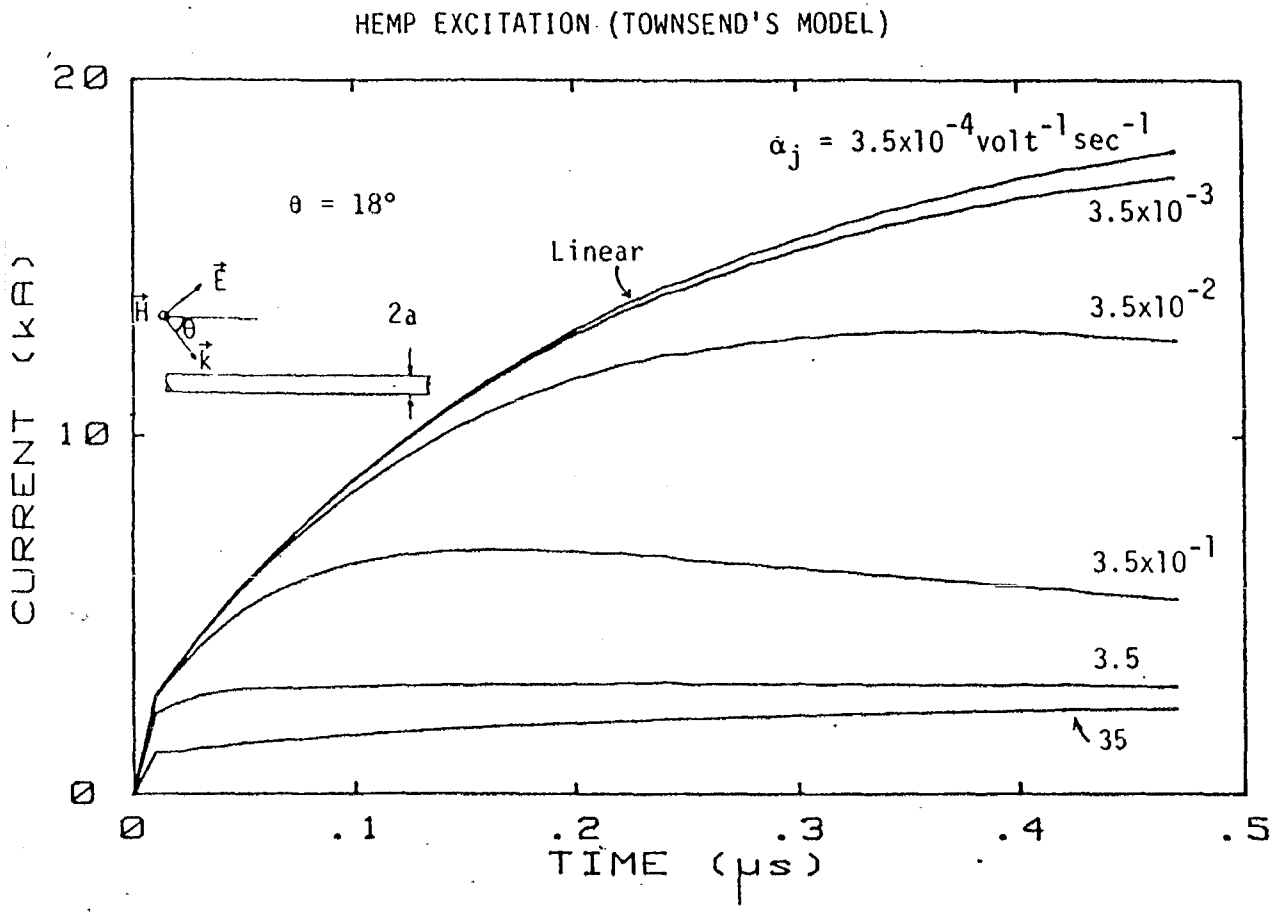

Fig. 2.2. HEMP-induced current in the wire for elevation angle $\theta = 18°$ and different values of α_j in Townsend's model for radius a = 1.407 cm and $E_c = 1.5 \times 10^6$ volt m^{-1}.

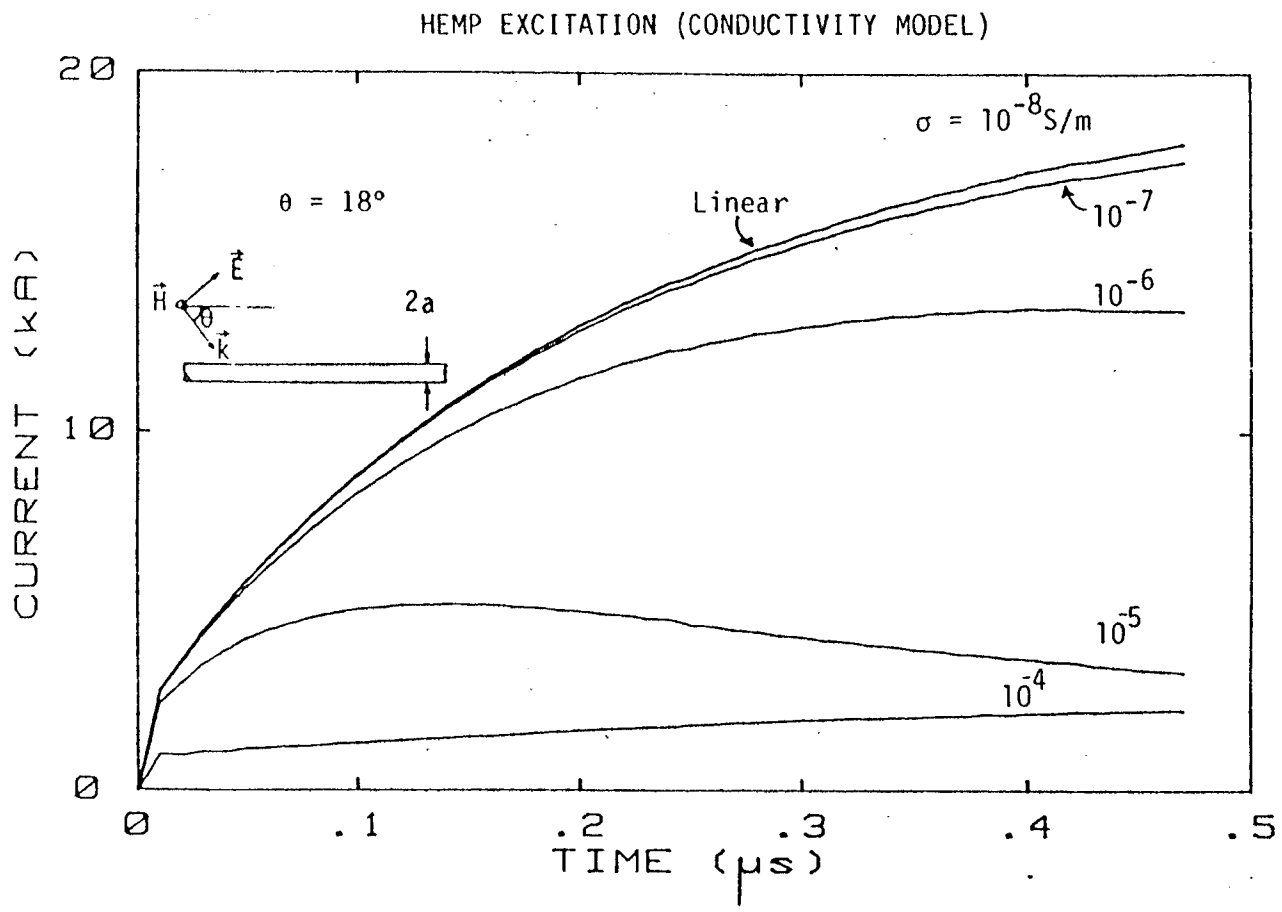

Fig. 2.3. HEMP-induced current in the wire for elevation angle $\theta = 18°$ and different values of σ in conductivity model for radius a = 1.407 cm and $E_c = 1.5 \times 10^6$ volt m^{-1}.

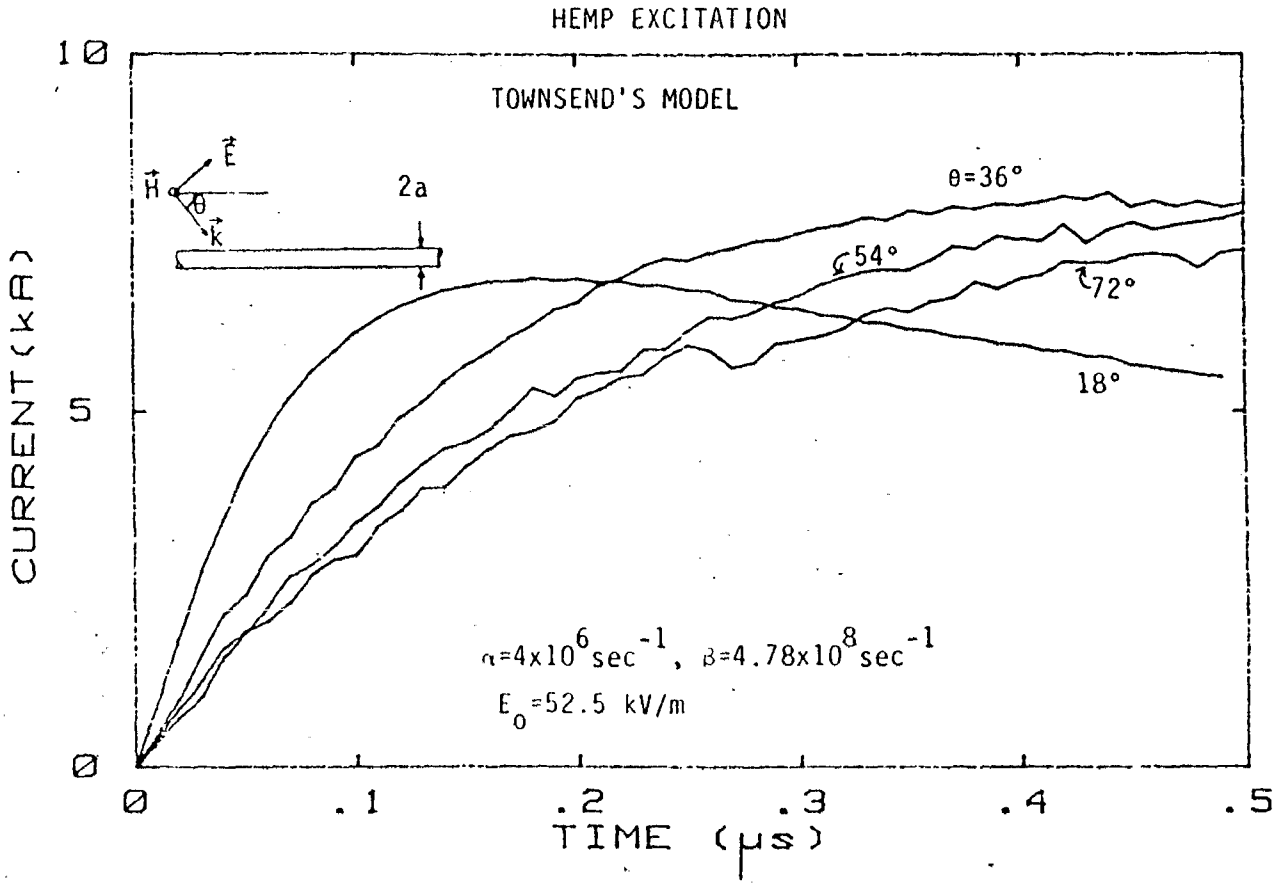

Fig. 2.4. HEMP-induced current in the wire for $\alpha_j = 3.5 \times 10^{-2}$ volt^{-1}sec^{-1} and different elevation angles in Townsend's model for radius a = 1.407 cm and $E_c = 1.5 \times 10^6$ volt m^{-1}.

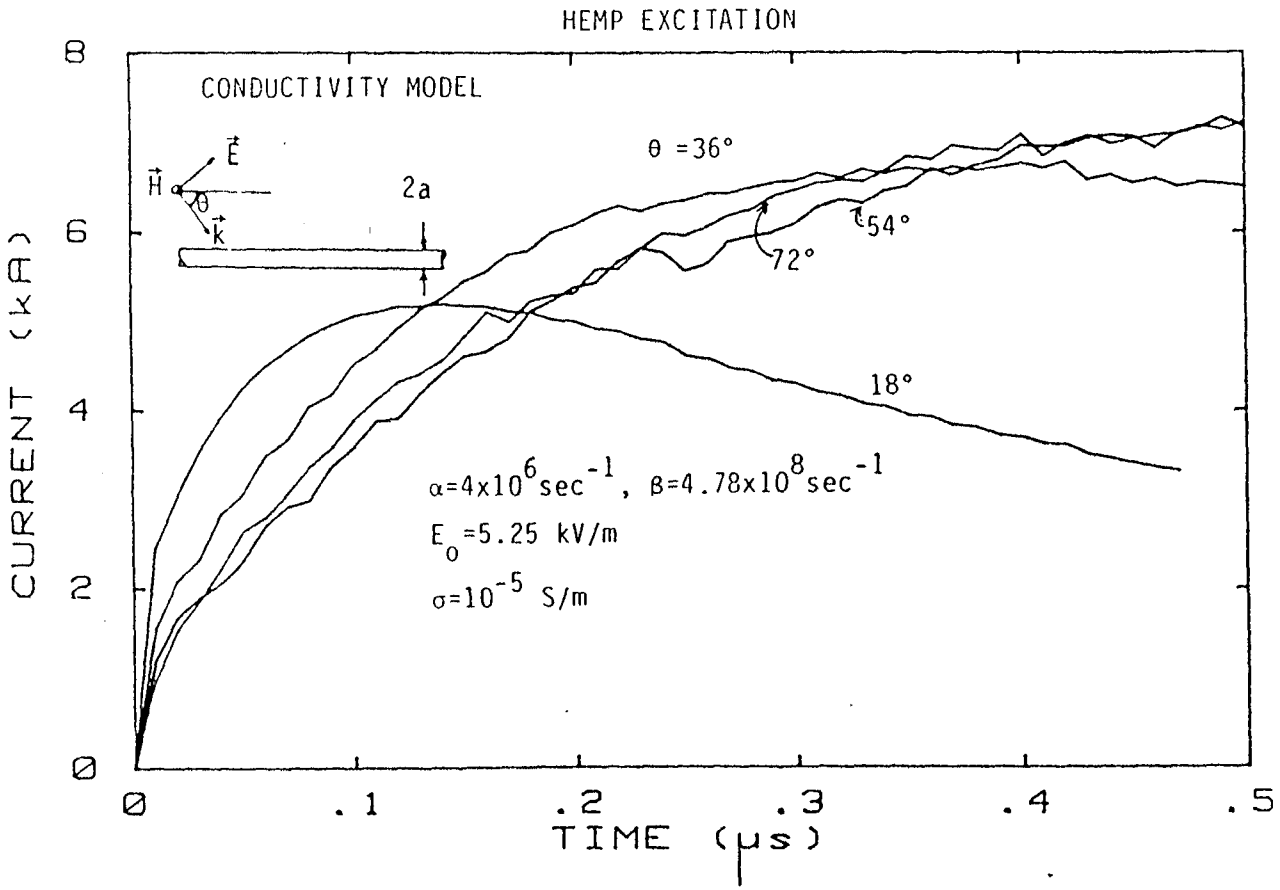

Fig. 2.5. HEMP-induced current in the wire for $\sigma = 10^{-5}$ S/m and for different elevation angles in conductivity model for radius a = 1.407 cm and $E_c = 1.5 \times 10^6$ volt m^{-1}.

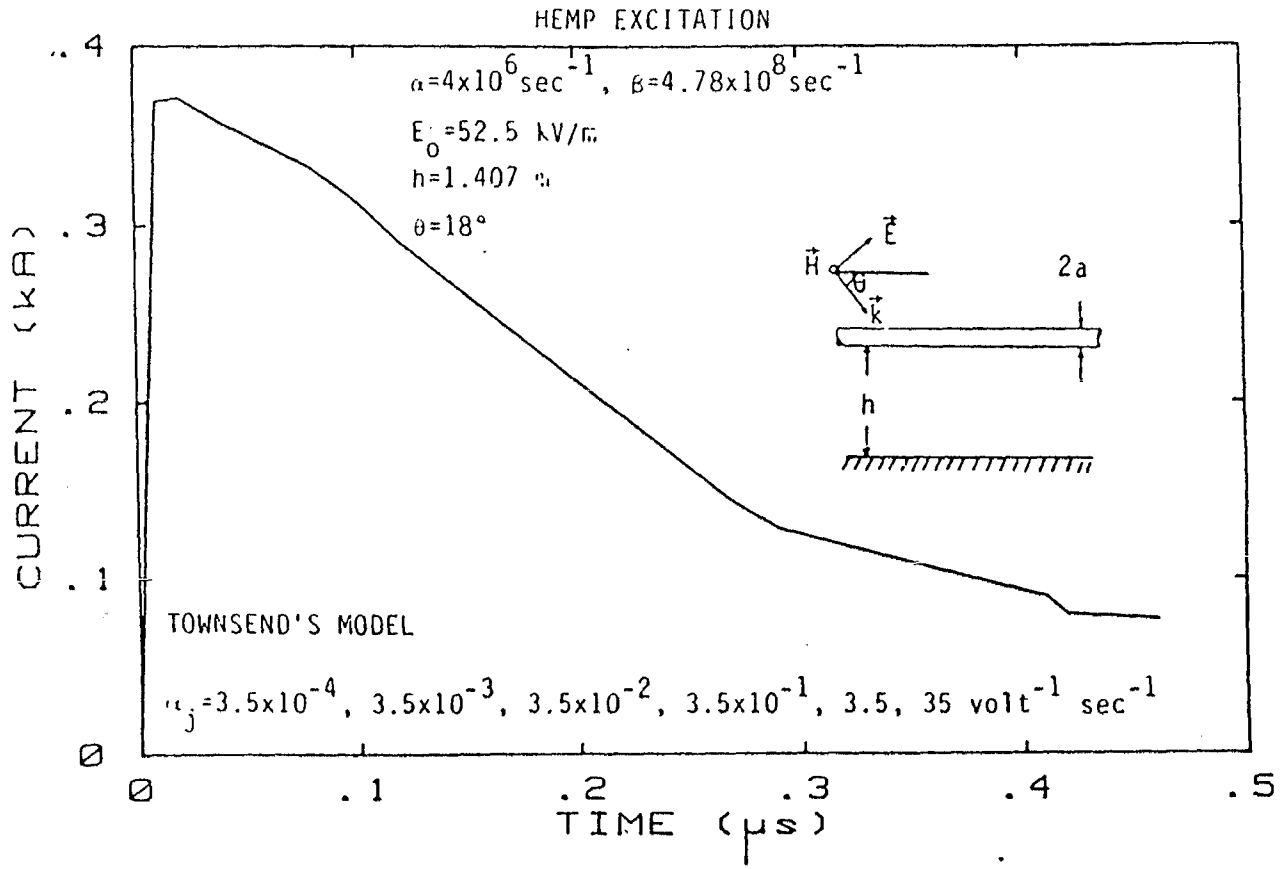

Fig. 2.6. HEMP-induced current in the wire for elevation angle $\theta = 18°$ and different values of α_j in Townsend's model for radius a = 1.407 cm and $E_c = 1.5 \times 10^6$ volt m^{-1}.

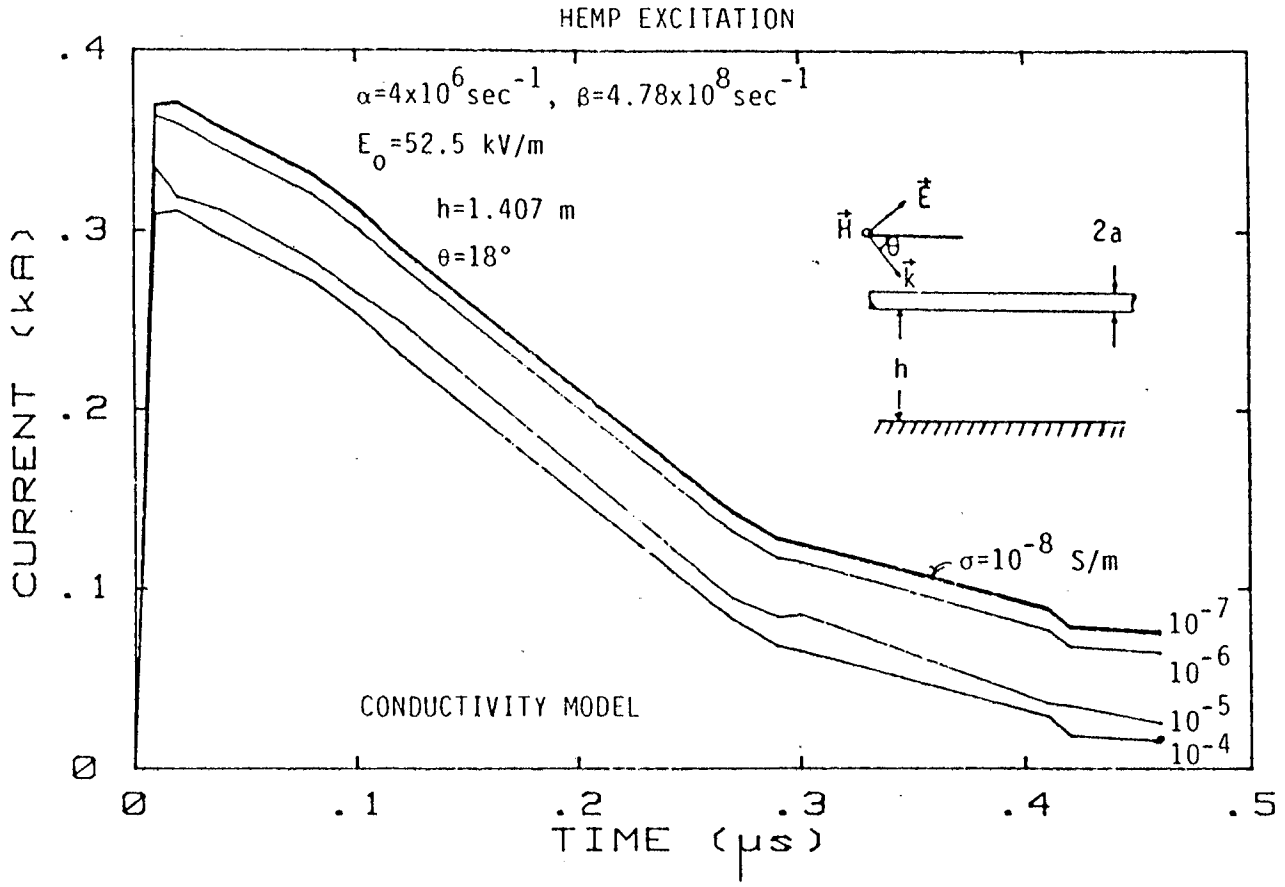

Fig. 2.7. HEMP-induced current in the wire in the presence of a perfectly conducting ground for elevation angle $\theta = 18°$ and different values of σ in conductivity model for radius a = 1.407 cm and $E_c = 1.5 \times 10^6$ volt m^{-1}.

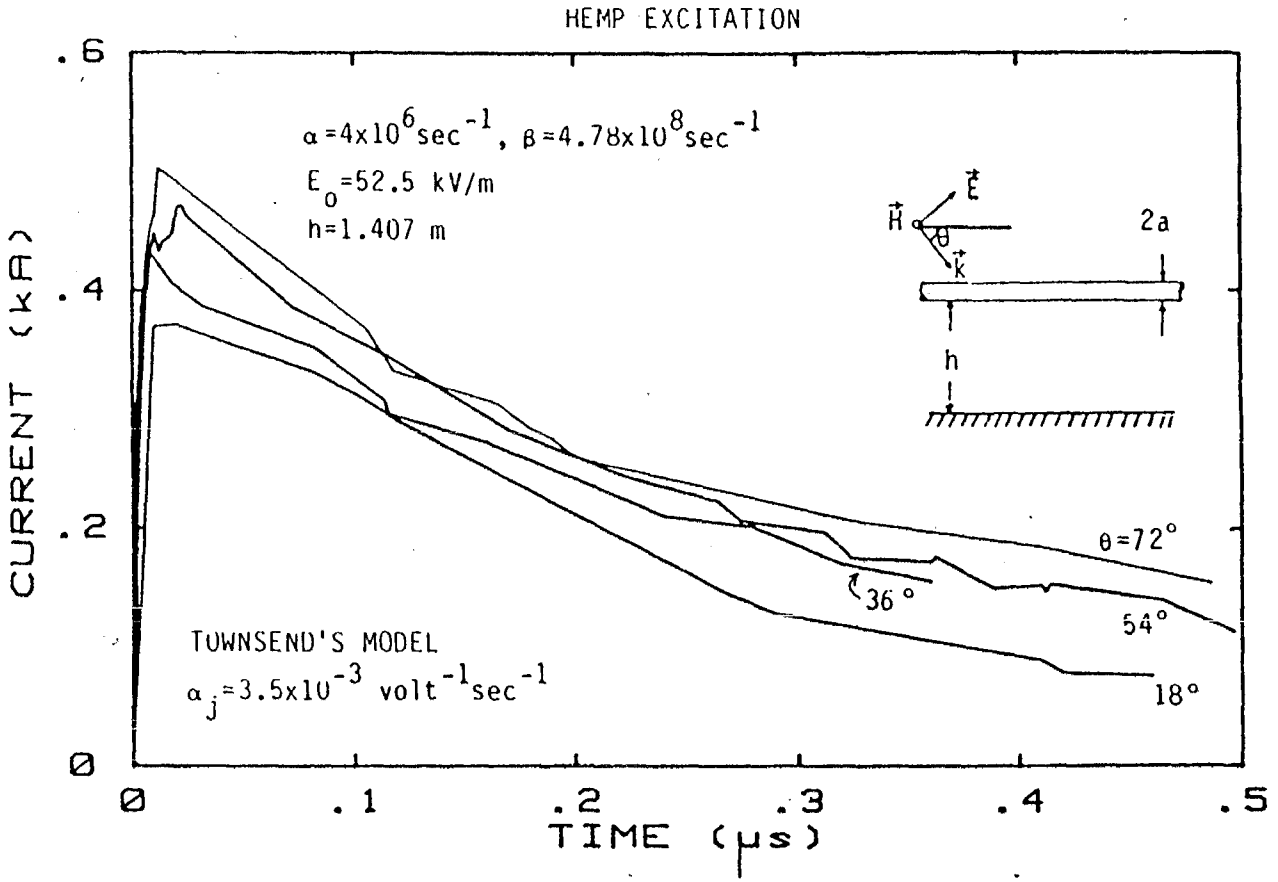

Fig. 2.8. HEMP-induced current in the wire in the presence of a perfectly conducting ground for $\alpha_j = 3.5 \times 10^{-3}$ volt^{-1}sec^{-1} and different elevation angles in Townsend's model for radius a = 1.407 cm and $E_c = 1.5 \times 10^{6}$ volt m^{-1}.

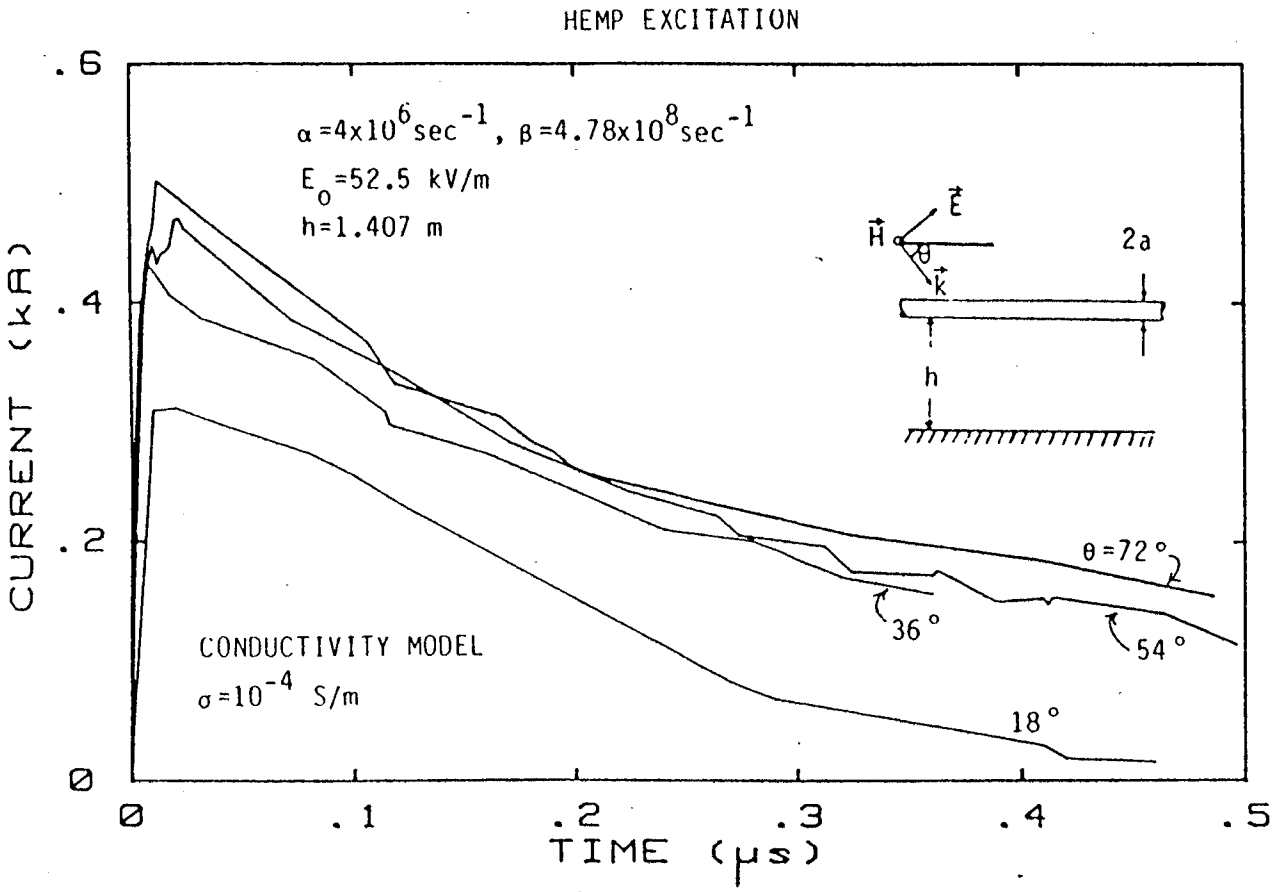

Fig. 2.9. HEMP-induced current in the wire in the presence of a perfectly conducting ground for $\sigma = 10^{-4}$ S/m and different elevation angles in conductivity model for radius a = 1.407 cm and $E_c = 1.5 \times 10^6$ volt m^{-1}.

LOCALIZED VOLTAGE SURGE (TOWNSEND'S MODEL, $\alpha_j = 3.5 \times 10^{-1} \text{volt}^{-1}\text{sec}^{-1}$)

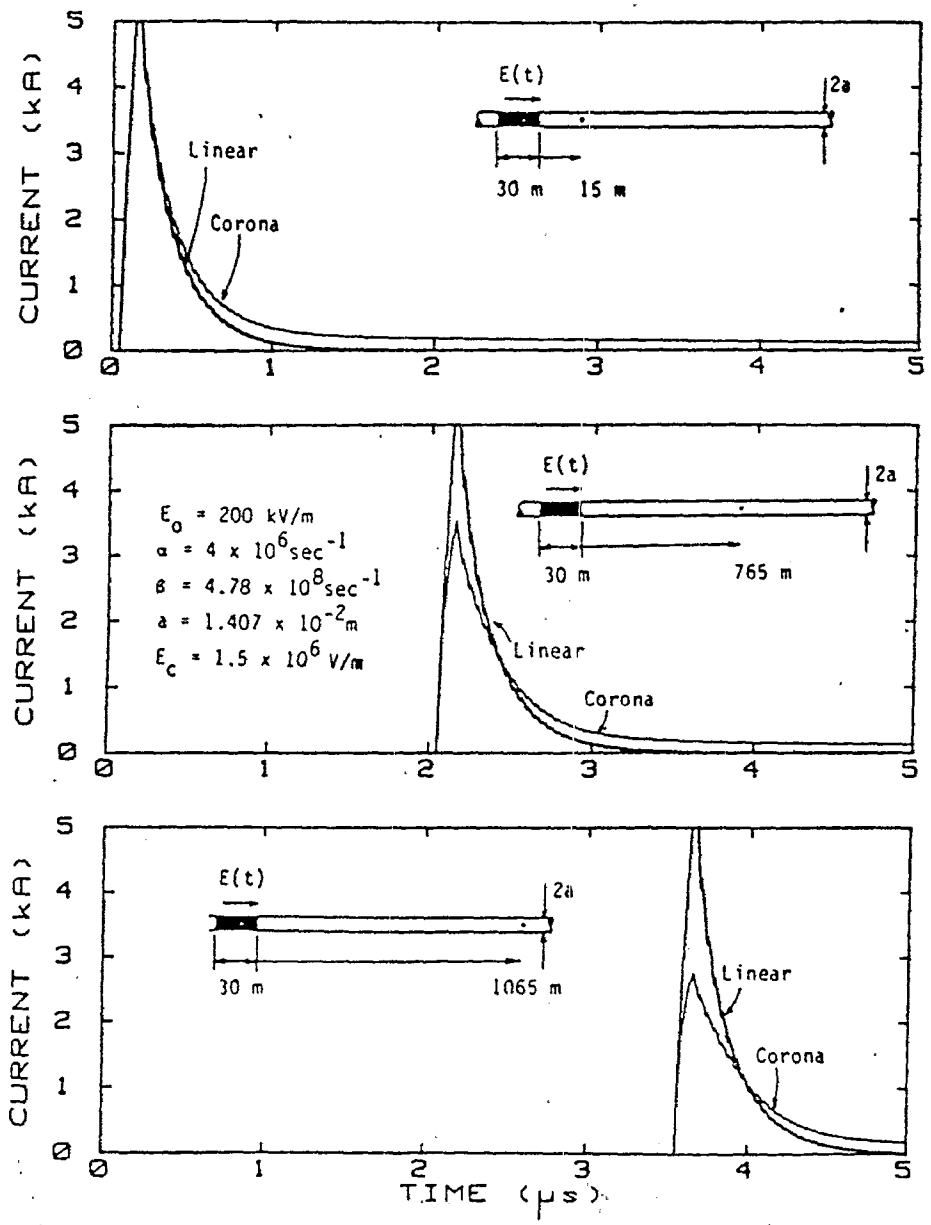

Fig. 2.10. Voltage surge-induced current in the wire at different distances from surge location in Townsend's model for $\alpha_j = 3.5 \times 10^{-1}$ volt^{-1}sec^{-1}.

LOCALIZED VOLTAGE SURGE (CONDUCTIVITY MODEL, $\sigma = 10^{-5}$ mhos/m)

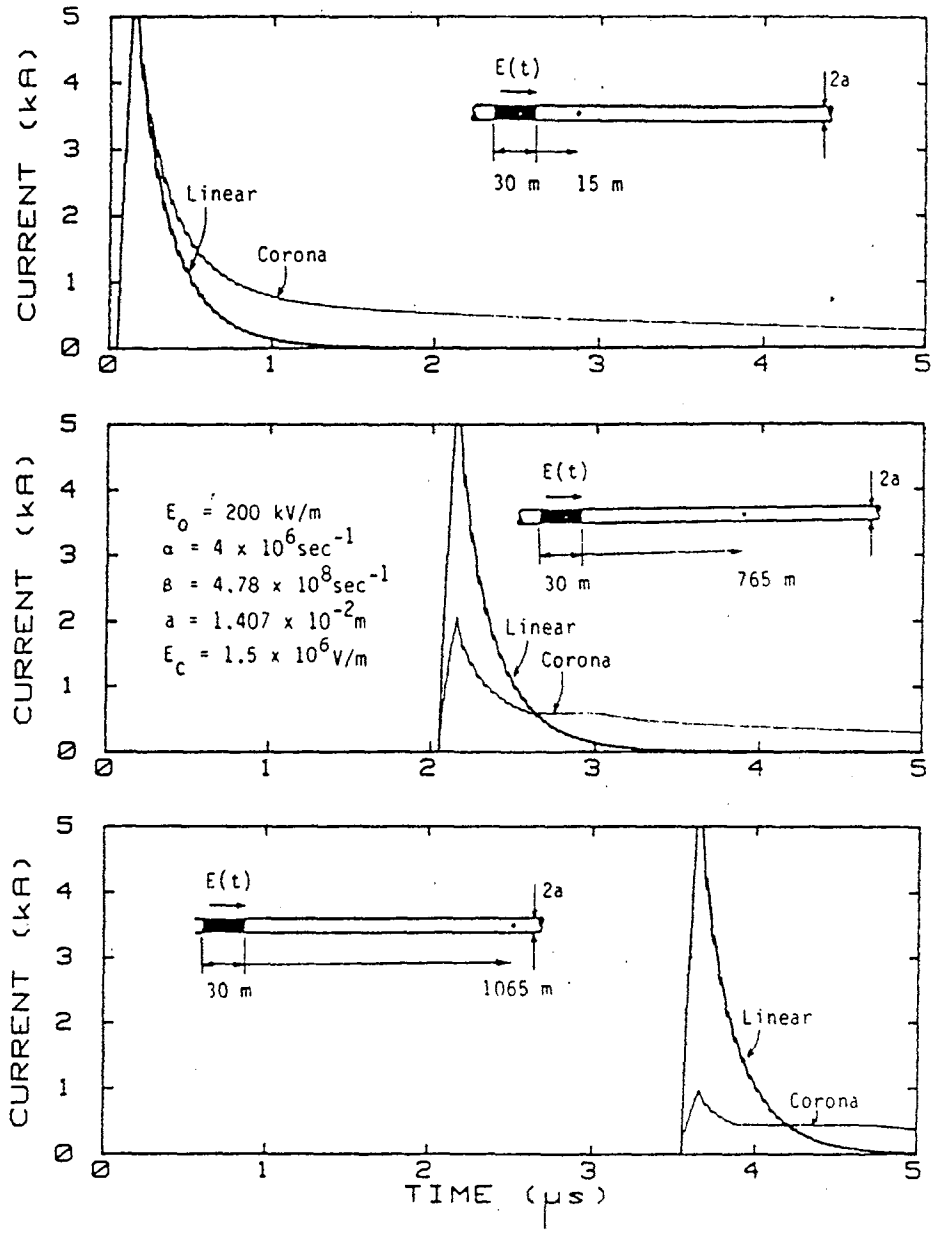

Fig. 2.11. Voltage surge-induced current in the wire at different distances from surge location in conductivity model for $\sigma = 10^{-5}$ S/m.

SEVERE LIGHTNING STRIKE (TOWNSEND'S MODEL)

(I_o = 100 kA, α = 1.43 x $10^4 sec^{-1}$, β = 4 x $10^6 sec^{-1}$, α_j = 3.5 x 10^{-3})

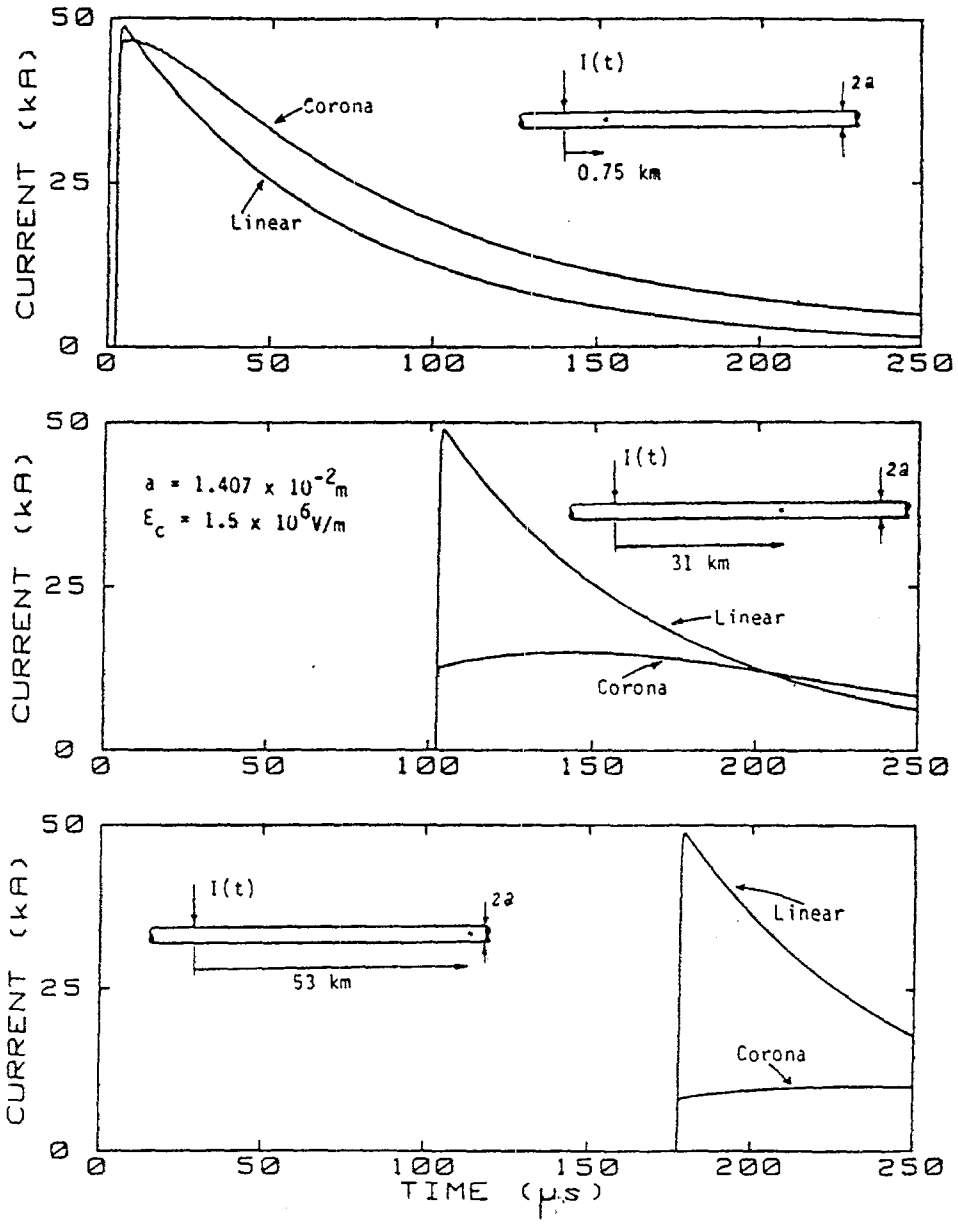

Fig. 2.12. Lightning strike-induced current in the wire at different distances from strike location in Townsend's model for α_j = 3.5 x $10^{-3} volt^{-1} sec^{-1}$.

SEVERE LIGHTNING STRIKE (CONDUCTIVITY MODEL)

(I_0 = 100 kA, $\alpha = 1.43 \times 10^4 sec^{-1}$, $\beta = 4 \times 10^6 sec^{-1}$, $\sigma_0 = 10^{-7}$ mho m^{-1})

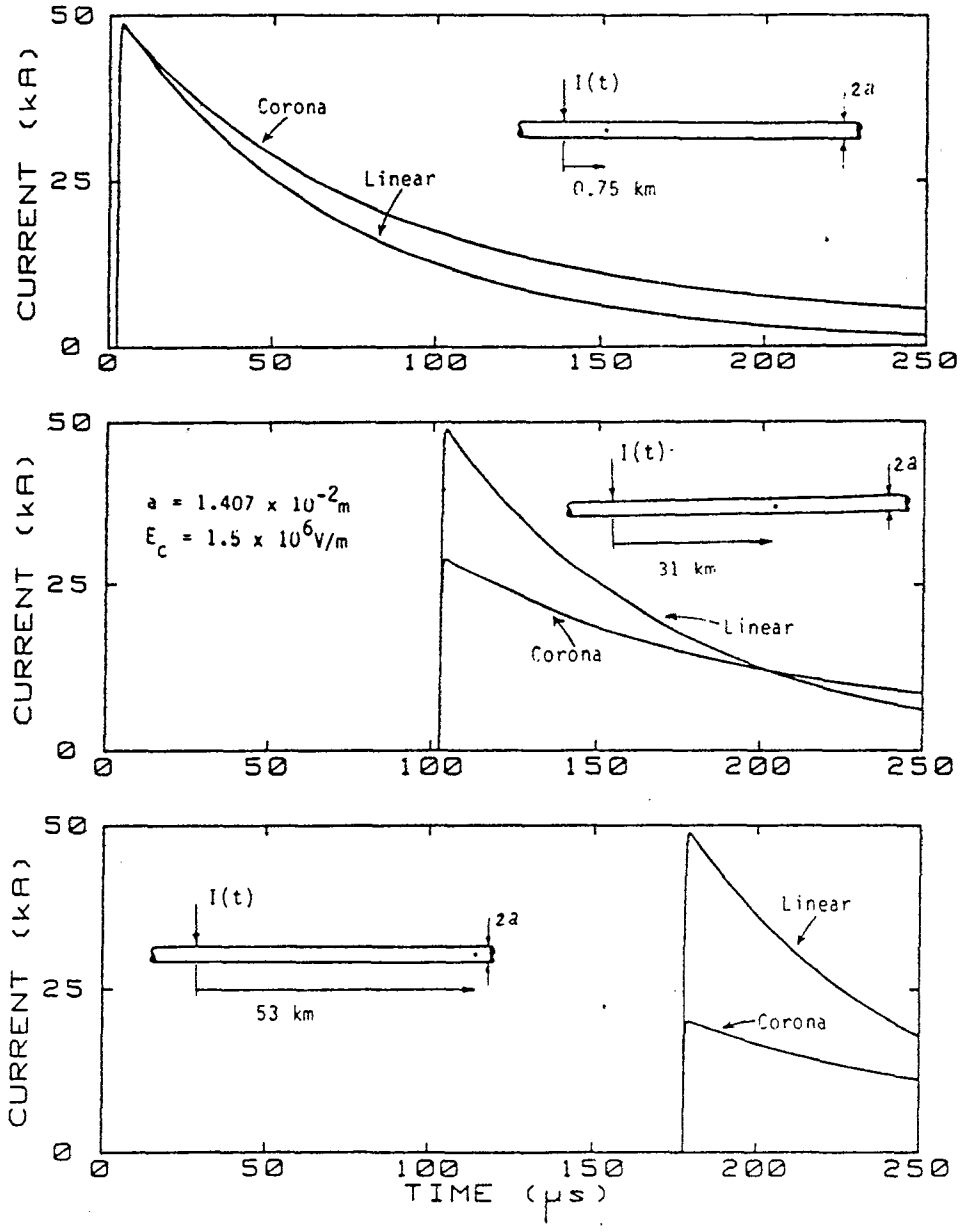

Fig. 2.13. Lightning strike-induced current in the wire at different distances from strike location in model conductivity model for $\sigma = 10^{-7}$ S/m.

2.6 COMPARISON OF THE ANALYTICAL RESULTS WITH TEST DATA AND RESULTS OF BAUM'S MODEL

In this part, the analytical results of this study are compared with the test results reported in the paper by Wagner and Lloyd[2] and also reported in a paper by Ovick and Kusic.[3] The analytical results are also compared with the results obtained from Baum's model.[4]

2.6.1 COMPARISON OF ANALYTICAL RESULTS WITH TEST DATA

In the paper by Wagner and Lloyd and also in the paper by Ovick and Kusic, some experimental data are shown. In the experimental setup, a very long wire of radius 1.32 cm lies at a height 26.4 m above the ground plane. The wire is excited by a voltage source with a double exponential waveform and voltage is measured at the different observation points. This experiment has been simulated in the computer using Townsend's and the conductivity models with the localized voltage source which generates the same waveform as that of the experiment before the corona occurs. The computer-simulated results at the same observation points are obtained. The results obtained from Townsend's models resemble the test more favorably than the results obtained from conductivity model. This enables one to find the proper value of α_j for the model. The comparison of the analytical results with the test data is shown in Fig. 2.14.

2.6.2 COMPARISON OF ANALYTICAL RESULTS WITH RESULTS OF BAUM'S MODEL

Baum formulated the corona problem using nonlinear transmission line equations.[4] The equations can be written as follows:

$$\frac{\partial V}{\partial z} = - L \frac{\partial I}{\partial t} + E_t^i \qquad (2.30)$$

$$\frac{\partial I}{\partial z} = - \frac{\partial Q}{\partial t} \qquad (2.31)$$

$$Q = C(Q)V \qquad (2.32)$$

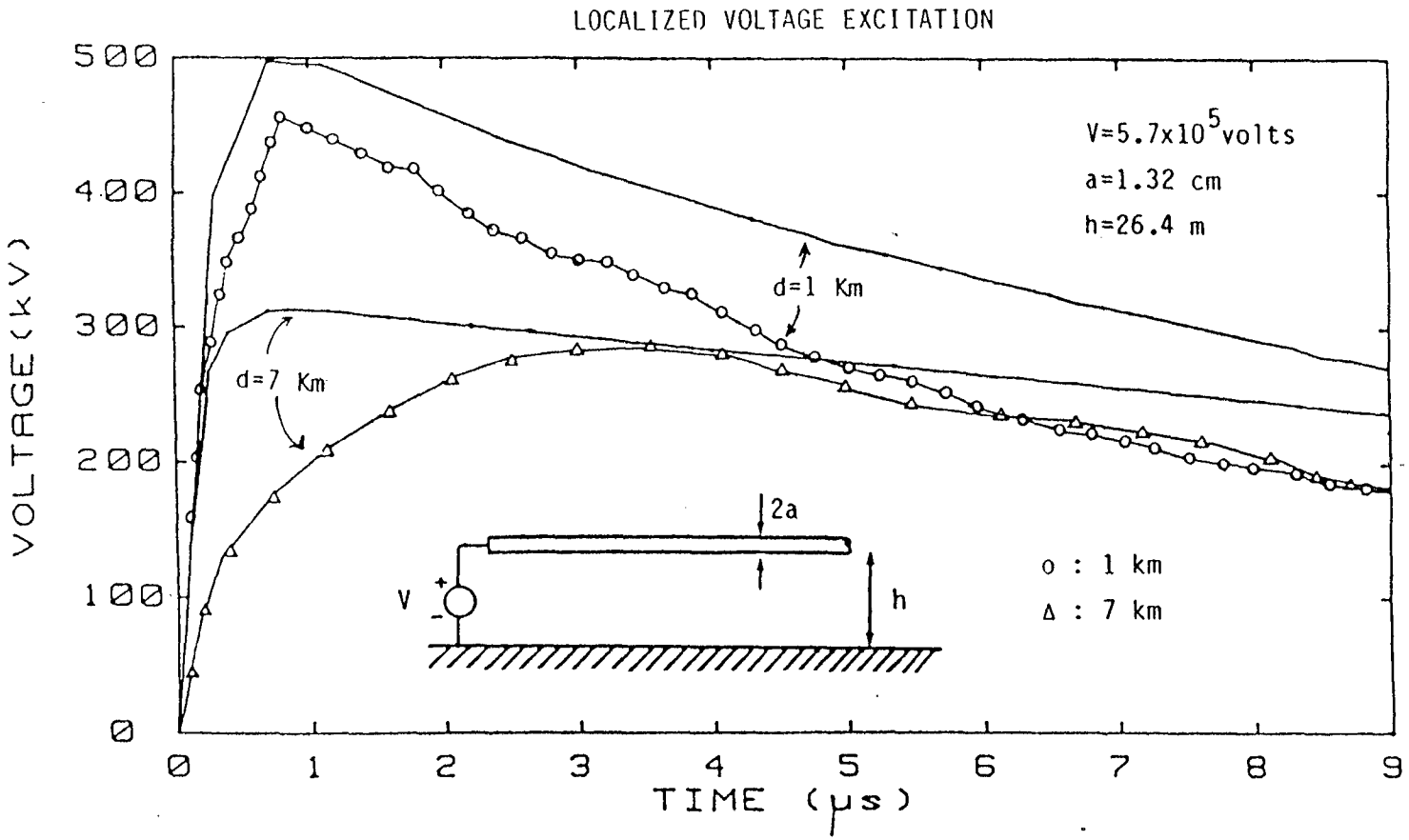

Fig. 2.14. Comparison of localized voltage induced current using Townsend's model for $\alpha_j = 2.64 \times 10^{-2}$ volt^{-1}sec^{-1} with experimental results (Refs. 2, 3) for radius $a = 1.32$ cm and $E_c = 1.5 \times 10^6$ volt m^{-1} at different distances d from the source. (o, Δ indicate experimental data)

where L is the inductance per unit length, C(Q) is the nonlinear capacitance per unit length, E_t^i is the tangential component of the incident field, Q is the charge per unit length, and V and I are the voltage and current in the wire, respectively. Baum has a solution for Q and I from this equation,i.e.,

$$Q + \frac{\cos^2\theta}{\ell n(2h/a)} Q \ell n \left(Q/4\pi\varepsilon_o h E_c\right) = \frac{2\pi\sin\theta\cos\theta}{\sqrt{\mu_o/\varepsilon_o}\,\ell n(2h/a)} E_o \int_0^{\tau} f(\tau')d\tau' \quad (2.33)$$

$$I = cQ/\cos\theta \quad (2.34)$$

where h = height of the wire

θ = elevation angle

a = radius of wire

E_c = critical voltage gradient

$E_o f(t)$ = incident electric field

$\tau = t - \frac{z\cos\theta}{c}$

This result is for the case where corona has already occurred, i.e., $Q > 2\pi a\varepsilon_o E_c$. However, when $Q < 2\pi a\varepsilon_o E_c$, Baum has the linear solution to the problem. That is

$$Q = \frac{2\pi\cot\theta}{\sqrt{\mu_o/\varepsilon_o}\,\ell n(2h/a)} E_o \int_0^{\tau} f(\tau')d\tau' \quad (2.35)$$

The analytical results obtained from Townsend's model have been compared with the results of Baum's model. The comparison is illustrated in Fig. 2.15. Additional curves for different elevation angles are shown in the appendix.

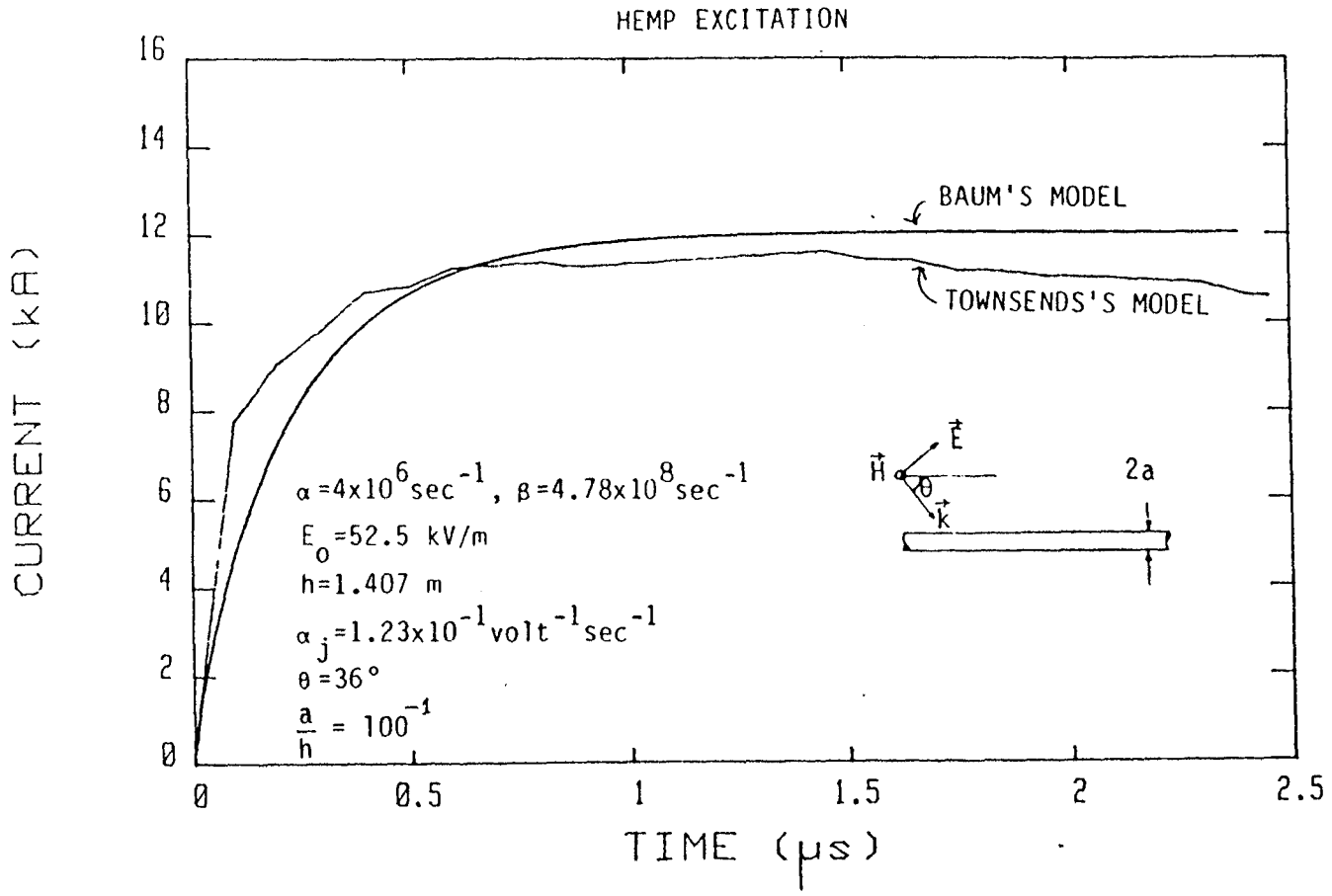

Fig. 2.15. Comparison of HEMP-induced current using Townsend's model for $\alpha_j = 1.23 \times 10^{-1}$ volt^{-1}sec^{-1} with Baum's model for elevation angle $\theta = 36°$, radius $a = 1.407$ cm and $E_c = 1.5 \times 10^6$ volt m^{-1}.

3. HEMP-INDUCED STRESSES ON LINE SUPPORTS IN T&D LINES

3.1 AN OVERVIEW

When a high-altitude electromagnetic pulse (HEMP) illuminates a large network of conductors, e.g., a power grid, large and fast transients can be induced on the network. The question of the susceptibility of the network's dielectric insulators naturally arises. Two different types of insulators will be studied, namely, the line supports and the transformer bushings. In this section, the HEMP-induced stresses across line supports will be calculated. The induced stresses across transformer bushings are relegated to the next section.

3.2 GEOMETRY OF THE PROBLEM

Figure 3.1 shows a typical 230-kV H-frame transmission line and a HEMP plane wave with the double exponential waveform incident on this system. The quantities to be calculated are the "potential difference", which is the line integral of HEMP-induced electric field across the line support, i.e., across A-C in Fig. 3.1, and the "potential difference" across the air gap between A-B in the same figure. To calculate these quantities, the interaction of HEMP with different scattering elements must be studied. These elements are the vertical line pole, the horizontal cross arm and the phase conductor above a finitely conducting ground. To calculate the "potential difference" between A and B, the interaction of HEMP with the vertical pole and the phase conductor is of relevance. The "potential difference" between A and C is calculated by considering the HEMP interaction with the horizontal cross arm and the phase conductor.

3.3 "POTENTIAL DIFFERENCE" ACROSS THE AIR GAP A-B

In evaluating the line integral of the electric field across the air gap A-B, the coupling of HEMP with the vertical pole and the phase conductor is to be considered. The formulation of the HEMP interaction

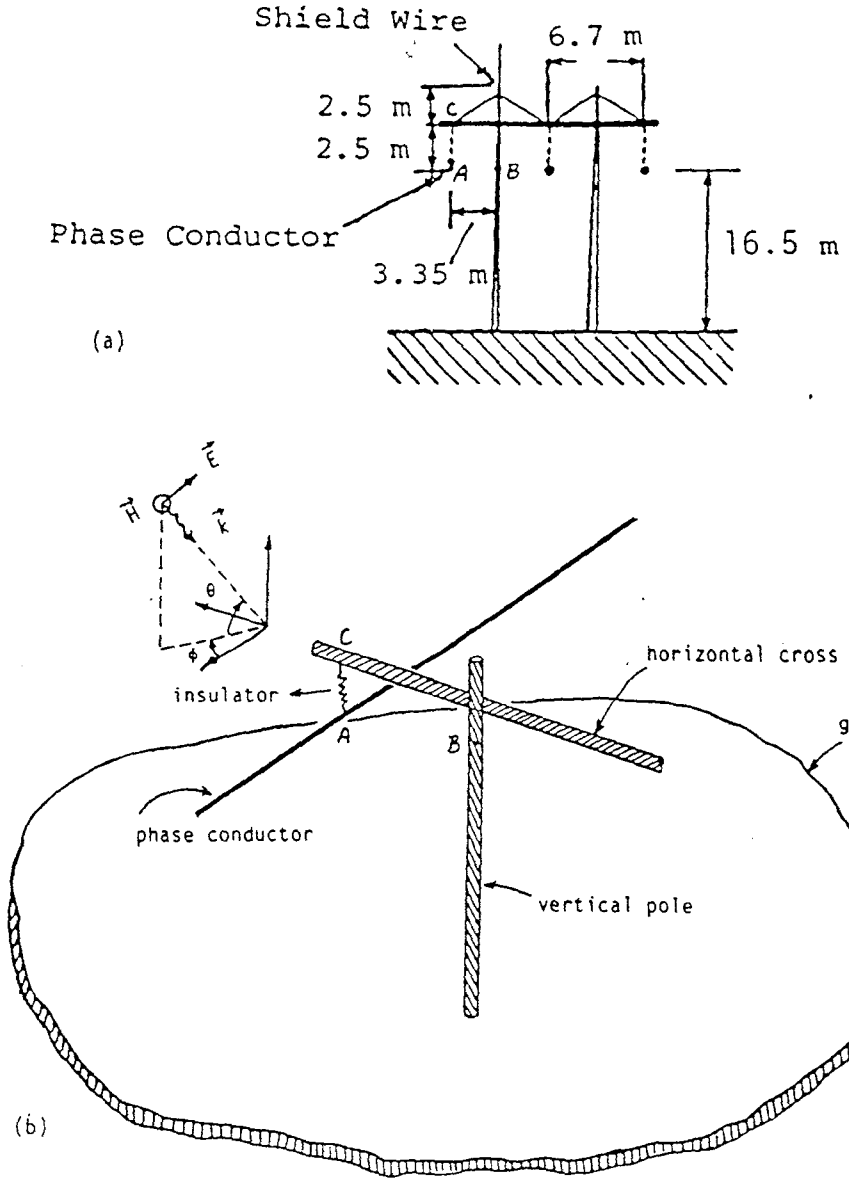

Fig. 3.1. A typical 230 kV H-frame transmission line (a) configuration at structure, (b) geometry of the problem of HEMP interaction with the transmission line.

with the vertical pole is similar to the formulation explained in Sect. 2, except that the corona current is zero. To evaluate the current and charge induced in the vertical pole, the following equations will be used:

$$\frac{\partial^2 I}{\partial z^2} - \frac{1}{c^2}\frac{\partial^2 I}{\partial t^2} = -\frac{4\pi\varepsilon_o}{\Omega}\frac{\partial E_t^i}{\partial t} \tag{3.1}$$

$$\frac{\partial I}{\partial z} = -\frac{\partial Q}{\partial t} \tag{3.2}$$

where $\Omega = 2\,\ell n\left[2(ct - z\sin\theta + a\cos\theta)/(r a\cos\theta)\right]$ for $ct - z\sin\theta + a\cos\theta > 0$, θ is the elevation angle, E_t^i is the tangential component of the incident field along the vertical pole, I is the current in the pole and Q is the charge per unit length in the pole. To solve these equations, method of characteristic is used and the charge per unit length at point B is calculated. From a knowledge of Q at B, induced electric field due to HEMP-coupling with the vertical pole is obtained. To evaluate the "potential difference" between A and B, the induced electric field across A-B due to HEMP interaction with the phase conductor is also needed.

To quantify the interaction of HEMP with the phase conductors, two different theories can be used: scattering and transmission-line theories. These two theories lead to similar results in later times. However, in early-times consideration, there will be differences. Figures 3.2 and 3.3 present the early-time responses of an infinitely long wire above a finitely conducting ground to HEMP using the two different theories. As can be seen, for different values of ground conductivity and for $\theta = 54°$, the responses differ at most by about 12%. For the smaller angle of incidence, whose curves are shown in the appendix, the difference is even less than this value. Therefore, the early-time responses obtained from two different methods are very much similar. Here and henceforth, the transmission-line theory is used in evaluating the HEMP-induced charge and current in the phase conductors. Solving the transmission line equations one gets[9]

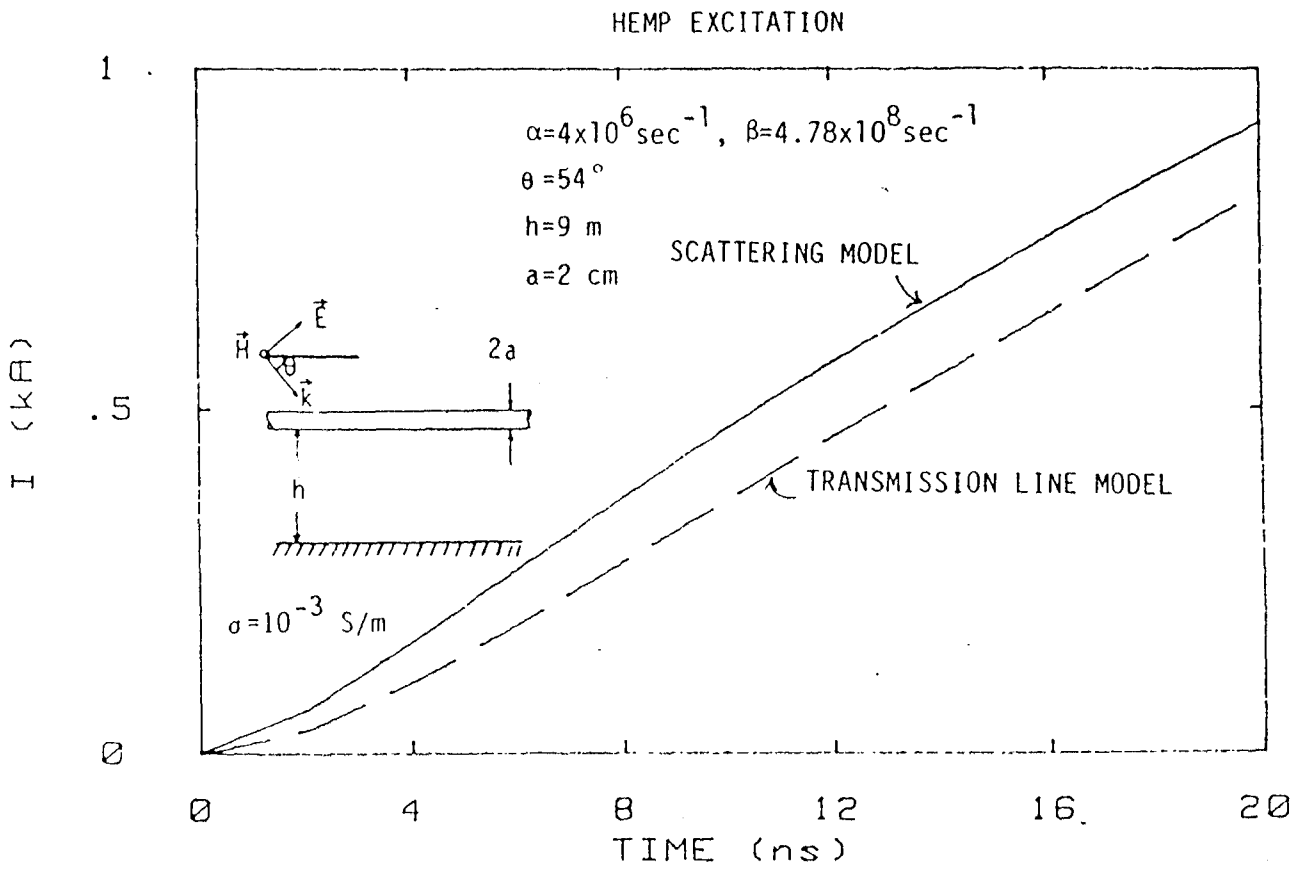

Fig. 3.2. Comparison of HEMP-induced current using scattering and transmission line models for elevation angle $\theta = 54°$ and ground conductivity $\sigma = 10^{-3}$ S/m.

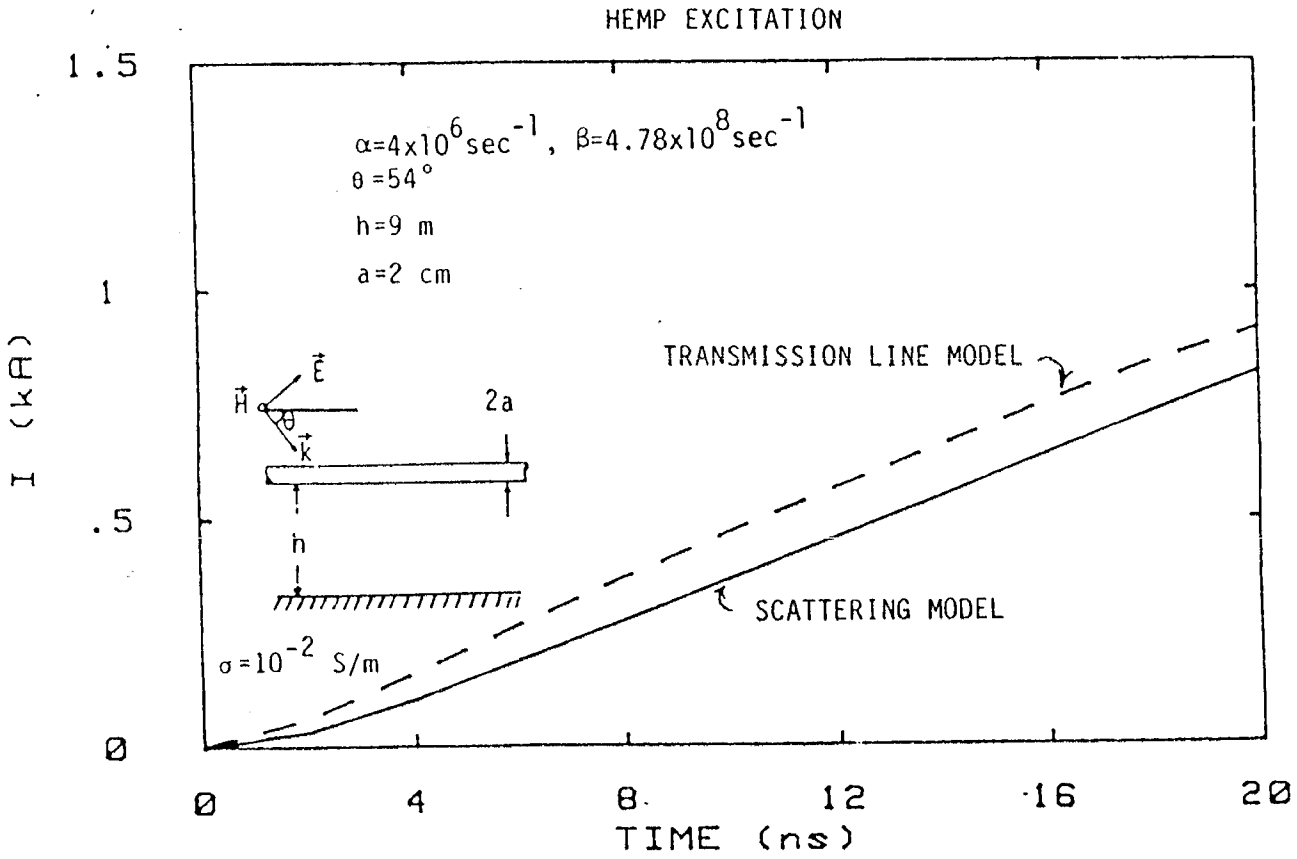

Fig. 3.3. Comparison of HEMP-induced current using scattering and transmission line models for elevation angle $\theta = 54°$ and ground conductivity $\sigma = 10^{-2}$ S/m.

$$I(t) = \frac{E_o\, c}{\sin\theta}\left[\frac{1}{\alpha}\left(1 - e^{-\alpha t}\right) \cdot \frac{1}{\beta}\left(1 - e^{-\beta t}\right)\right] \quad \text{for} \quad 0 < t < t_o$$

$$= \frac{E_o c}{\sin\theta}\left\{\frac{1}{\alpha}\left[\left(e^{\alpha t_o} - 1\right) e^{-\alpha t} + \frac{4}{\sin\theta}\sqrt{\frac{\alpha\tau_e}{\pi}}\, e^{-\alpha t'}\int_0^{\sqrt{\alpha t'}} e^{u^2} du\right]\right. \qquad (3.3)$$

$$\left. - \frac{1}{\beta}\left[\left(e^{\beta t_o} - 1\right) e^{-\beta t} + \frac{4}{\sin\theta}\sqrt{\frac{\beta\tau_e}{\pi}}\, e^{-\beta t'}\int_0^{\sqrt{\beta t'}} e^{u^2} du\right]\right\}$$

$$\text{for } t > t_o$$

where $t_o = \frac{2h\sin\theta}{c}$, h is the height of the wire, $t' = t - t_o$, E_o is the amplitude of the incident field with a double exponential time function given by Eq. (2.27), θ is the elevation angle, $\tau_e = \frac{\varepsilon_o}{\sigma}$ (σ = conductivity of the ground) and c is the vacuum speed of light. With a knowledge of I, Q can be calculated using the following relation:

$$Q = \frac{I\cos\theta}{c} \qquad (3.4)$$

From Q, the electric field across the air gap A-B can be evaluated, and hence the line integral of the electric fields across A-B. The line integral or the "potential difference" is calculated for two different values of ground conductivity (e.g. $\sigma = 10^{-2}$ and 10^{-3} S/m) and for different elevation angles (e.g. θ = 18°, 36°, and 54°). In this calculation h is taken to be 9.75 m. However, the height of the wire at the pole is 16.5 m, but due to wire sagging the average height is 9.75 m. ϕ is taken to be zero, since this value of ϕ, among other values of ϕ, provides the highest "potential difference" in the air gap. Figures 3.4 through 3.6 illustrate the potential differences across air gap A-B for different values of σ and θ. As can be seen, the major contribution to this potential difference is from the HEMP-coupling with the phase

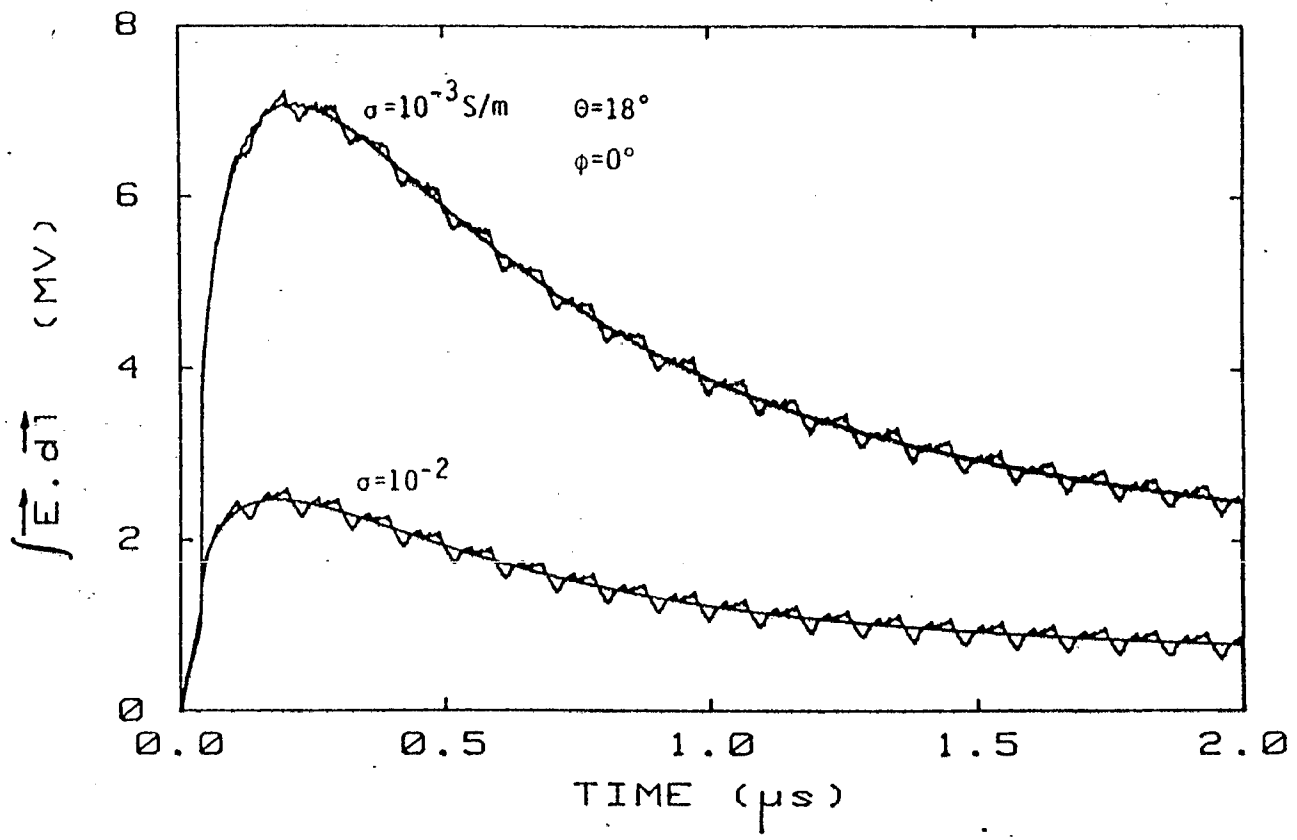

Fig. 3.4. Calculated HEMP-induced "Potential Difference" between the phase conductor and the vertical pole for the elevation angle $\theta=18°$ and for two different values of ground conductivity σ.

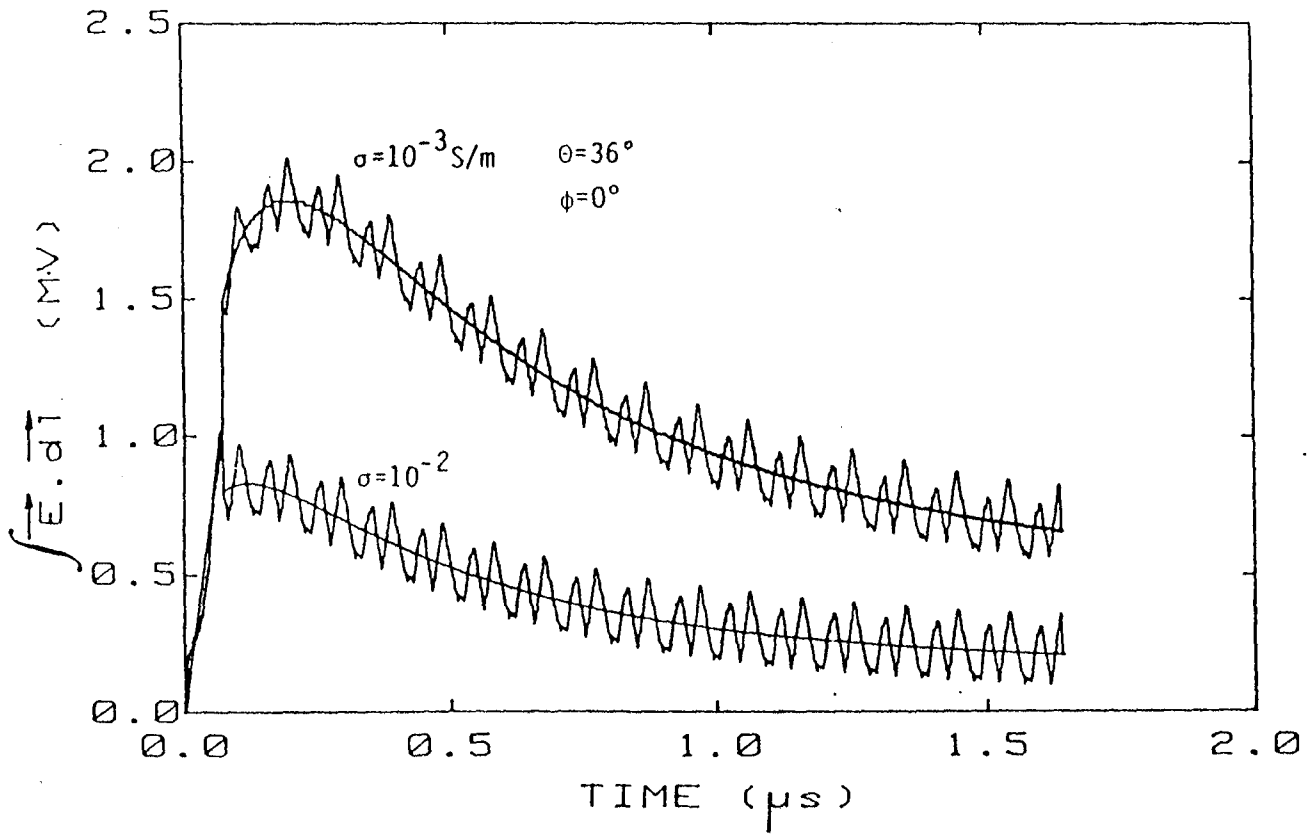

Fig. 3.5. Calculated HEMP-induced "Potential Difference" between the phase conductor and the vertical pole for the elevation angle $\theta=36°$ and for two different values of ground conductivity σ.

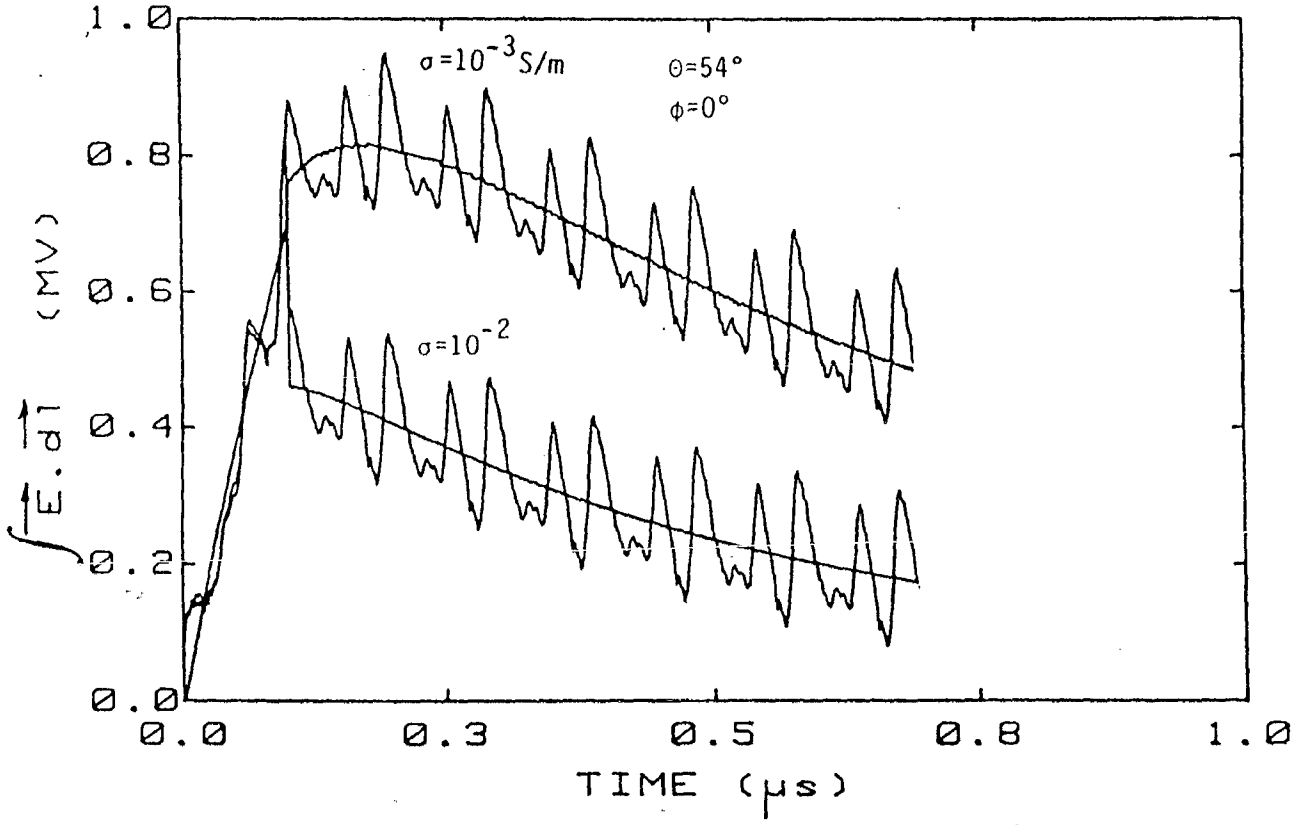

Fig. 3.6. Calculated HEMP-induced "Potential Difference" between the phase conductor and the vertical pole for the elevation angle $\theta=54°$ and for two different values of ground conductivity σ.

conductors. The vertical pole contribution appears to be small ripples in the results. Figure 3.7 presents the rise time, the fall time and the peak value of the HEMP-induced potential difference between A-B for different elevation angles. The small wiggles over the ripples are numerical noises.

3.4 "POTENTIAL DIFFERENCE" ACROSS THE LINE SUPPORT A-C

Using an approach similar to the one used in the evaluation of "potential difference" across air gap A-B, the "potential difference" across the line support can be calculated. In this calculation, the azimuthal angle ϕ is also one of the parameters. Figures 3.8 through 3.14 show the HEMP-induced potential differences across the line support for different elevation angle θ, azimuthal angles ϕ, and ground conductivities σ. Additional curves are presented in the appendix. As can be seen from the figures, for $\phi = 0°$ the whole contribution is from HEMP-coupling with the phase conductors. As ϕ increases the contribution of phase conductor to the potential difference decreases, and the contribution of the horizontal cross arm increases. When $\phi = 90°$, the whole contribution is due to the horizontal cross arm. Figures 3.15 through 3.20 present the rise-time, fall-time and the peak value of the HEMP-induced potential difference across the line support.

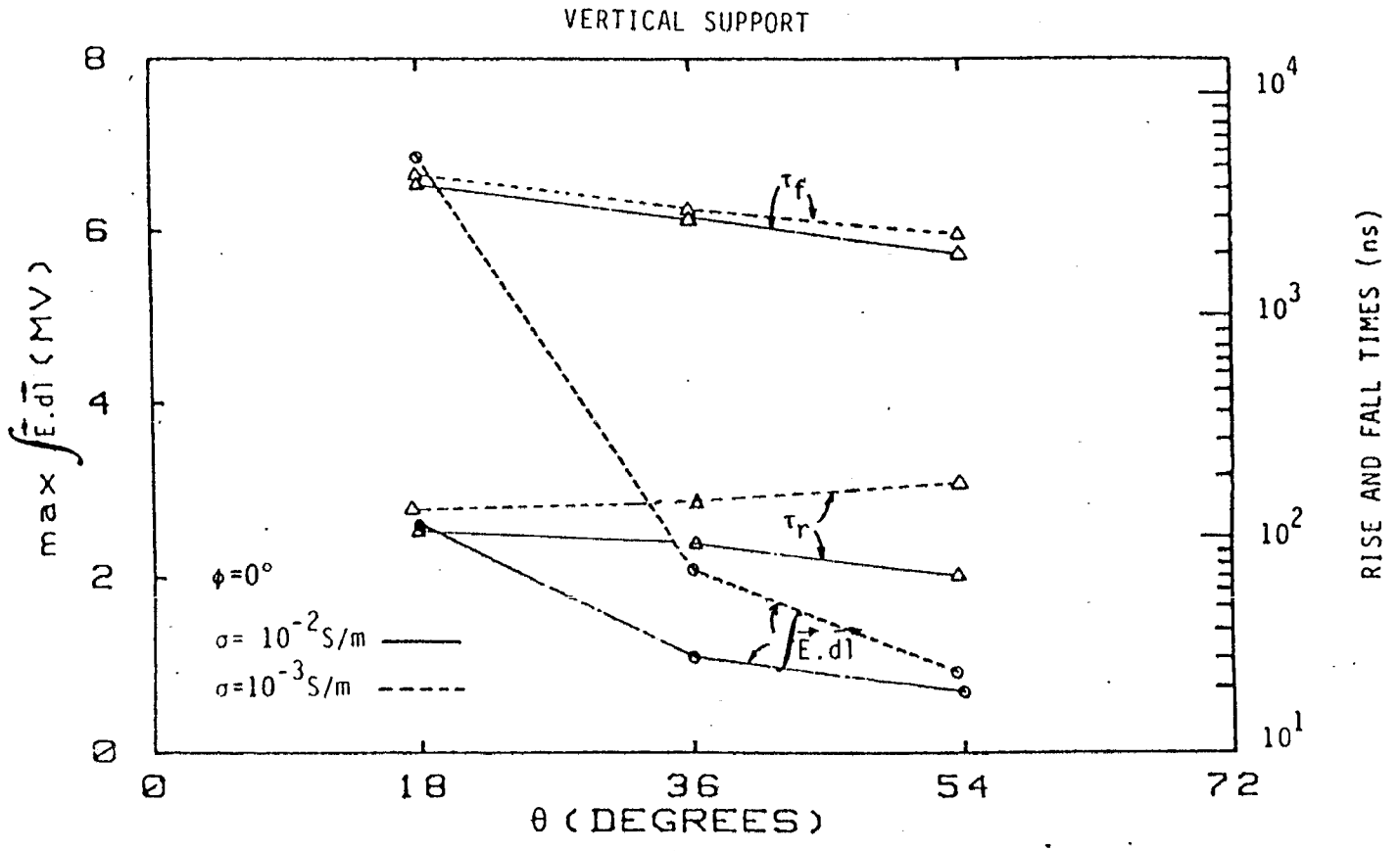

Fig. 3.7. Rise time, fall time, and maximum value of HEMP-induced "Potential Difference" between the phase conductor and the vertical pole as function of elevation angle θ for two different values of ground conductivity σ.

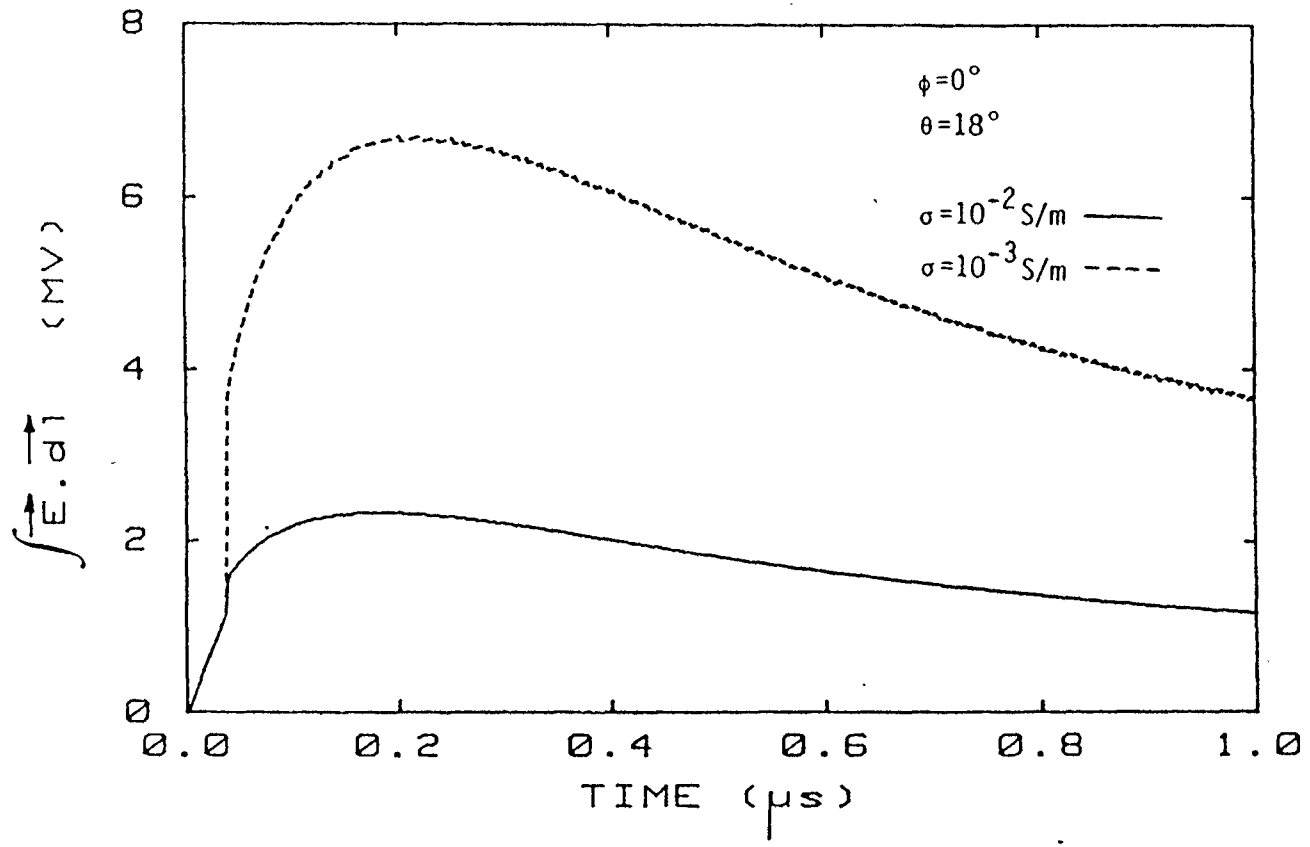

Fig. 3.8. Calculated HEMP-induced "Potential Difference" between the phase conductor and the horizontal cross arm for azimuthal angle $\phi=0°$, elevation angle $\theta=18°$, and for two different values of ground conductivity σ.

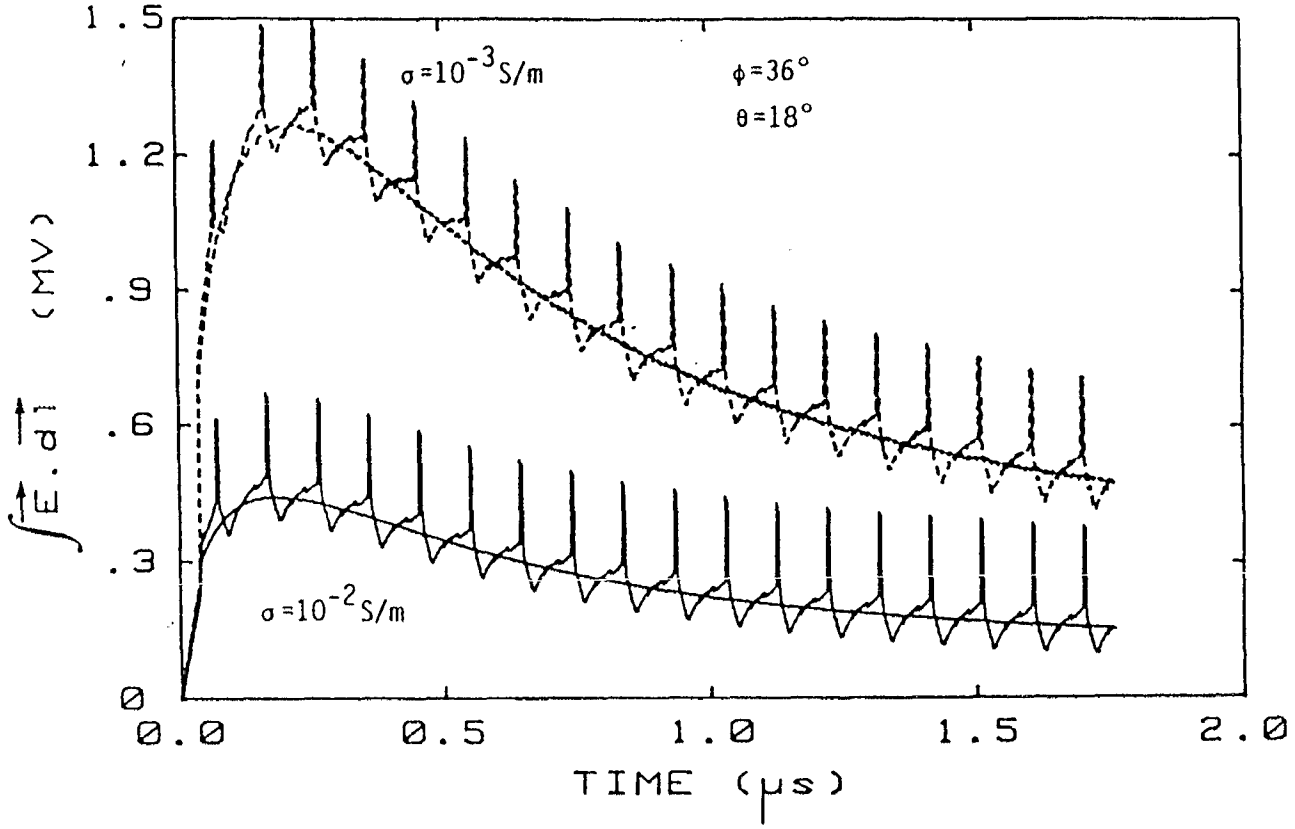

Fig. 3.9. Calculated HEMP-induced "Potential Difference" between the phase conductor and the horizontal cross arm for azimuthal angle $\phi=36°$, elevation angle $\theta=18°$, and for two different values of ground conductivity σ.

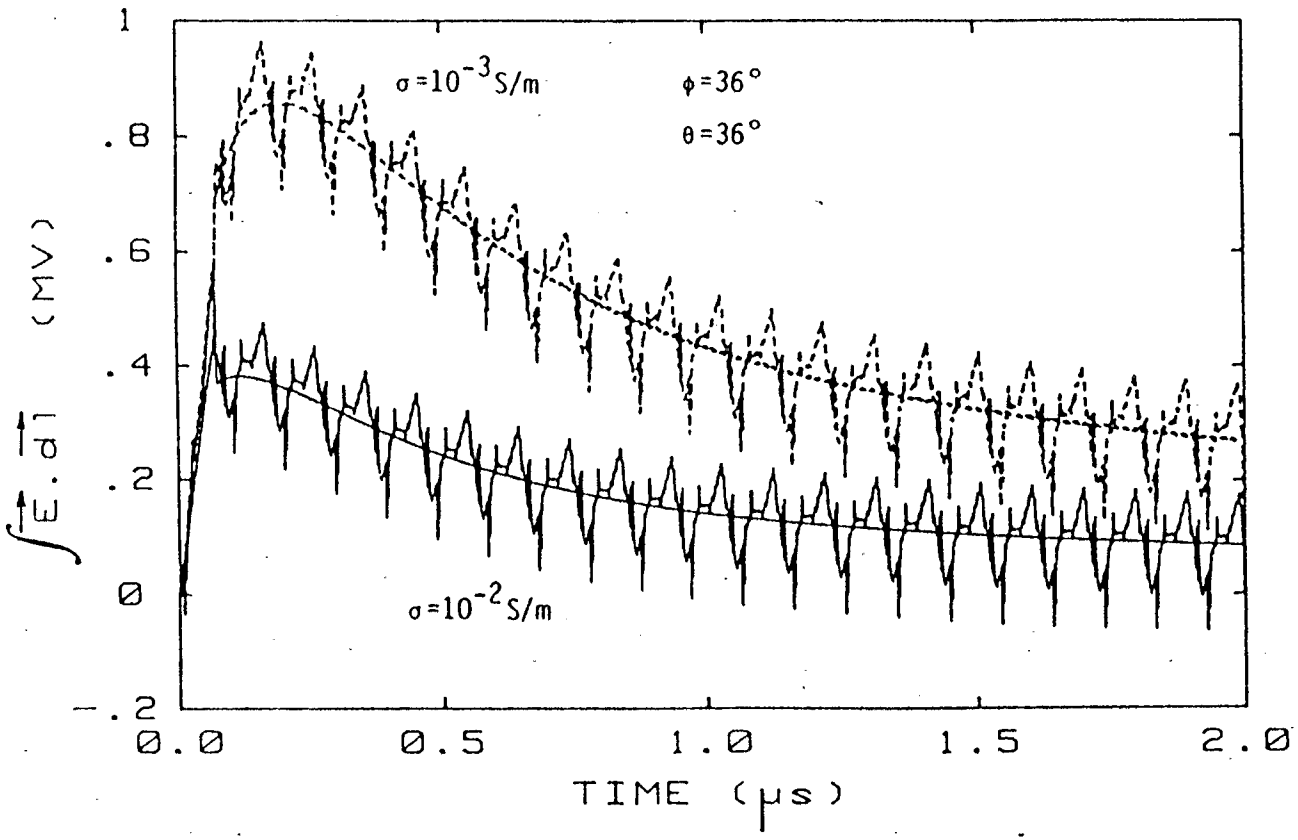

Fig. 3.10. Calculated HEMP-induced "Potential Difference" between the phase conductor and the horizontal cross arm for azimuthal angle $\phi=36°$, elevation angle $\theta=36°$, and for two different values of ground conductivity σ.

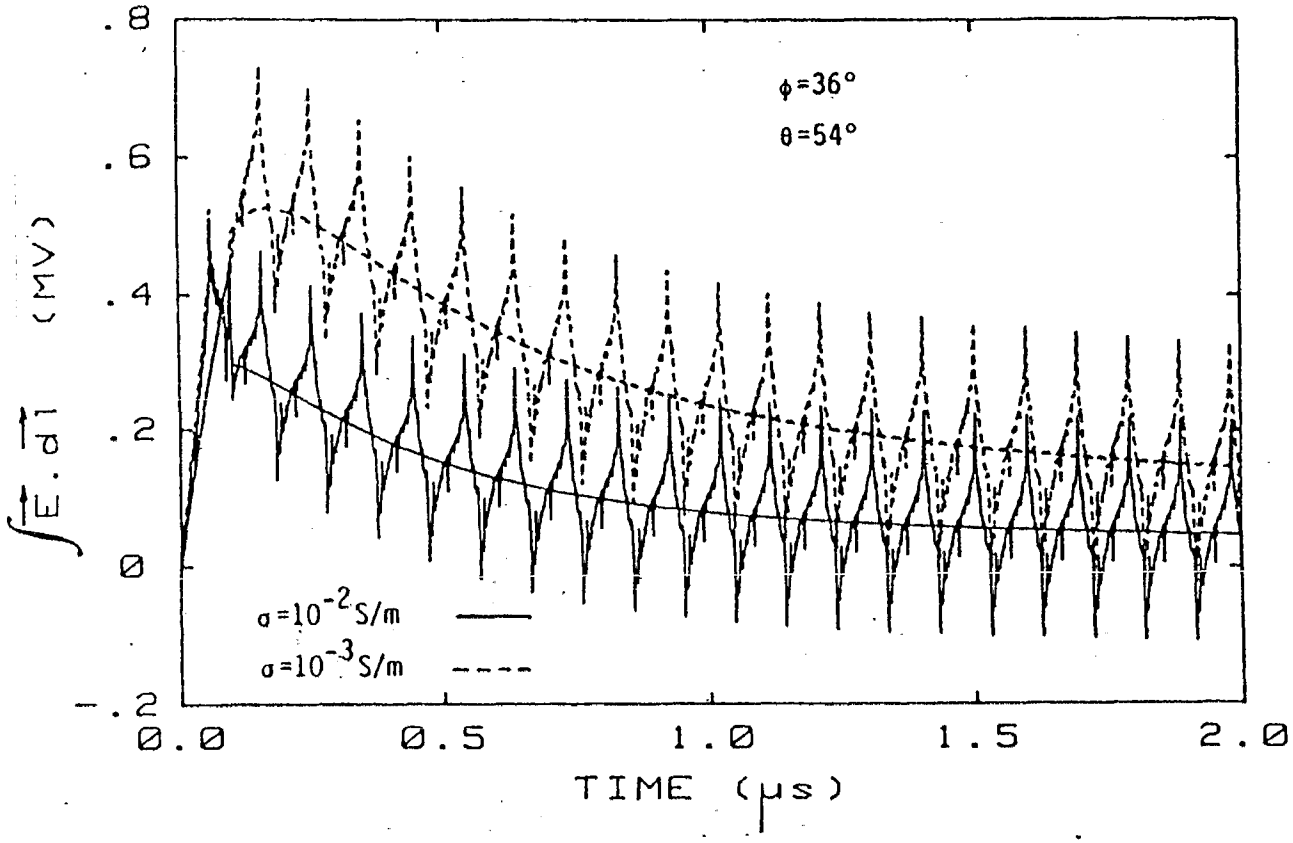

Fig. 3.11. Calculated HEMP-induced "Potential Difference" between the phase conductor and the horizontal cross arm for azimuthal angle ϕ=36°, elevation angle θ=54°, and for two different values of ground conductivity σ.

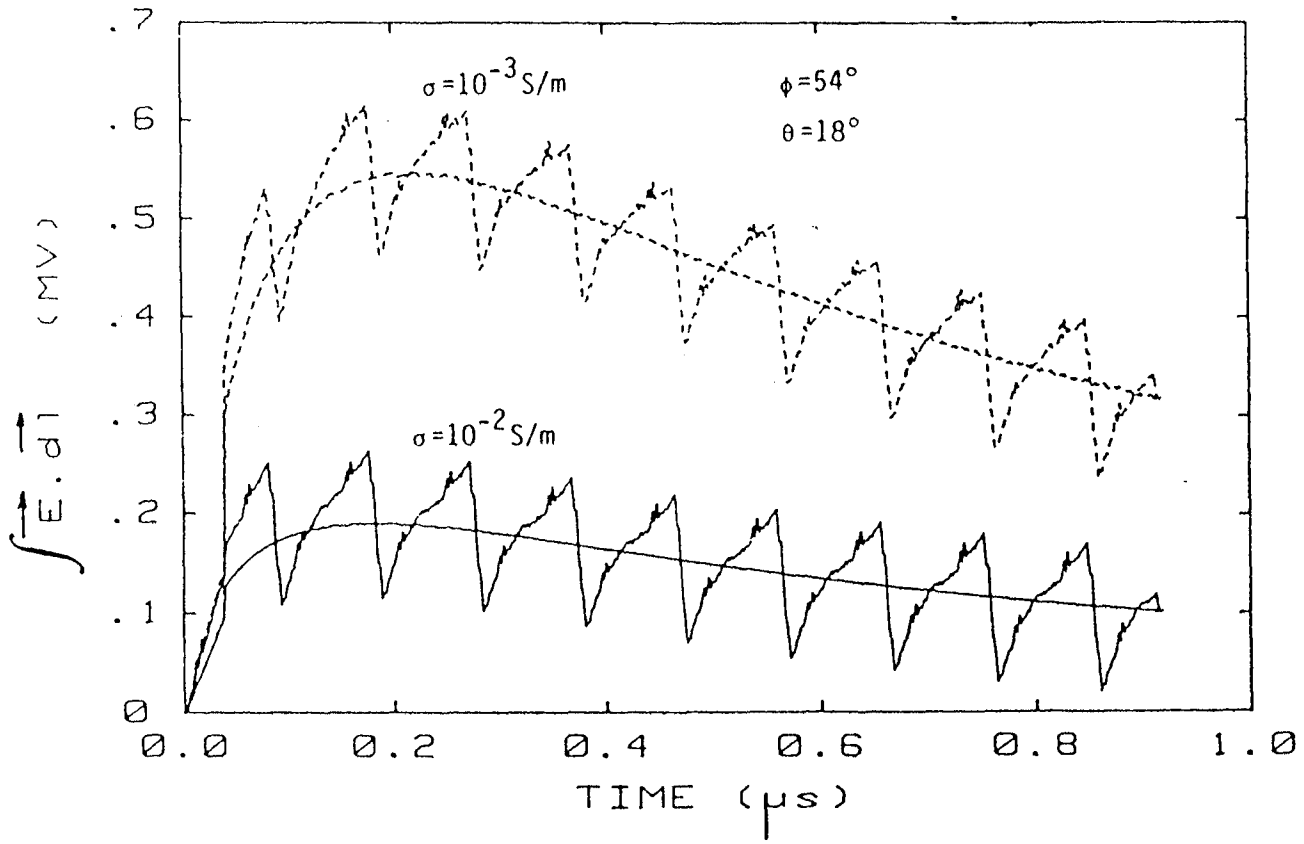

Fig. 3.12. Calculated HEMP-induced "Potential Difference" between the phase conductor and the horizontal cross arm for azimuthal angle $\phi=54°$, elevation angle $\theta=18°$, and for two different values of ground conductivity σ.

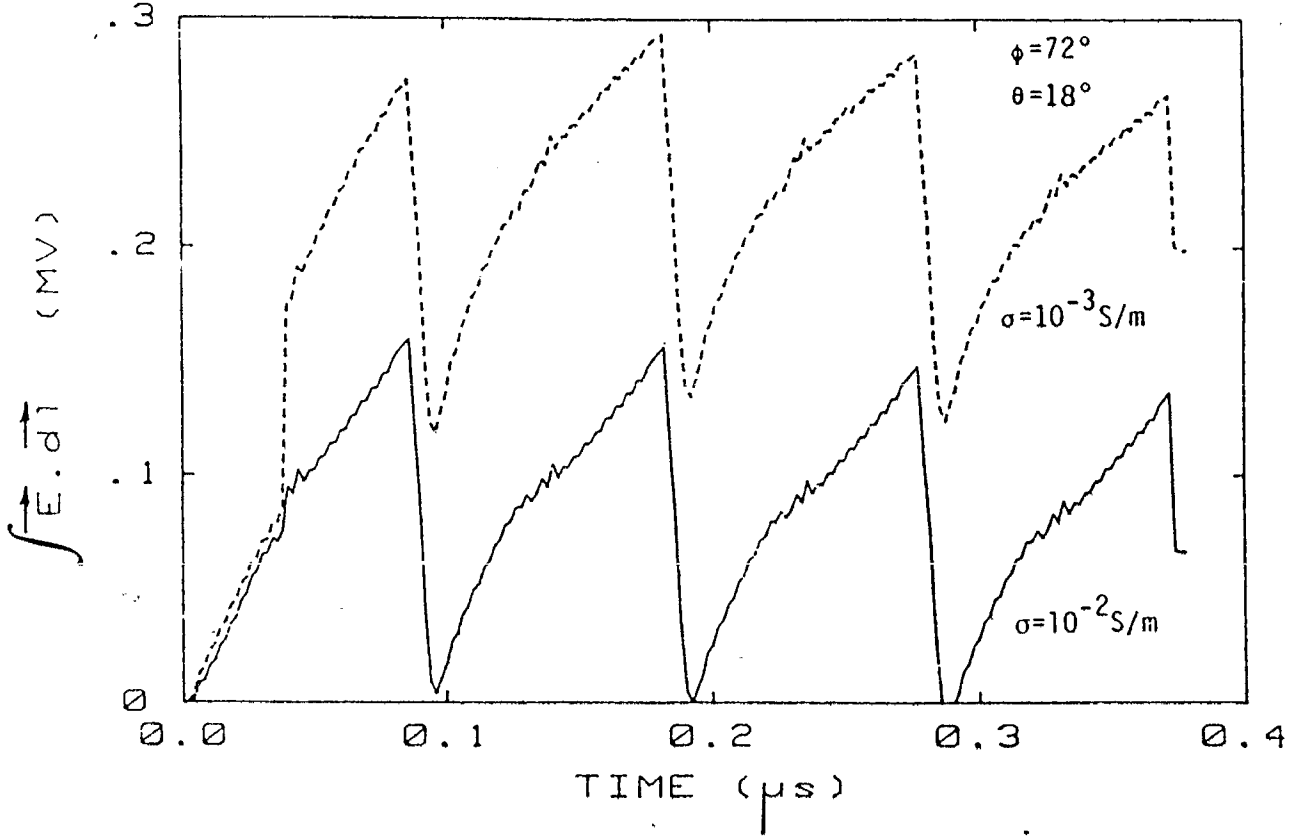

Fig. 3.13. Calculated HEMP-induced "Potential Difference" between the phase conductor and the horizontal cross arm for azimuthal angle ϕ=72°, elevation angle θ=18°, and for two different values of ground conductivity σ.

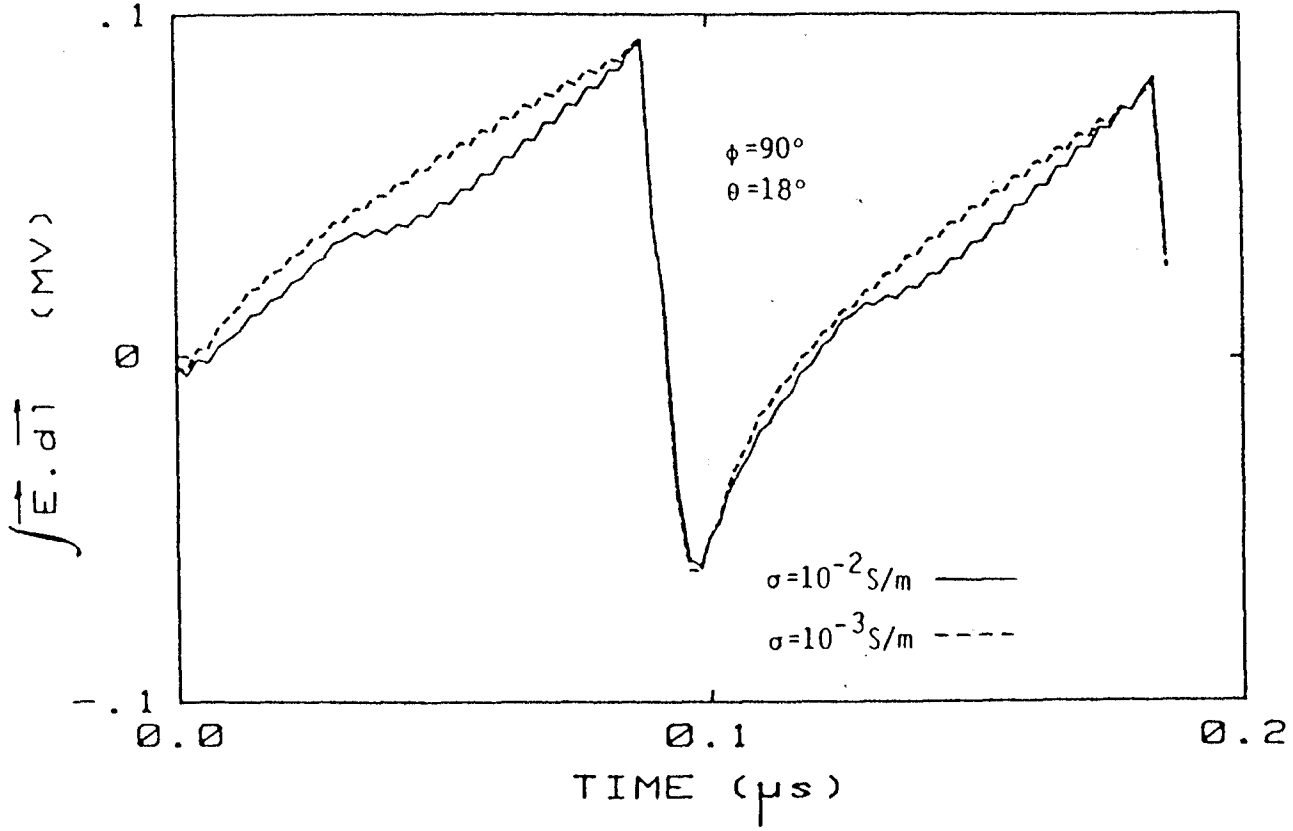

Fig. 3.14. Calculated HEMP-induced "Potential Difference" between the phase conductor and the horizontal cross arm for azimuthal angle ϕ=90°, elevation angle θ=18°, and for two different values of ground conductivity σ.

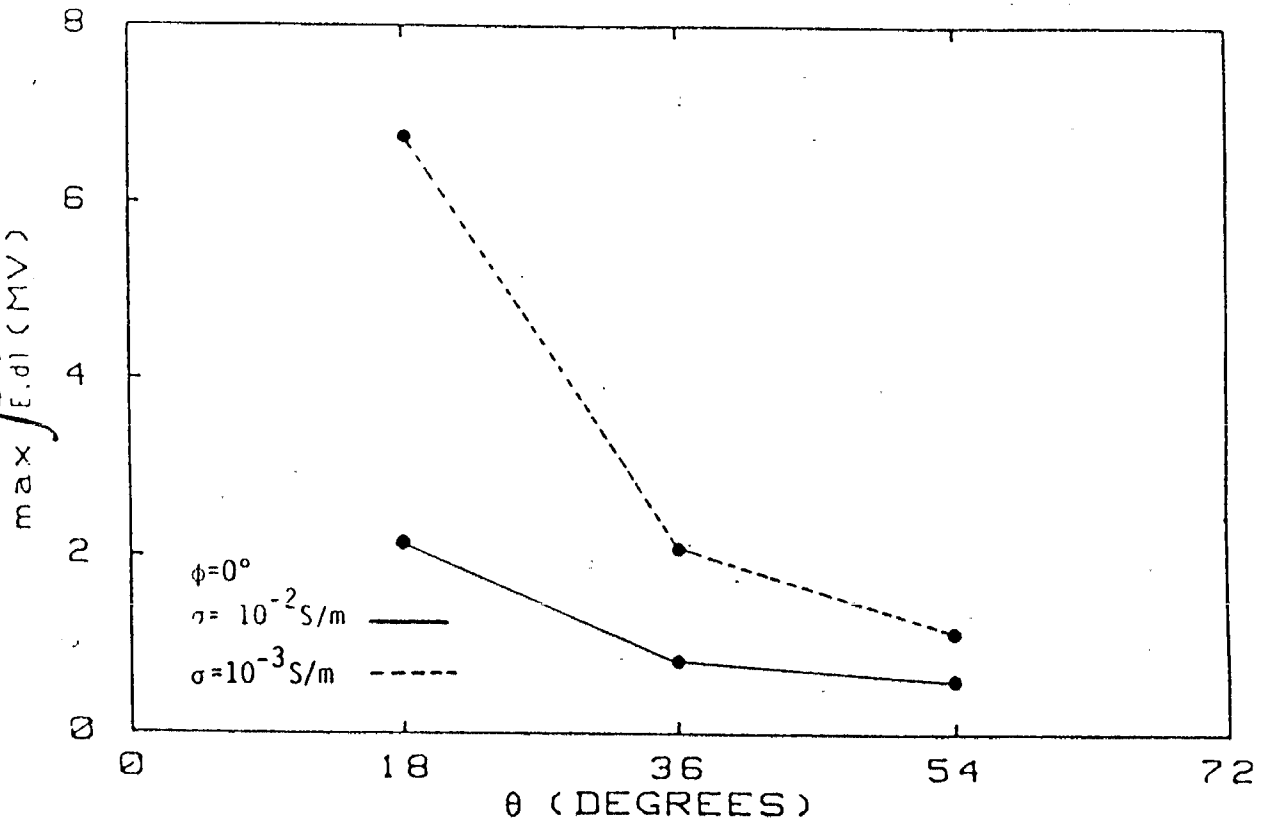

Fig. 3.15. Rise time, fall time and maximum value of HEMP-induced "Potential Difference" between the phase conductor and the horizontal cross arm as function of elevation angle θ for azimuthal angle $\phi=0^{\circ}$, and for two different values of ground conductivity σ.

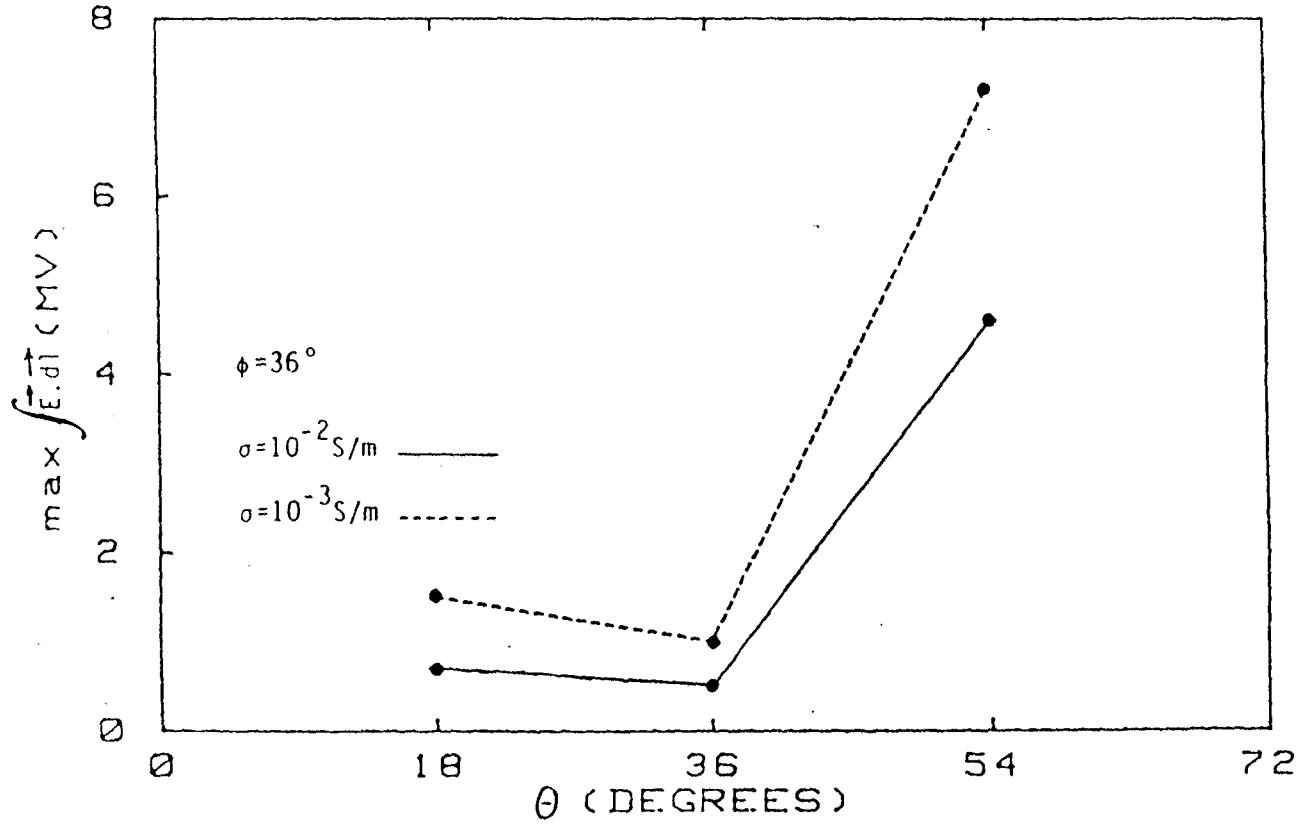

Fig. 3.16. Maximum value of HEMP-induced "Potential Difference" between the phase conductor and the horizontal cross arm as function of elevation angle θ for azimuthal angle $\phi=36°$ and for two different values of ground conductivity σ.

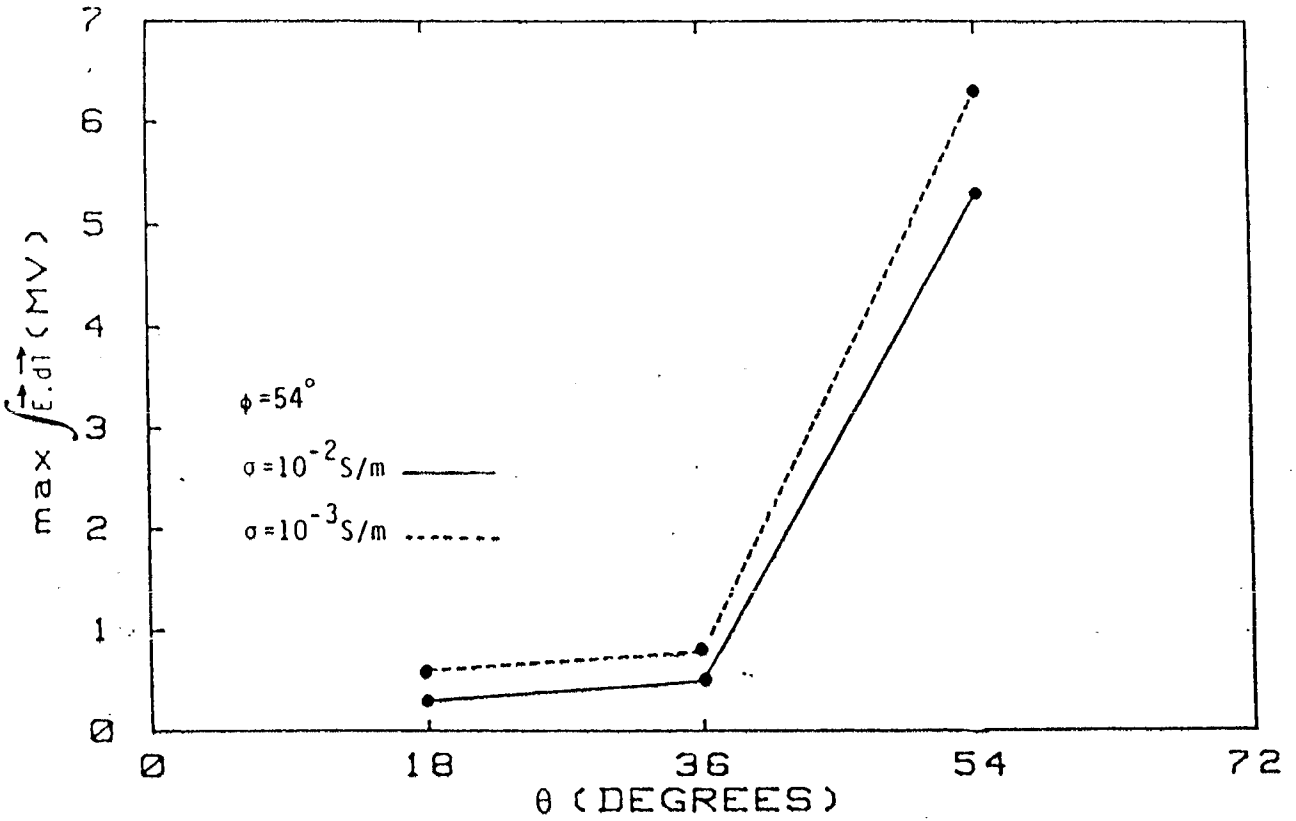

Fig. 3.17. Maximum value of HEMP-induced "Potential Difference" between the phase conductor and the horizontal cross arm as function of elevation angle θ for azimuthal angle $\phi=54°$, and for two different values of ground conductivity σ.

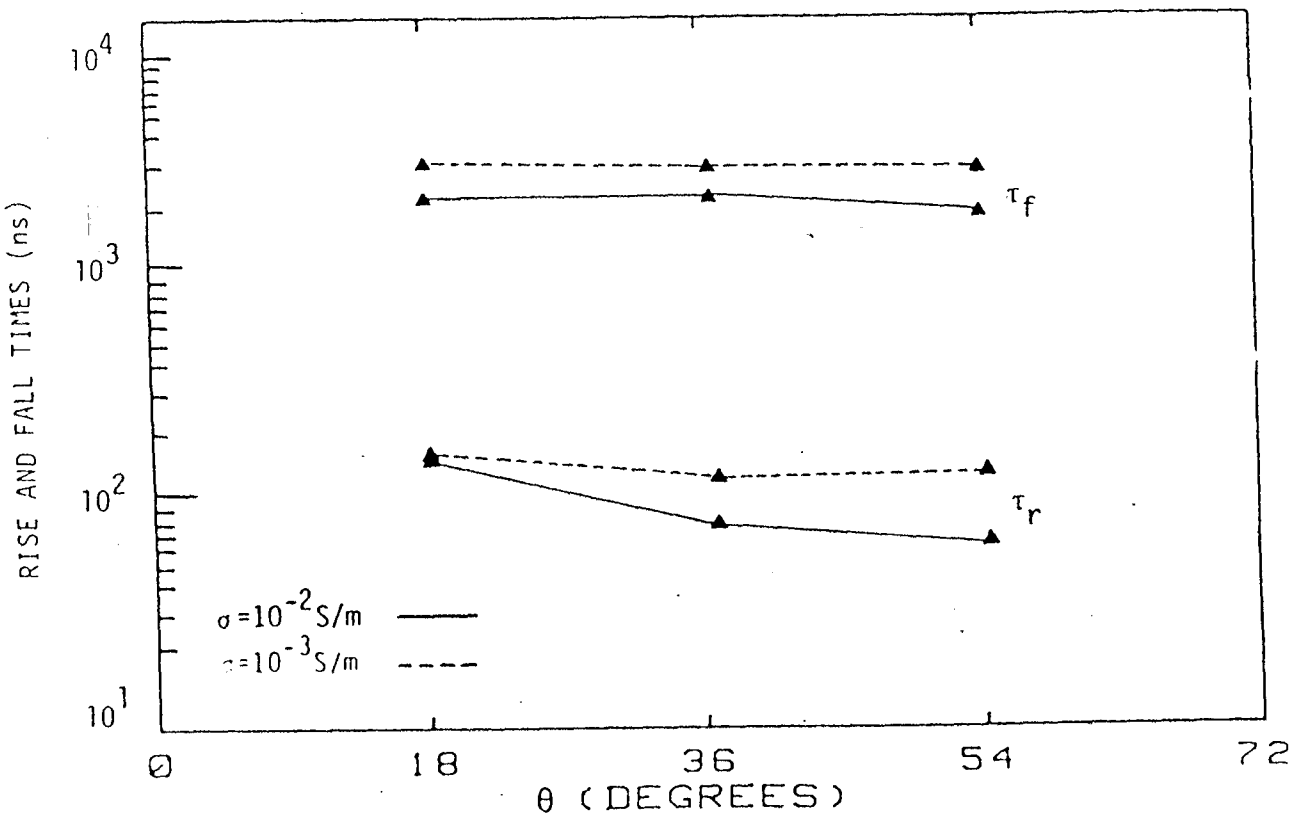

Fig. 3.18. Rise time and fall time of HEMP-induced "Potential Difference" between the phase conductor and the horizontal cross arm as function of elevation angle θ for azimuthal angle $\phi=0^\circ$ and for two different values of ground conductivity σ.

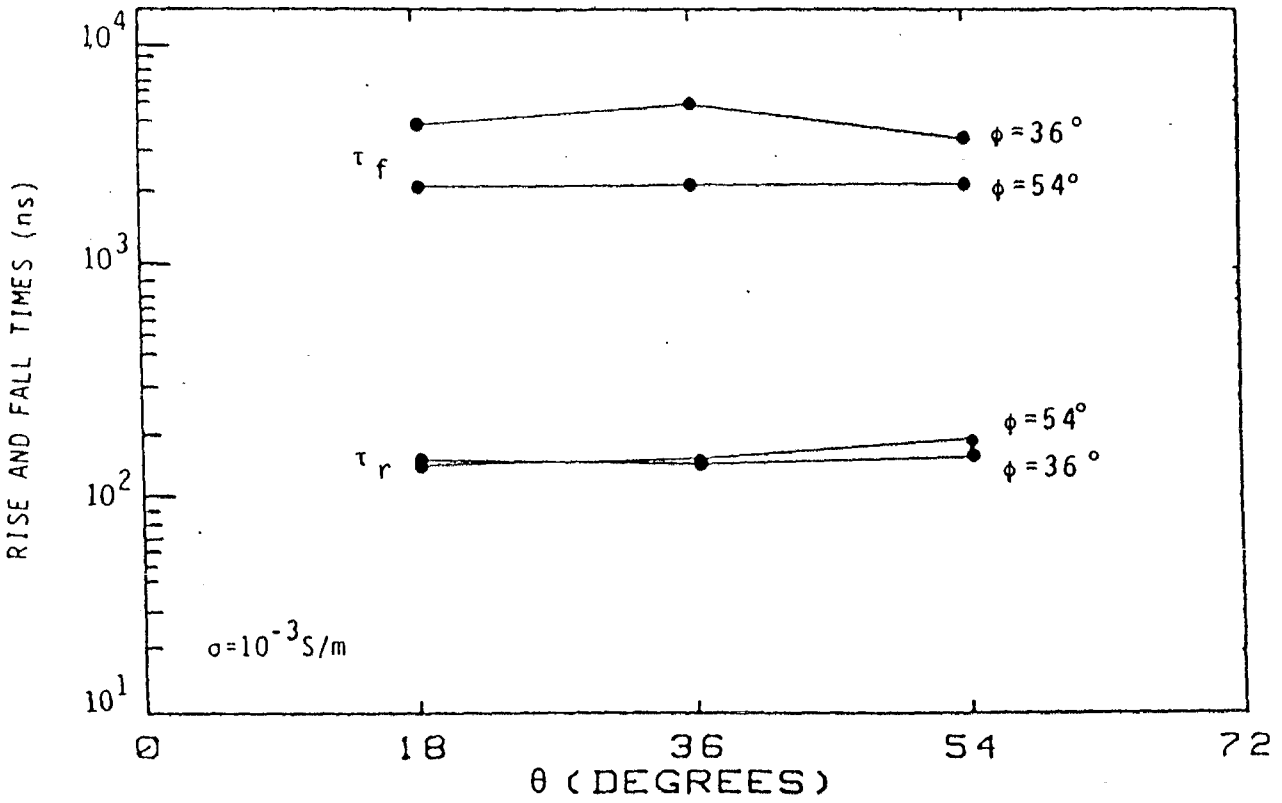

Fig. 3.19. Rise time and fall time of HEMP-induced "Potential Difference" between the phase conductor and the horizontal cross arm as function of elevation angle θ for ground conductivity $\sigma = 10^{-3}$ S/m and for two different values of azimuthal angle ϕ.

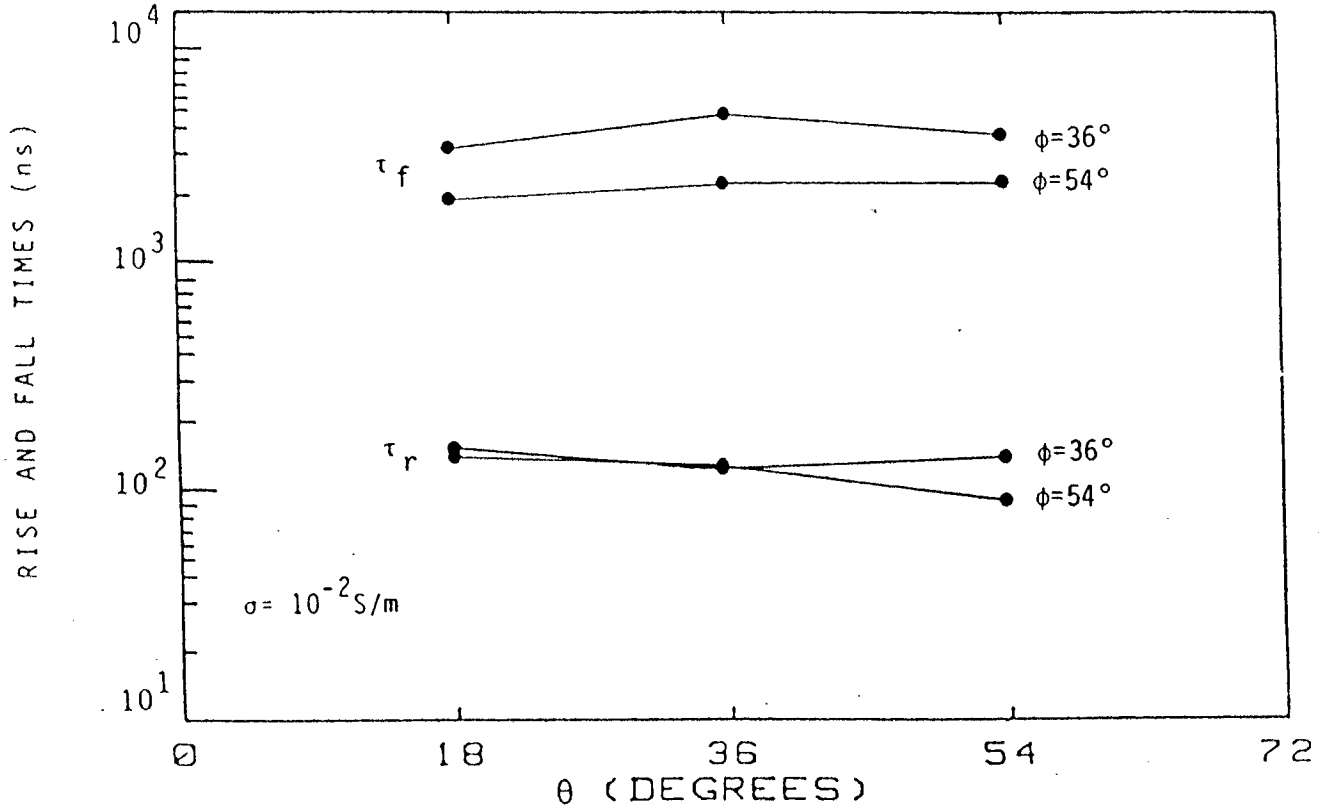

Fig. 3.20. Rise time and fall time of HEMP-induced "Potential Difference" between the phase conductor and the horizontal cross arm as function of elevation angle θ for ground conductivity $\sigma = 10^{-2}$ S/m and for two different values of azimuthal angle ϕ.

4. HEMP-INDUCED STRESSES ON TRANSFORMER BUSHINGS

4.1 AN OVERVIEW

As was mentioned in Sect. 3, when a transmission or distribution line system is exposed to HEMP, fast and large transients are induced in the system, and consequently the susceptibility of dielectric insulators in the system is of concern. One type of such dielectric insulators is transformer bushing. A typical form of transformer bushings is shown in Fig. 4.1. In this section the HEMP-induced stresses across transformer bushings are calculated.

4.2 GEOMETRY OF THE PROBLEM

Figure 4.2 illustrates the simplified geometry of the problem. The induced potential difference across the transformer bushing is the quantity of interest. To find this potential difference, one can make use of the Thévenin equivalent circuit which is characterized by the open-circuit voltage across A-B (in the absence of the bushing) and also the input impedance between A, B. To evaluate the open-circuit voltage, one can just assume that the horizontal, semi-infinite line is connected to the vertical element of the line and the vertical element is extended to the ground, but not connected to the ground. As was explained in Vance's book,[9] the vertical line can be taken to be a conical transmission line with its upper end connected to the horizontal transmission line. Consequently, the input impedance of the combination is still the characteristic impedance of the horizontal transmission line which is

$$Z_0 = \frac{1}{2\pi}\sqrt{\frac{\mu_0}{\varepsilon_0}}\,\ell n\,(2h/a) \qquad (4.1)$$

To obtain the open-circuit voltage between the lower end of the vertical element and the ground, the interaction of HEMP with the horizontal semi-infinite transmission line and the vertical element is needed. Following

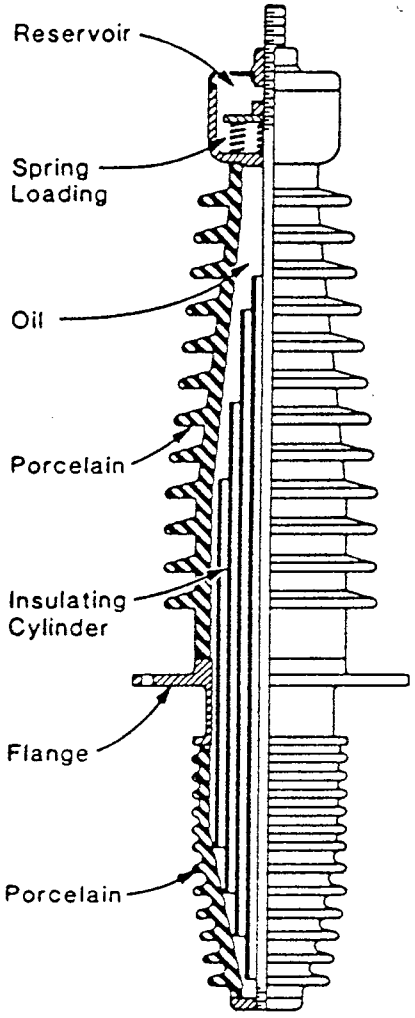

High voltage class oil impregnated capacitor bushing

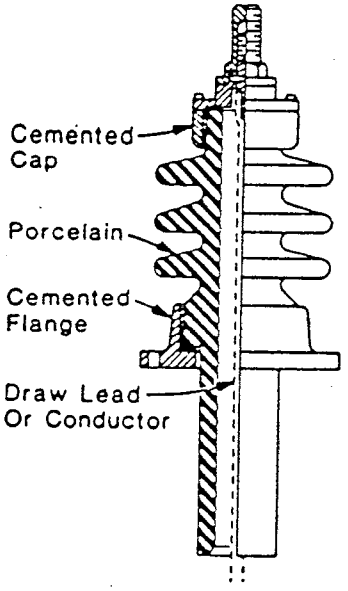

Distribution class procelain bushing

Fig. 4.1. Two types of transformer bushings.

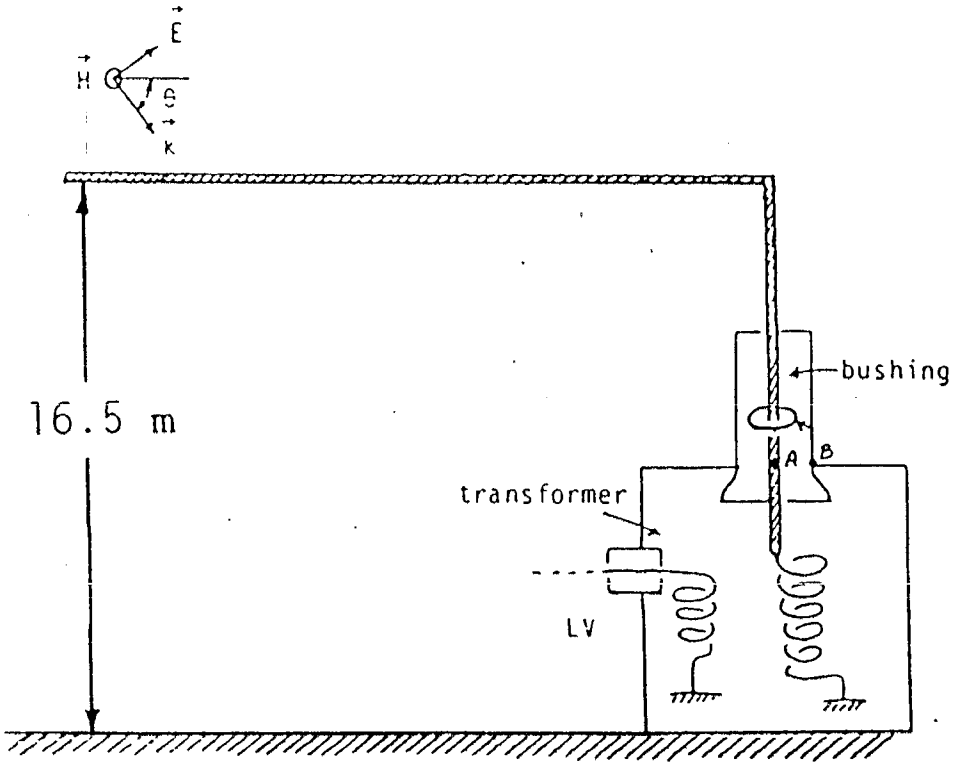

Fig. 4.2. Simplified geometry of the problem of calculating HEMP-induced stresses across transformer bushings.

the formulas in Vance's book, the open-circuit voltage due to the HEMP interaction with the horizontal transmission line and the vertical element can be calculated for two different values of ground conductivity. The incident wave is again taken to be a double exponential function given by Eq. 2.27. The electric field vector is in the plane of the horizontal and vertical transmission lines. The results are presented in Figs. 4.3 through 4.6. Figure 4.7 shows the rise time, the fall time and the maximum values of the open-circuit voltage versus elevation angle θ for two different values of ground conductivity. As can be seen, the early-time decrease in the open-circuit voltage is due to the interaction of HEMP with the vertical element. The interaction of HEMP with the horizontal line dominates and is the major contribution to the induced open-circuit voltage.

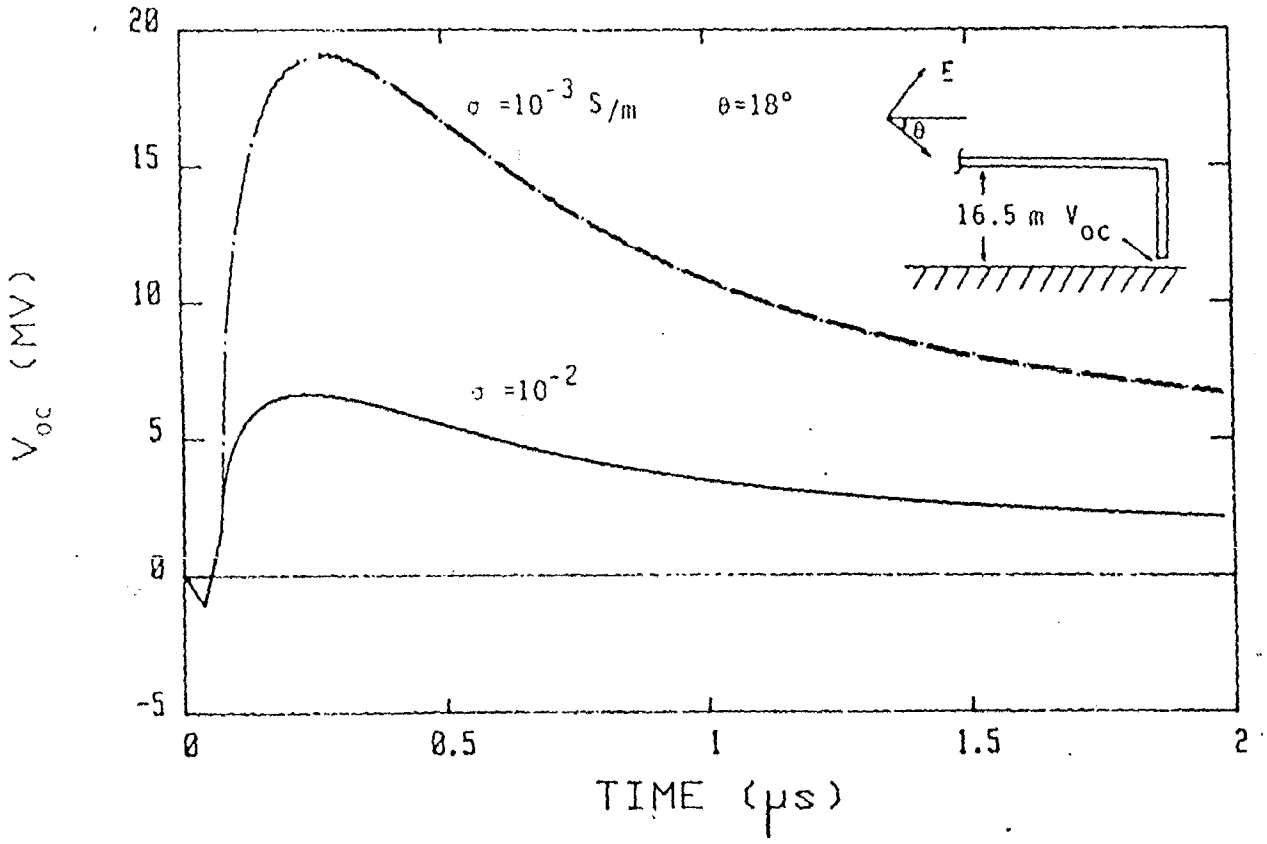

Fig. 4.3. Calculated HEMP-induced open-circuit voltage at the transformer bushing for incident angle θ = 18° and for two different values of ground conductivity σ.

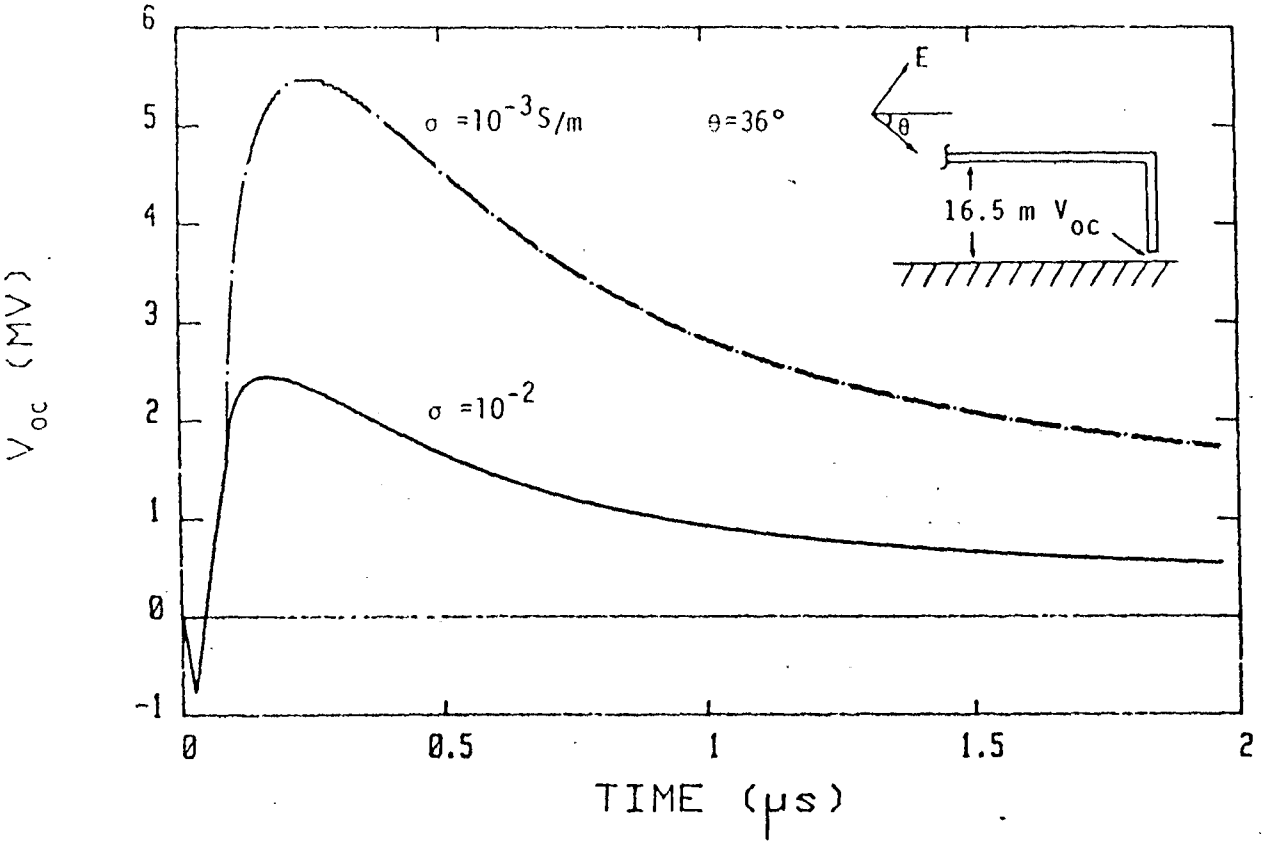

Fig. 4.4. Calculated HEMP-induced open-circuit voltage at the transformer bushing for incident angle θ = 36° and for two different values of ground conductivity σ.

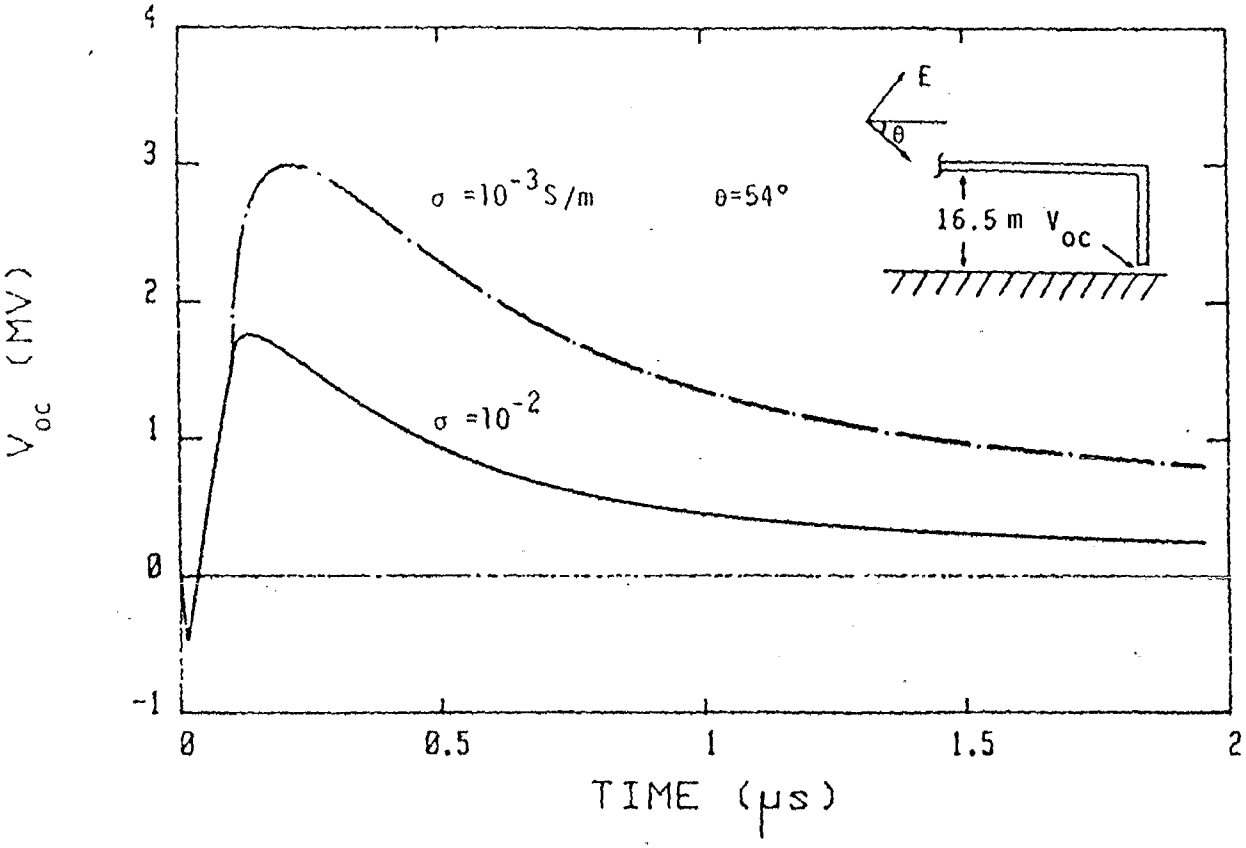

Fig. 4.5. Calculated HEMP-induced open-circuit voltage at the transformer bushing for incident angle θ = 54° and for two different values of ground conductivity σ.

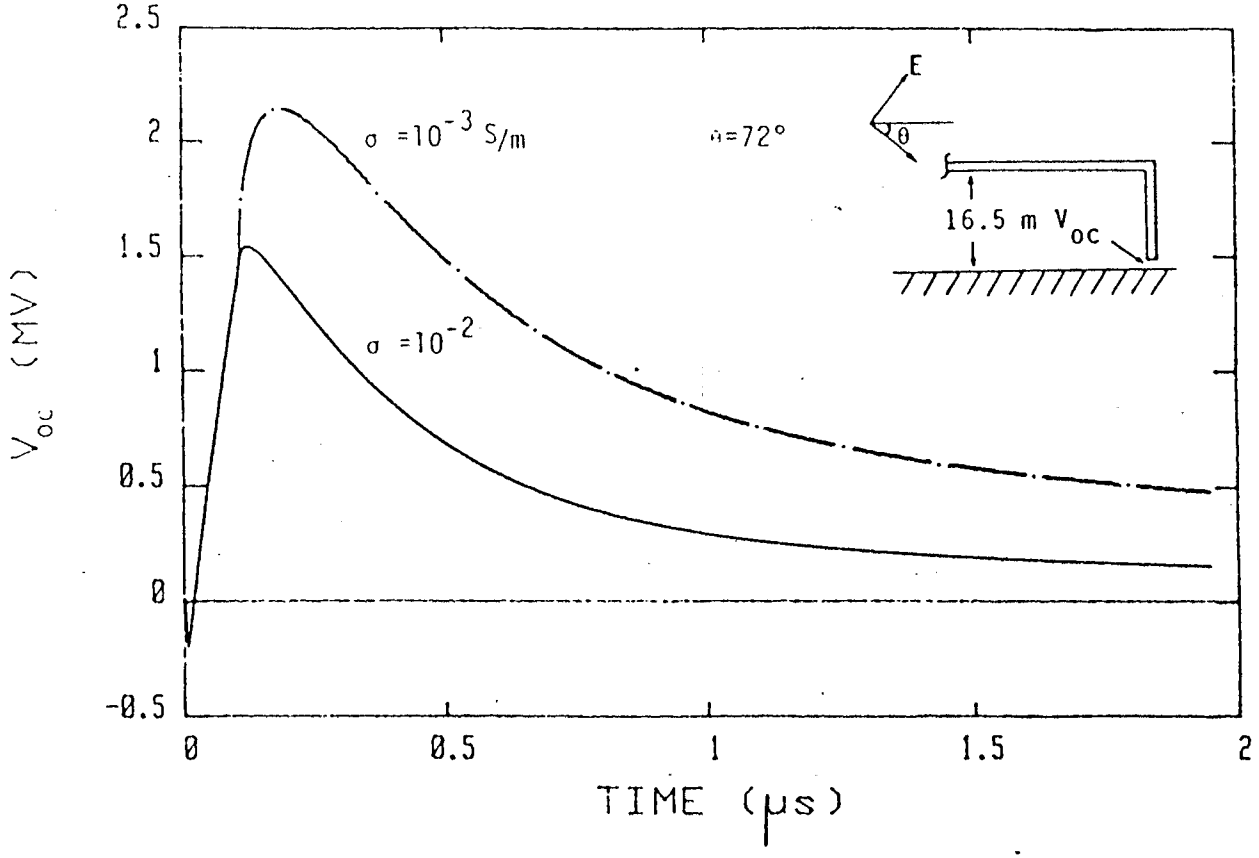

Fig. 4.6. Calculated HEMP-induced open-circuit voltage at the transformer bushing for incident angle θ = 72° and for two different values of ground conductivity σ.

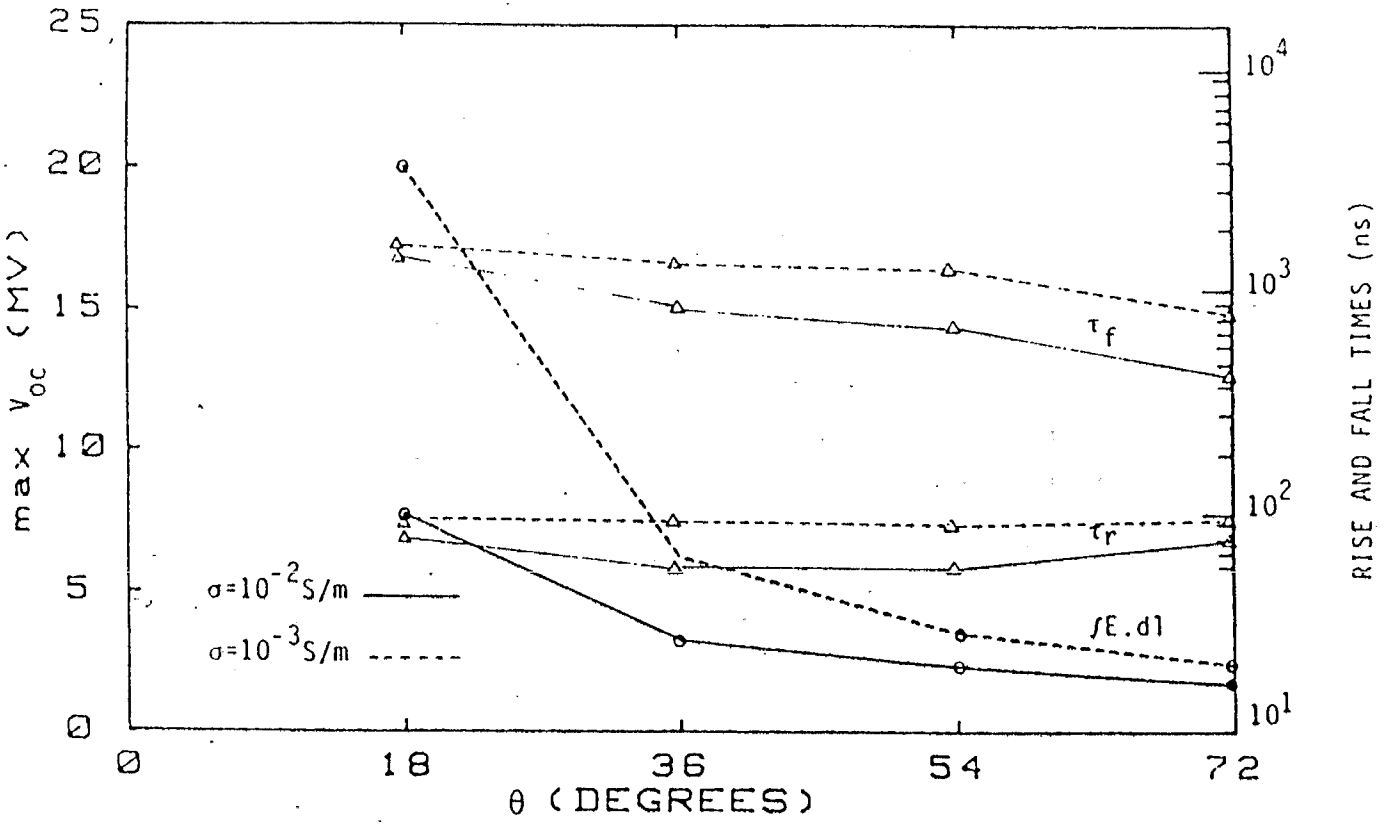

Fig. 4.7. Rise time, fall time, and maximum value of HEMP-induced open-circuit voltage at the transformer bushing as function of elevation angle θ for two different values of ground conductivity σ.

5. SUMMARY

This report comprises a study of corona effects on induced transients in transmission and distribution lines and also a study of HEMP-induced stresses on dielectric insulators such as line supports and transformer bushings.

Section 1 is an introduction to the problem.

Section 2 deals with the corona problem in which two different corona models and three different excitation mechanisms are analyzed. The two different corona models are Townsend's model and the conductivity model. The three different excitations are a HEMP plane wave, a localized voltage source, and a current source injected on a point of the wire. In all cases, the excitation is taken to be a double exponential time function. The charge and current induced in a very long, straight wire excited by the above sources have been calculated by the method of characteristics. The results show that the corona has the effect of reducing the maximum value of the induced current as much as 30% of the value without corona and also the effect of decreasing its rate of rise by a factor of 40%. The results obtained are compared with some available experimental data, and in some cases, a good agreement is observed. The analytical results are also compared with those of Baum's model, and again a good agreement is found.

Section 3 treats the HEMP-induced stresses across dielectric line supports and the air gaps between phase conductors and line poles. A typical 230-kV, H-frame transmission line is taken for consideration. The "potential difference", which is defined to be the line integral of the induced electric field across the air gap or the line support, has been calculated. Generally, the results illustrate that the major contribution to the potential difference across the line support and the gap comes from the HEMP interaction with the phase conductors, and the coupling of HEMP with the vertical pole and with the horizontal cross arm is of less importance. The potential difference can be as high as 7 MV across the air gap and across the line support. The rise time of the potential

difference is about 100 ns, and the fall time is about 2-3 μs. The results also reveal that the higher value of the ground conductivity is, the less the HEMP-induced stresses become.

Section 4 is concerned with the HEMP-induced stresses across transformer bushings. The parameters of a Thévenin equivalent circuit, which represents the induced stress, are calculated. The open-circuit voltage can be as large as few tens of MVs. The rise time is in the order of 100 ns and the fall time 800 ns. The results also illustrate that the HEMP coupling with the horizontal part of the line has a dominant effect on the open-circuit voltage. The higher value of ground conductivity results in lower value for the open circuit voltage. The impedance of the equivalent circuit is the characteristic impedance of the horizontal part of the line. The results obtained in this section can be utilized in the design of pulsers for testing the susceptibility of transformer bushings.

REFERENCES

1. K.S.H. Lee, F.C. Yang, and N. Engheta, "Interaction of High-Altitude Electromagentic Pulse with Transmission and Distribution Lines: An Early-Time Consideration," Interaction Notes, Note 435, Air Force Weapons Laboratory, Albuqueurque, NM November 1983.

2. C.F. Wagner and B.L. Lloyed, "Effects of Corona on Traveling Waves," Transactions of the American Institute of Elect. Engineers, Power Apparatus and Systems, Vol. 74, October 1955, pp. 858-872.

3. N.L. Ovick and G.L. Kusic, "Including Corona Effects forTravelling Waves on Transmission Lines," IEEE Transactions of Power Engineering Society, 1984.

4. C. Baum, "Effect of Corona on the Response of Infinite-length Transmission Lines to Incident Plane Waves," Interaction Notes, Note 443, Air Force Weapons Laboratory, Albuquerque, NM, November 1983.

5. G.B. Whitham, Linear and Nonlinear Waves, Wiley-Interscience Publications New York, 1974.

6. K.S.H. Lee and L. Marin, "SGEMP for Resonant Structures," Theoretical Notes, Note 199, Air Force Weapons Laboratory, Albuquerque, NM, September1974.

7. J. Lam, "Theoretical Study of the Electrical Corona on a Long wire," Interaction Note, Note 305, Air Force Weapons Laboratory, Albuquerque, NM, June 1976.

8. J.S. Townsend, "Die Ionisation der Gase," Handbuch der Radiologie Band I, Akademischer Verlag, Leipzig, 1920. See also J. D. cobine, Gaseous Conductors,Dover Publications, New York, 1958.

9. E.F. Vance, Coupling to Shielded Cables, Wiley-Intersciences Publications, New York, 1978.

APPENDIX

In this appendix, additional curves are presented in the following order:

- Figures A1 through A14 for the induced currents in the wire using Townsend's and the conductivity models for different values of α_j and σ and different elevation angles
- Figures A15 through A20 for the induced currents in the wire in the presence of the perfectly conducting ground using Townsend's and the conductivity models
- Figures A21 through A25 for the localized voltage source-induced current in the wire using Townsend's and the conductivity models
- Figures A26 and A27 for the lightning strike-induced current in the wire using Townsend's and the conductivity models
- Figures A28 through A30 for comparison of the analytical results with the results of Baum's model
- Figures A31 through A34 for comparison of transmission line theory with the scattering theory
- Figures A35 through A40 for the calculated "potential difference" across the line support for different elevation angles, different azimuthal angles, and different values of ground conductivity

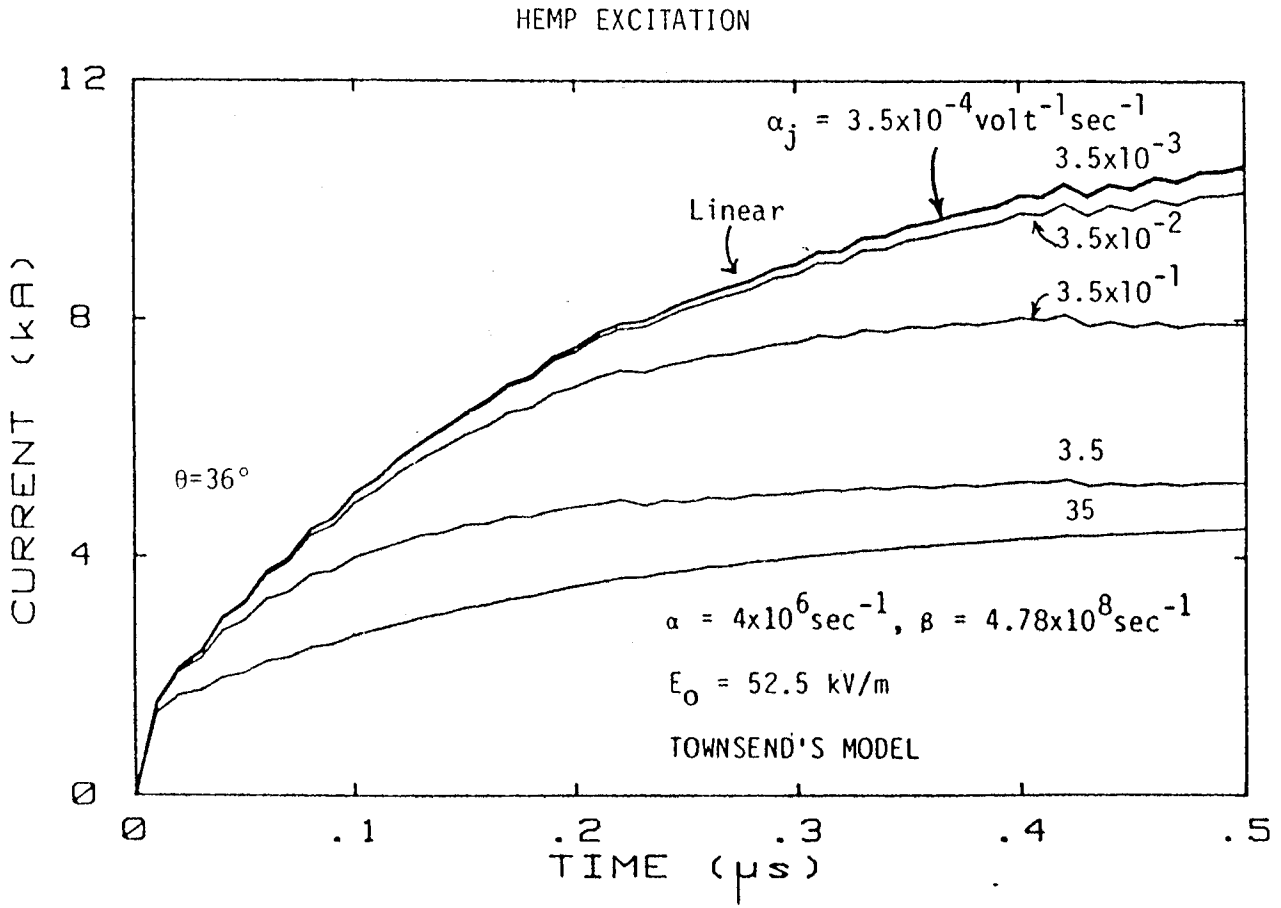

Fig. A1. HEMP-induced current in the wire for elevation angle θ = 36° and different values of α_j in Townsend's model for radius a = 1.407 cm and $E_c = 1.5 \times 10^6$ volt m^{-1}.

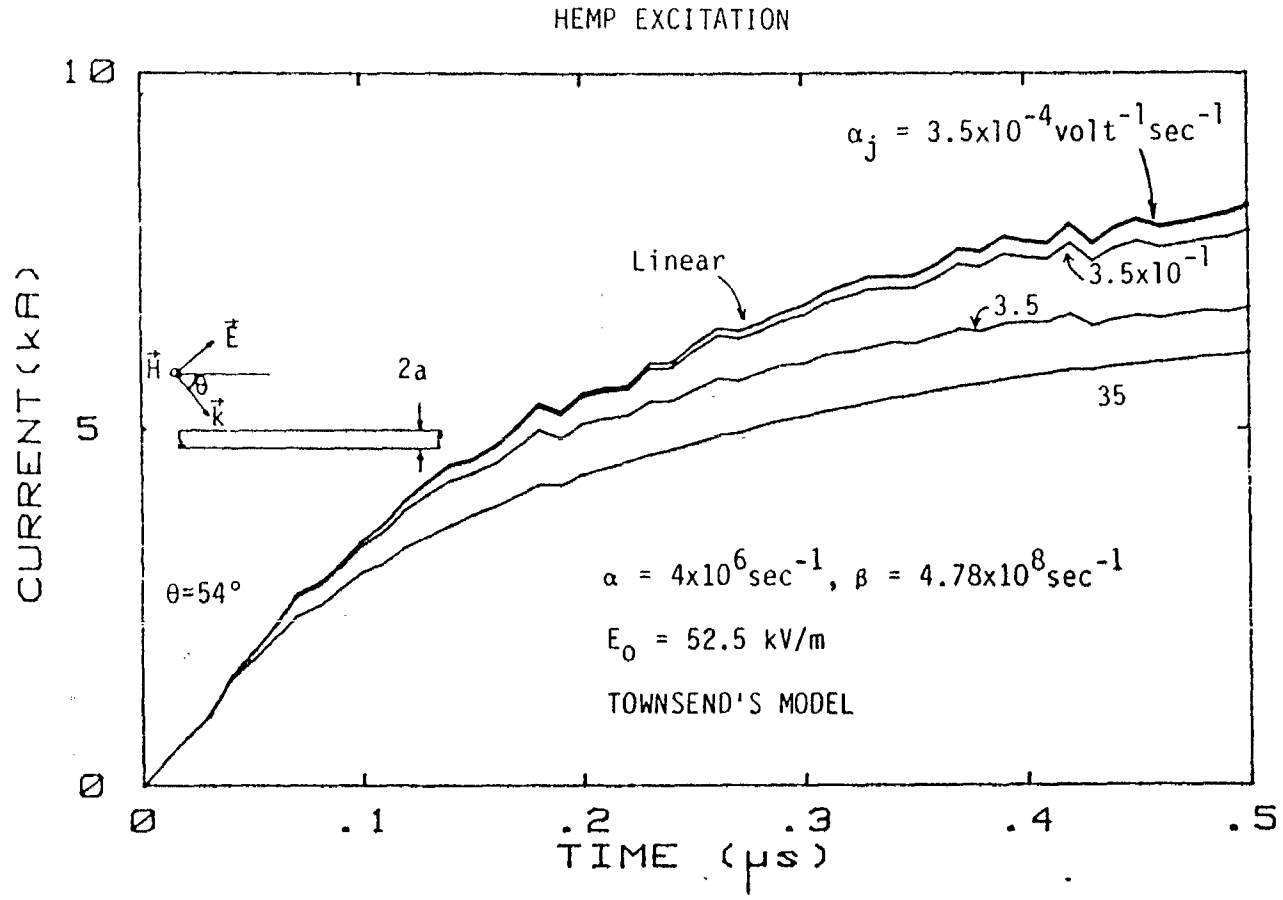

Fig. A2. HEMP-induced current in the wire for elevation angle θ = 54°and different values of α_j in Townsend's model for radius a = 1.407 cm and $E_c = 1.5 \times 10^{6}$volt m^{-1}.

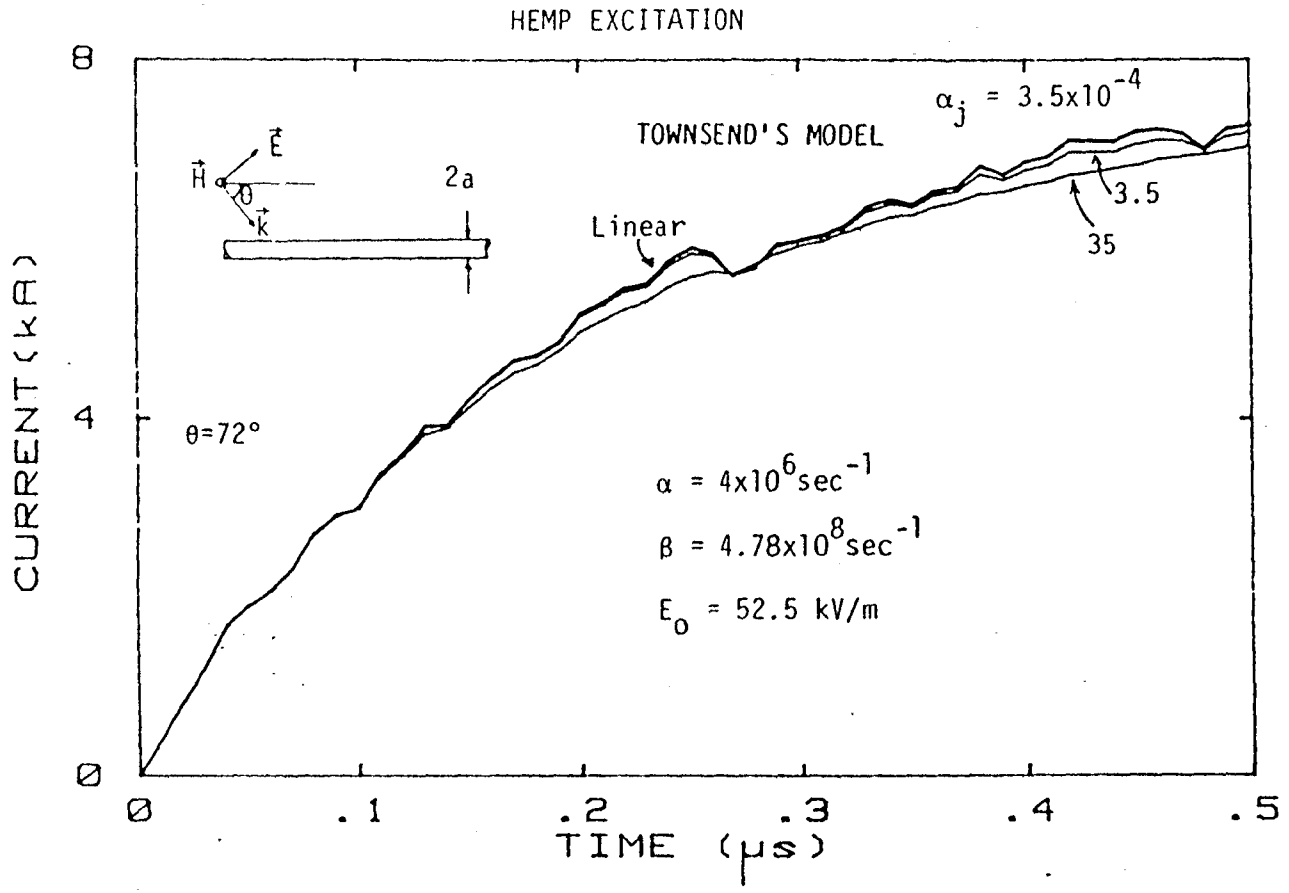

Fig. A3. HEMP-induced current in the wire for elevation angle $\theta = 72°$ and different values of α_j in Townsend's model for radius a = 1.407 cm and $E_c = 1.5 \times 10^{6}$ volt m^{-1}.

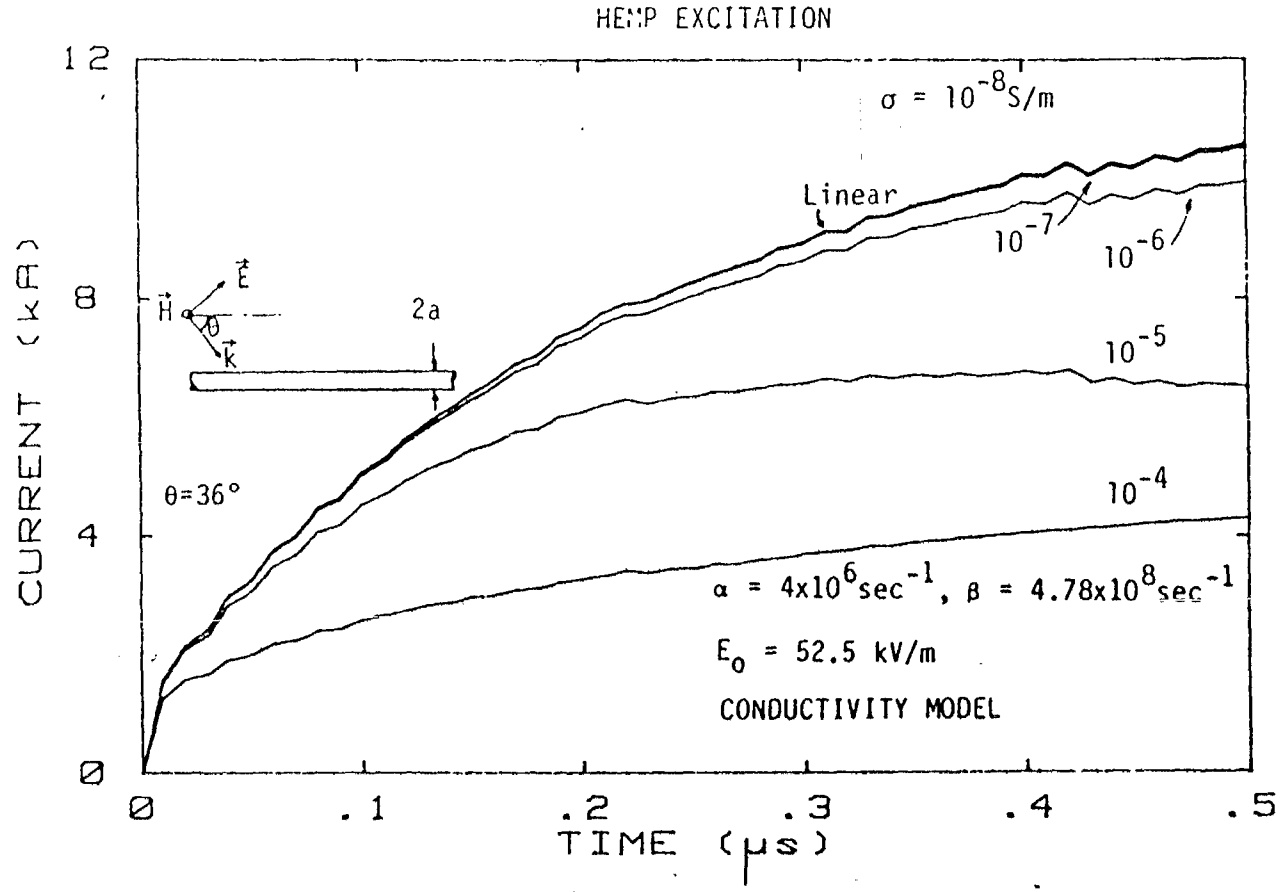

Fig. A4. HEMP-induced current in the wire for elevation angle $\theta = 36°$ and different values of σ in conductivity model for radius a = 1.407 cm and $E_c = 1.5 \times 10^6$ volt m^{-1}.

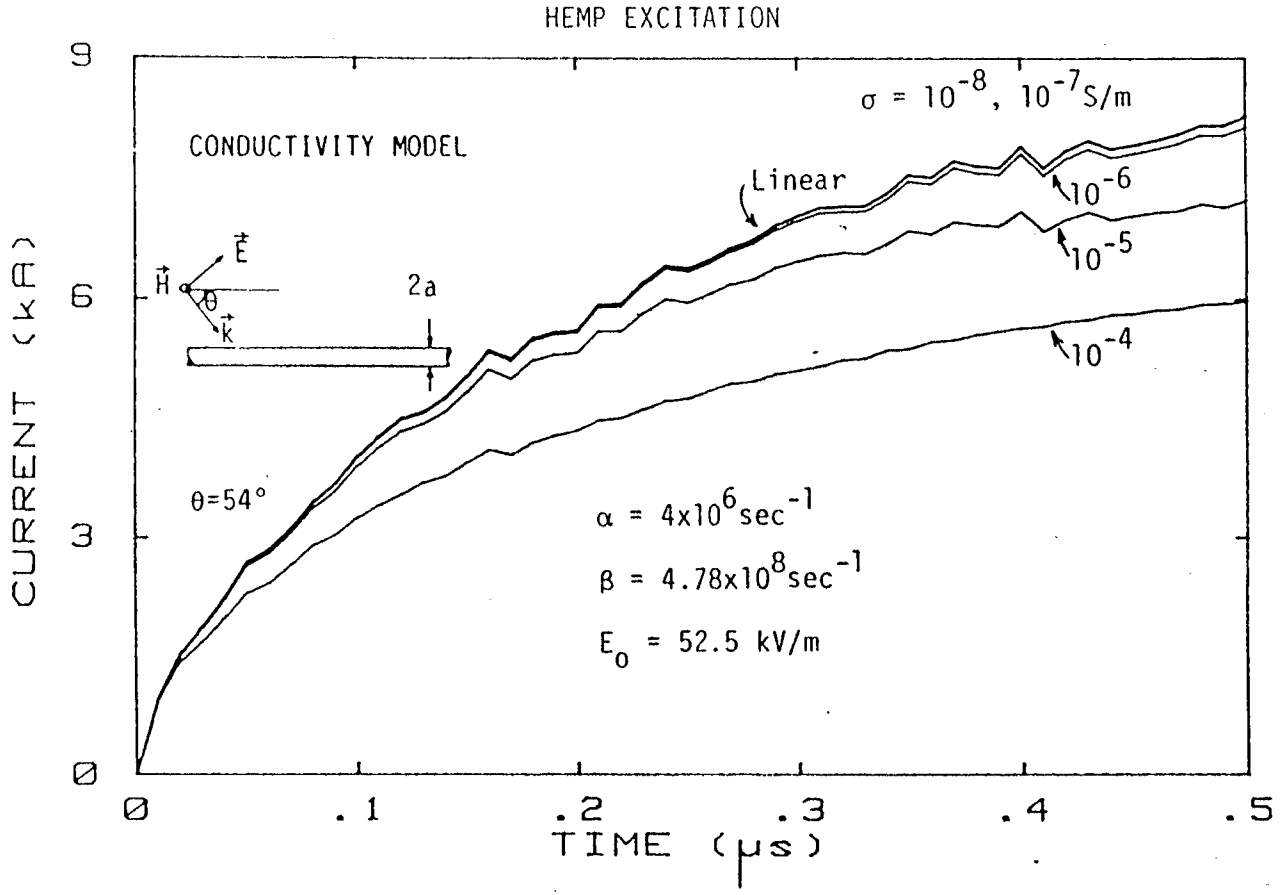

Fig. A5. HEMP-induced current in the wire for elevation angle $\theta = 54°$ and different values of σ in conductivity model for radius a = 1.407 cm and $E_c = 1.5 \times 10^6$ volt m^{-1}.

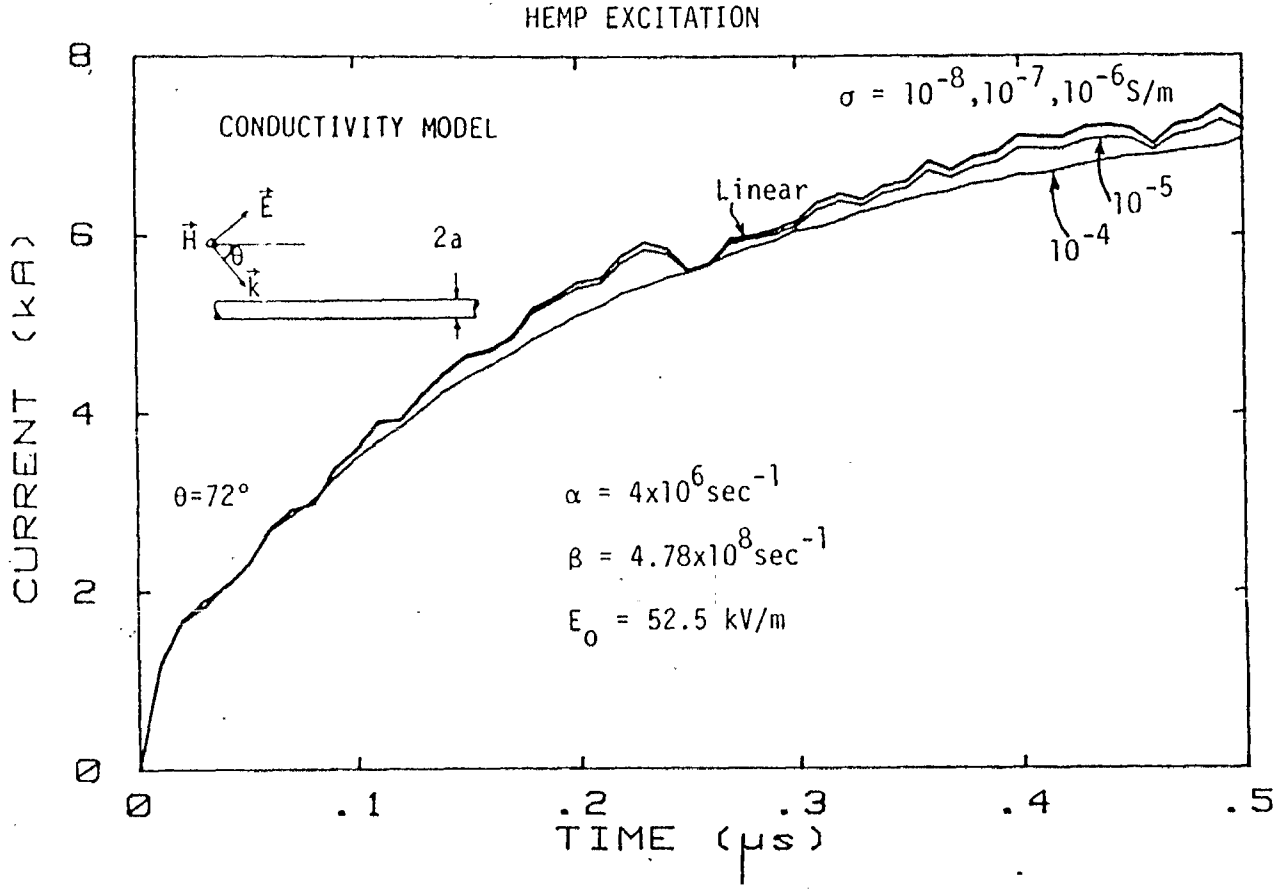

Fig. A6. HEMP-induced current in the wire for elevation angle $\theta = 72°$ and different values of σ in conductivity model for radius a = 1.407 cm and $E_c = 1.5 \times 10^6$ volt m^{-1}.

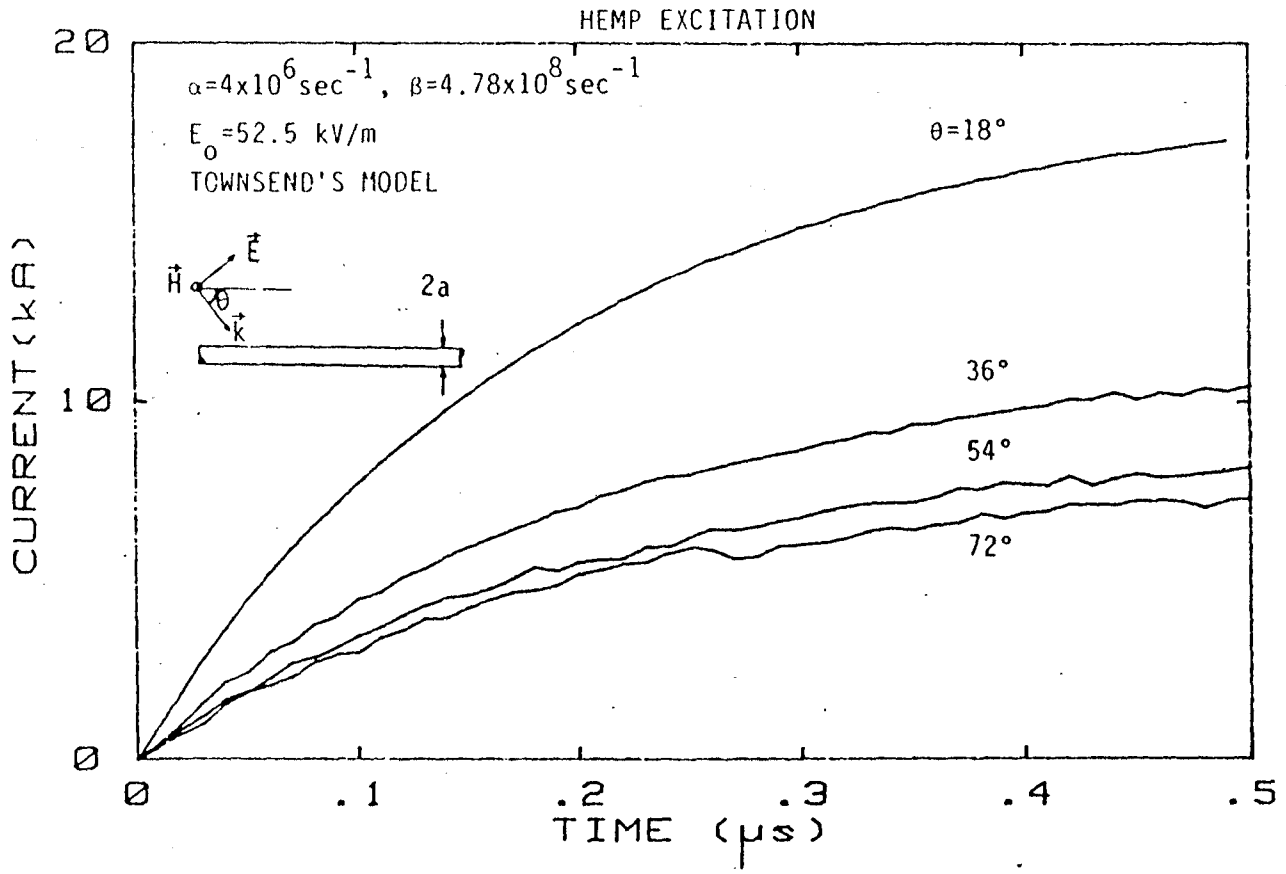

Fig. A7. HEMP-induced current in the wire for $\alpha_j = 3.5 \times 10^{-4}$ volt^{-1}sec^{-1} and different elevation angles in Townsend's model for radius a = 1.407 cm and $E_c = 1.5 \times 10^6$ volt m^{-1}.

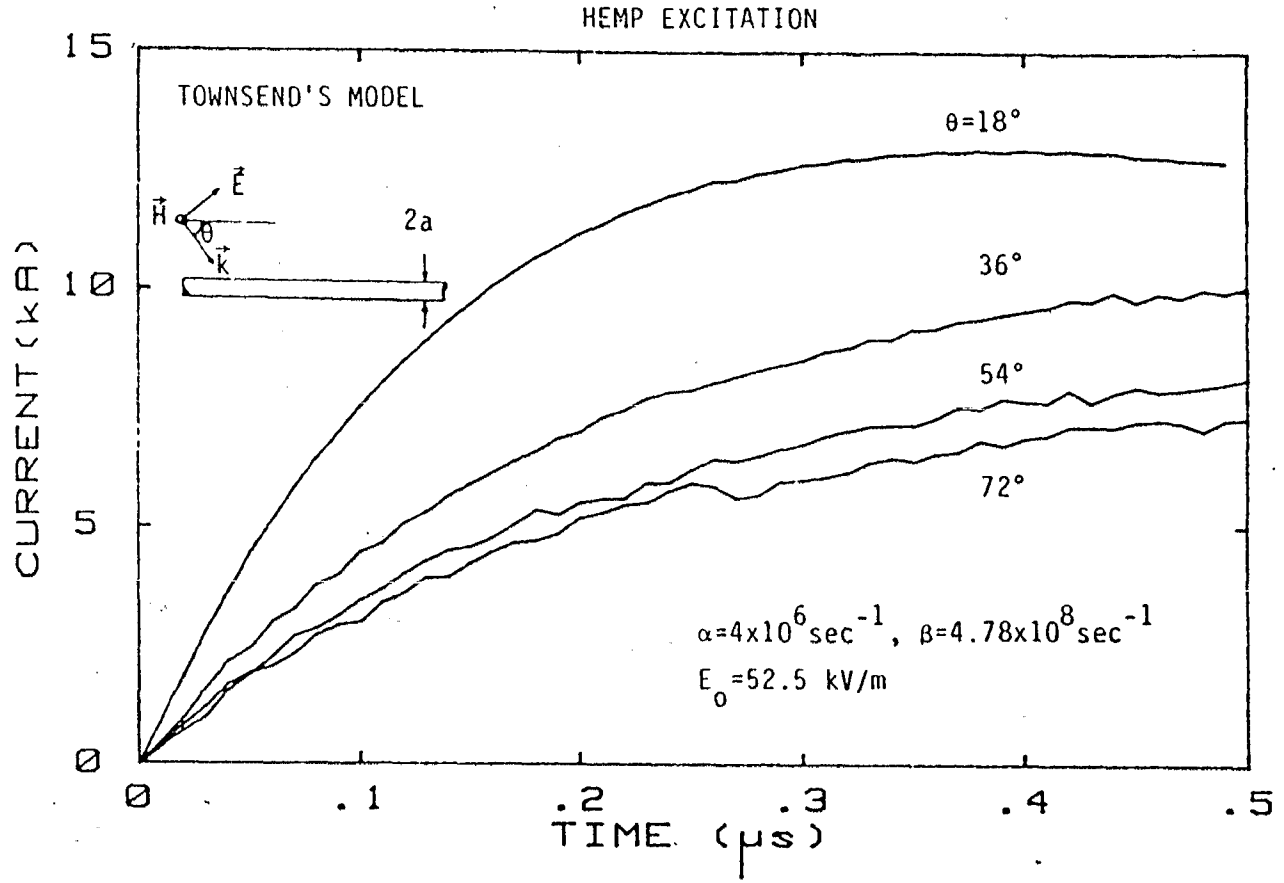

Fig. A8. HEMP-induced current in the wire for $\alpha_j = 3.5 \times 10^{-3}$ volt^{-1}sec^{-1} and different elevation angles in Townsend's model for radius a = 1.407 cm and $E_c = 1.5 \times 10^6$ volt m^{-1}.

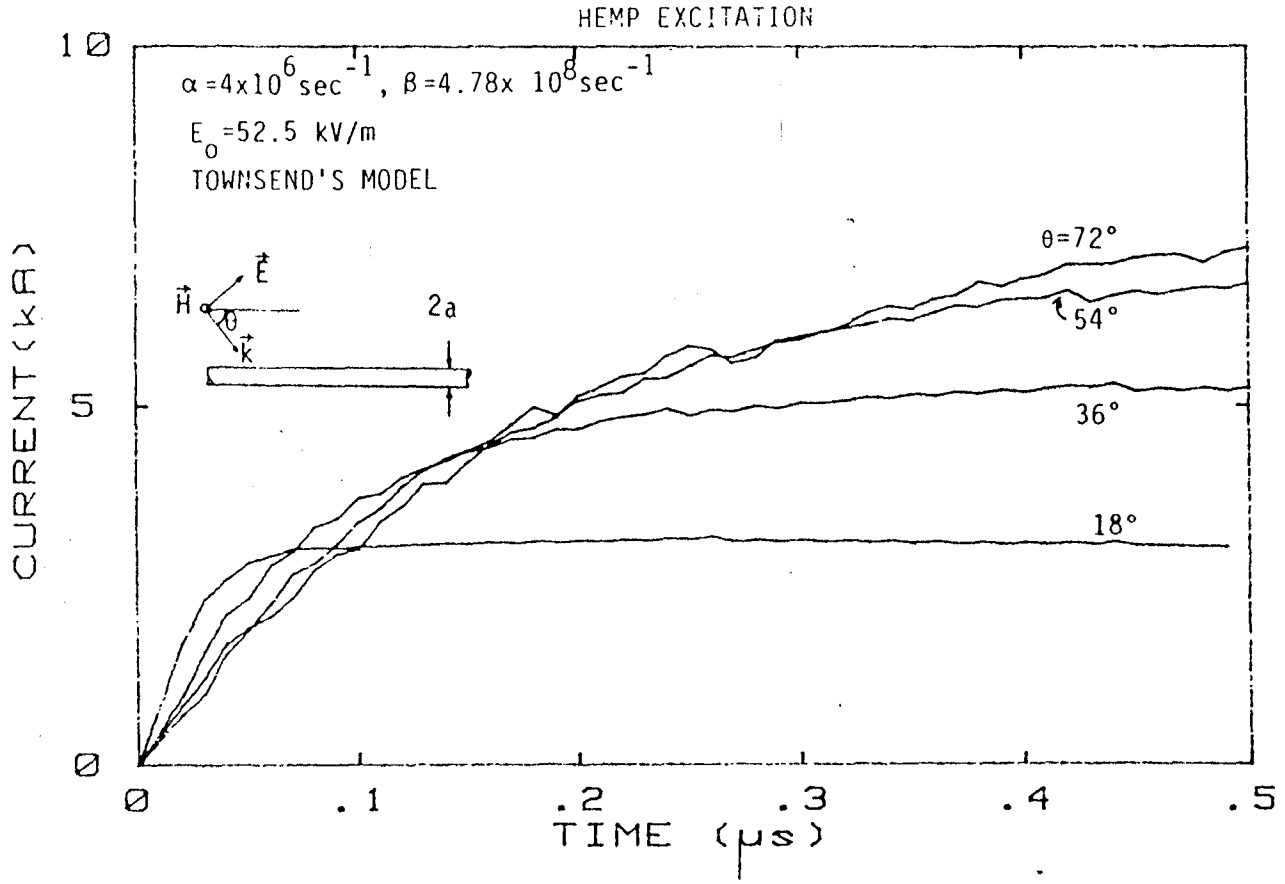

Fig. A9. HEMP-induced current in the wire for $\alpha_j = 3.5 \times 10^{-1}$ volt^{-1}sec^{-1} and different elevation angles in Townsend's model for radius a = 1.407 cm and $E_c = 1.5 \times 10^6$ volt m^{-1}.

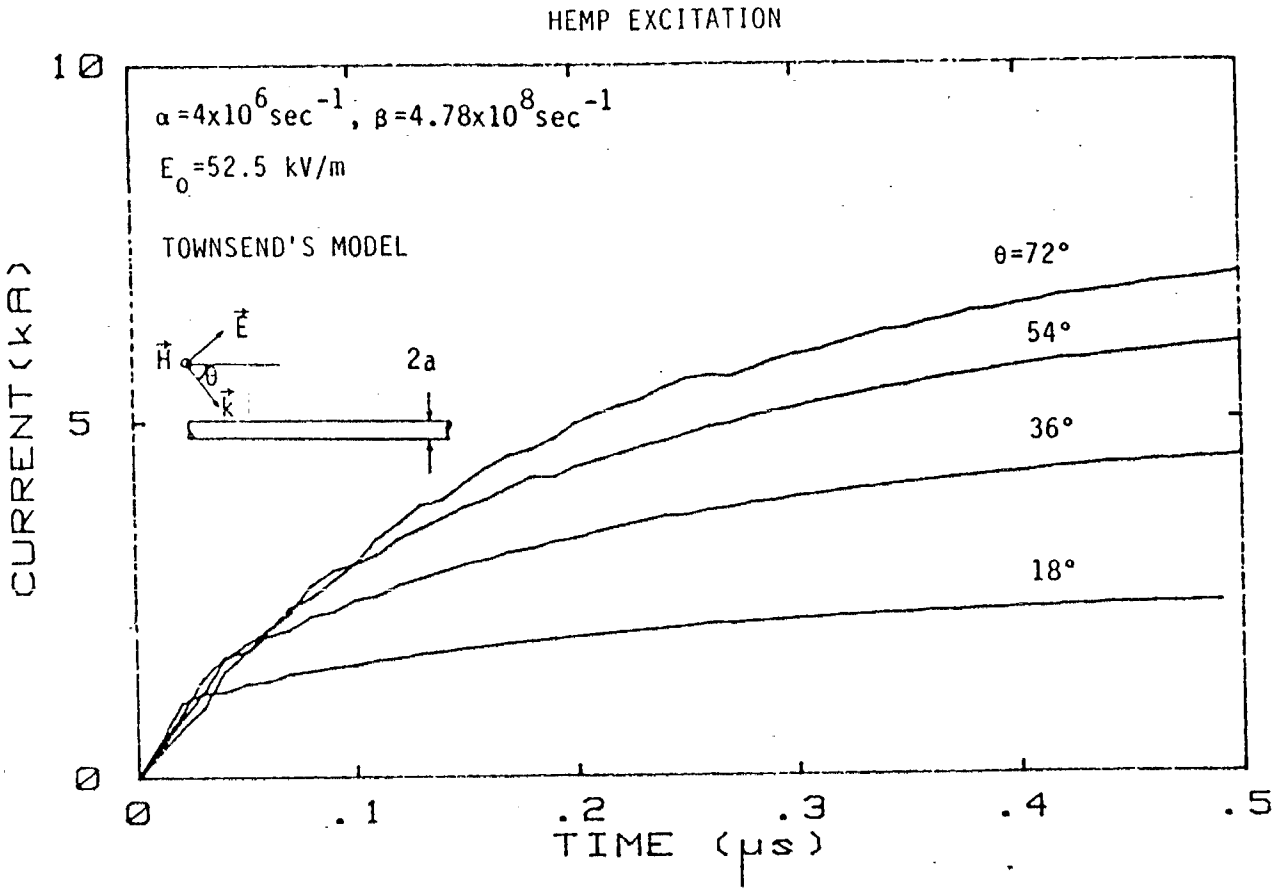

Fig. A10. HEMP-induced current in the wire for $\alpha_j = 3.5$ volt^{-1}sec^{-1} and different elevation angles in Townsend's model for radius a = 1.407 cm and $E_c = 1.5 \times 10^6$ volt m^{-1}.

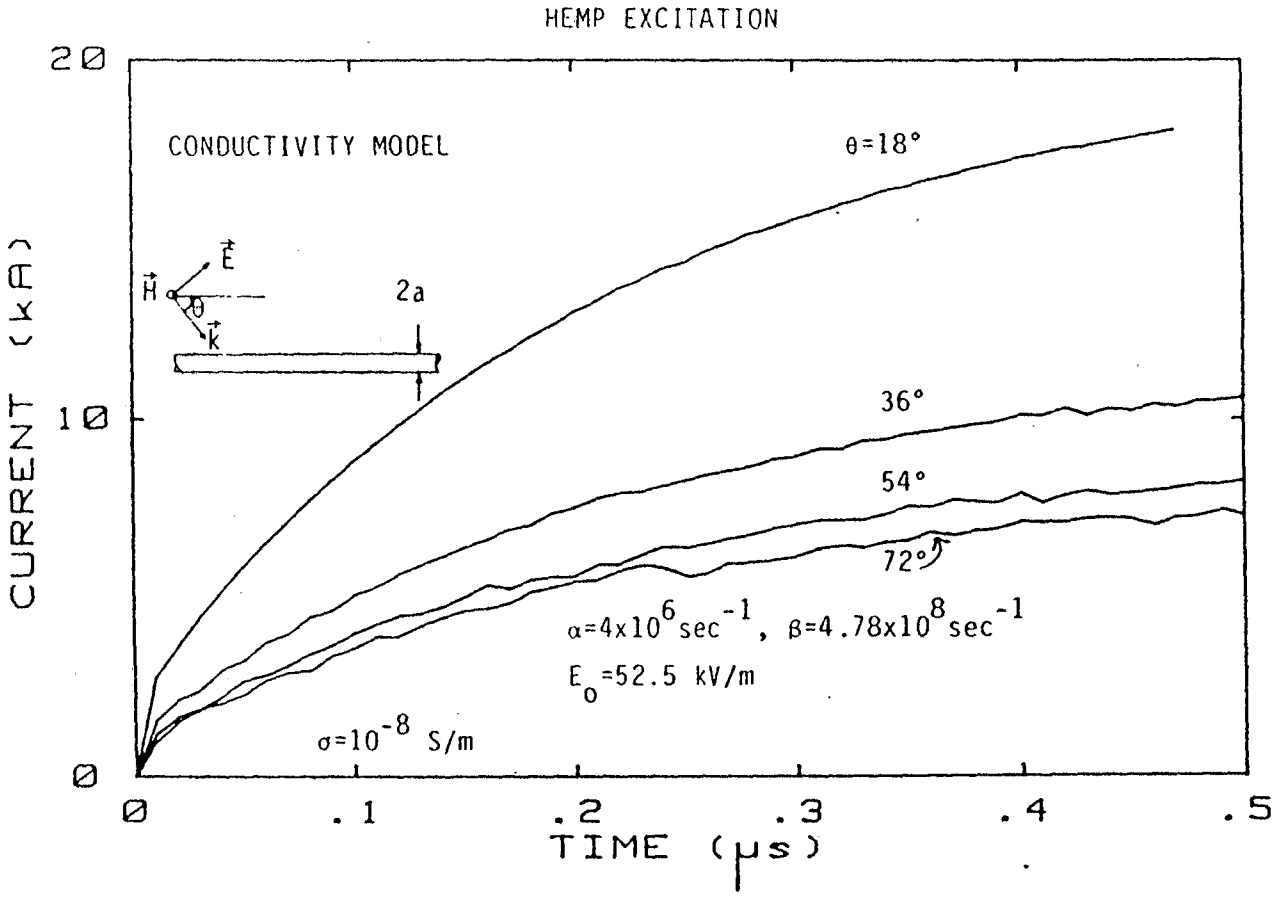

Fig. A11. HEMP-induced current in the wire for $\sigma = 10^{-8}$ S/m and for different elevation angles in conductivity model for radius a = 1.407 cm and $E_c = 1.5 \times 10^6$ volt m^{-1}.

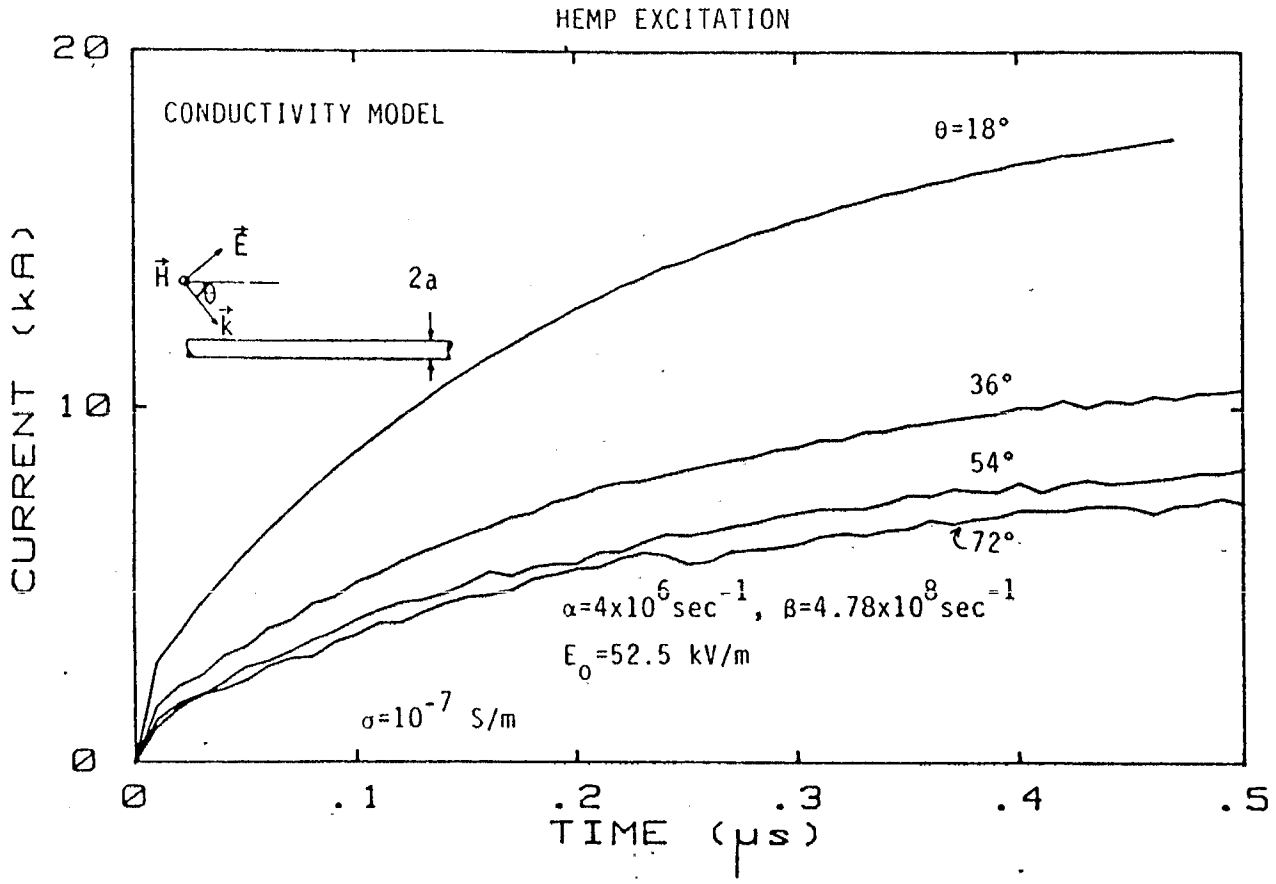

Fig. A12. HEMP-induced current in the wire for $\sigma = 10^{-7}$ S/m and for different elevation angles in conductivity model for radius a = 1.407 cm and $E_c = 1.5 \times 10^6$ volt m^{-1}.

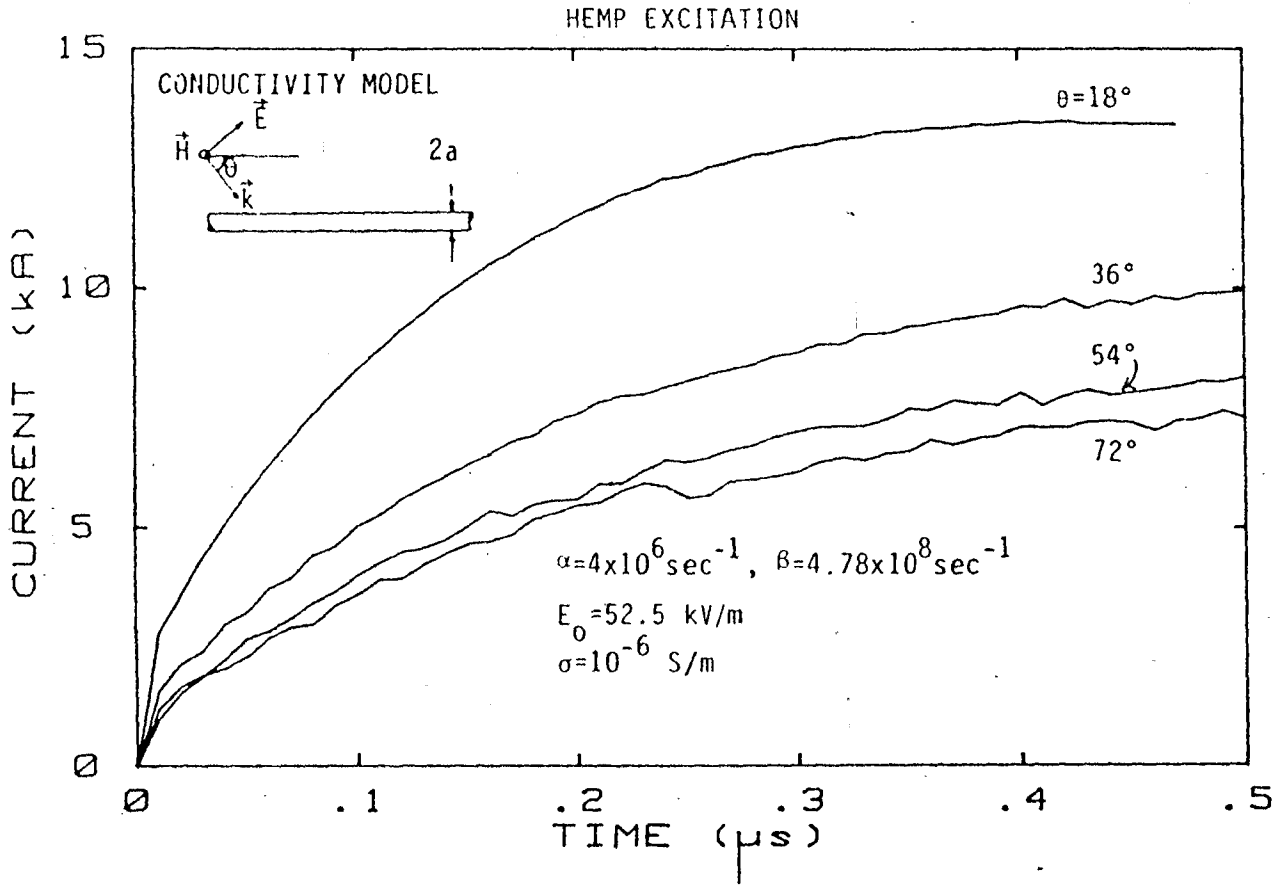

Fig. A13. HEMP-induced current in the wire for $\sigma = 10^{-6}$ S/m and for different elevation angles in conductivity model for radius a = 1.407 cm and $E_c = 1.5 \times 10^{6}$ volt m^{-1}.

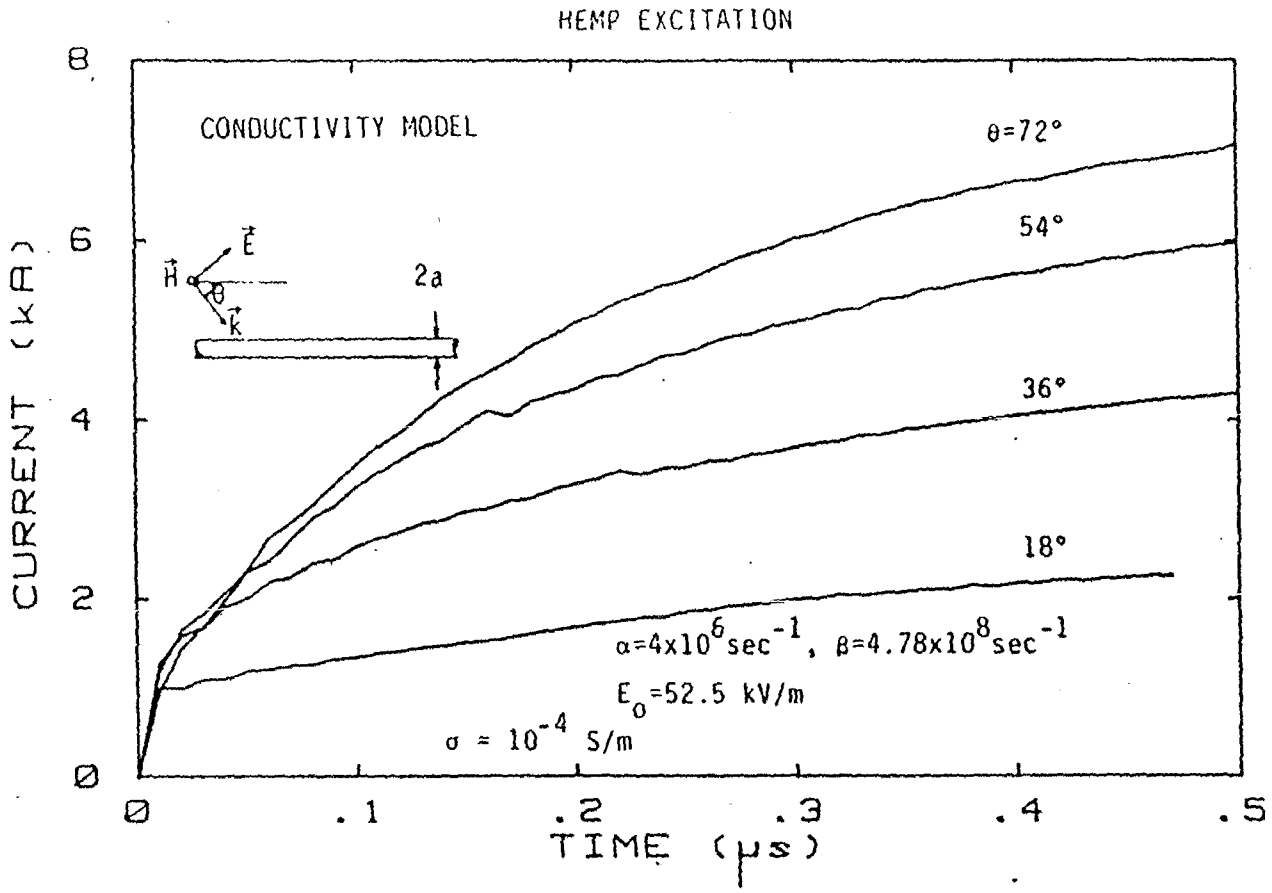

Fig. A14. HEMP-induced current in the wire for $\sigma = 10^{-4}$ S/m and for different elevation angles in conductivity model for radius a = 1.407 cm and $E_c = 1.5 \times 10^6$ volt m^{-1}.

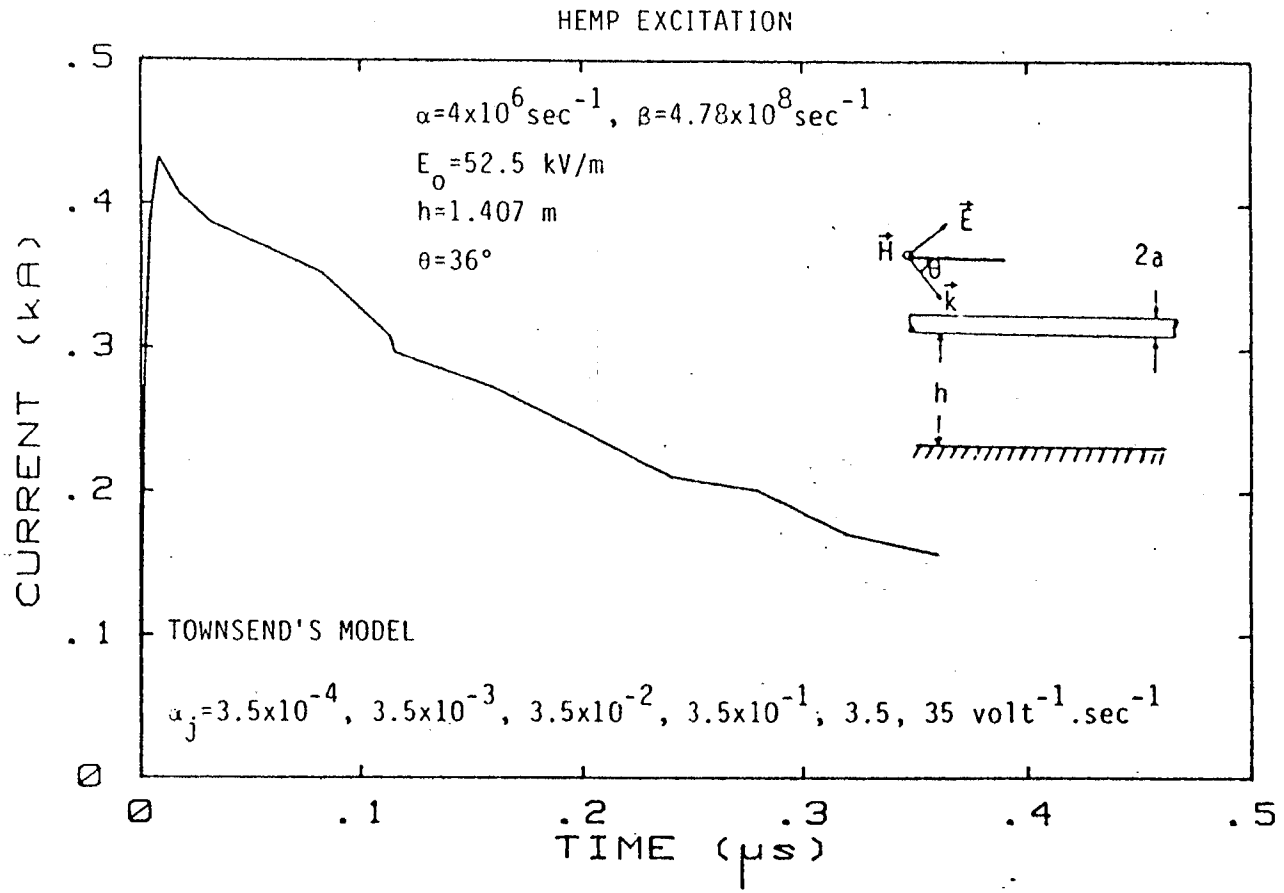

Fig. A15. HEMP-induced current in the wire for elevation angle $\theta = 36°$ and different values of α_j in the Townsend's model for radius a = 1.407 cm and $E_c = 1.5 \times 10^6$ volt m^{-1}.

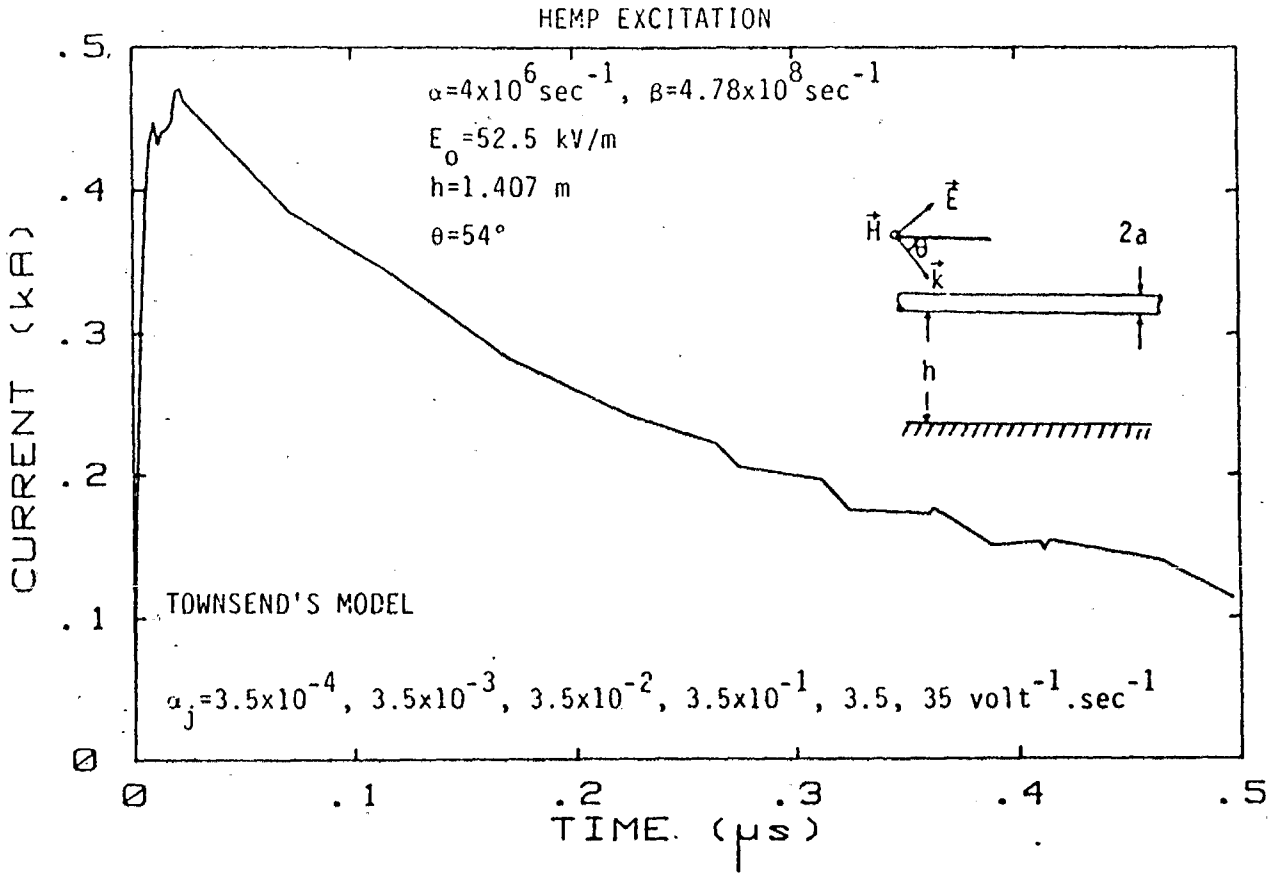

Fig. A16. HEMP-induced current in the wire for elevation angle $\theta = 54°$ and different values of α_j in Townsend's model for radius a = 1.407 cm and $E_c = 1.5 \times 10^6$ volt m^{-1}.

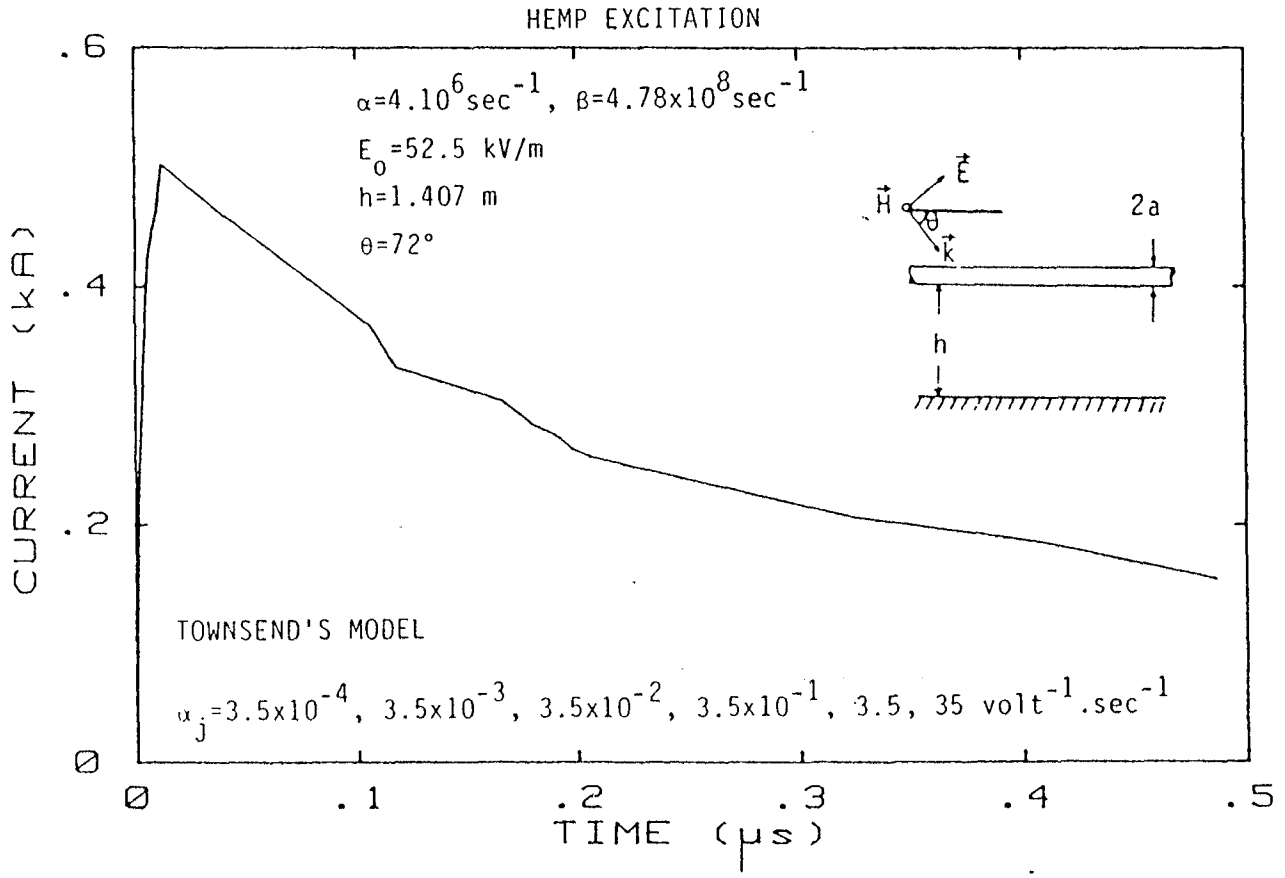

Fig. A17. HEMP-induced current in the wire in the presence of a perfectly conducting ground for elevation angle $\theta = 72°$ and different values of α_j in Townsend's model for radius a = 1.407 cm and $E_c = 1.5 \times 10^6$ volt m^{-1}.

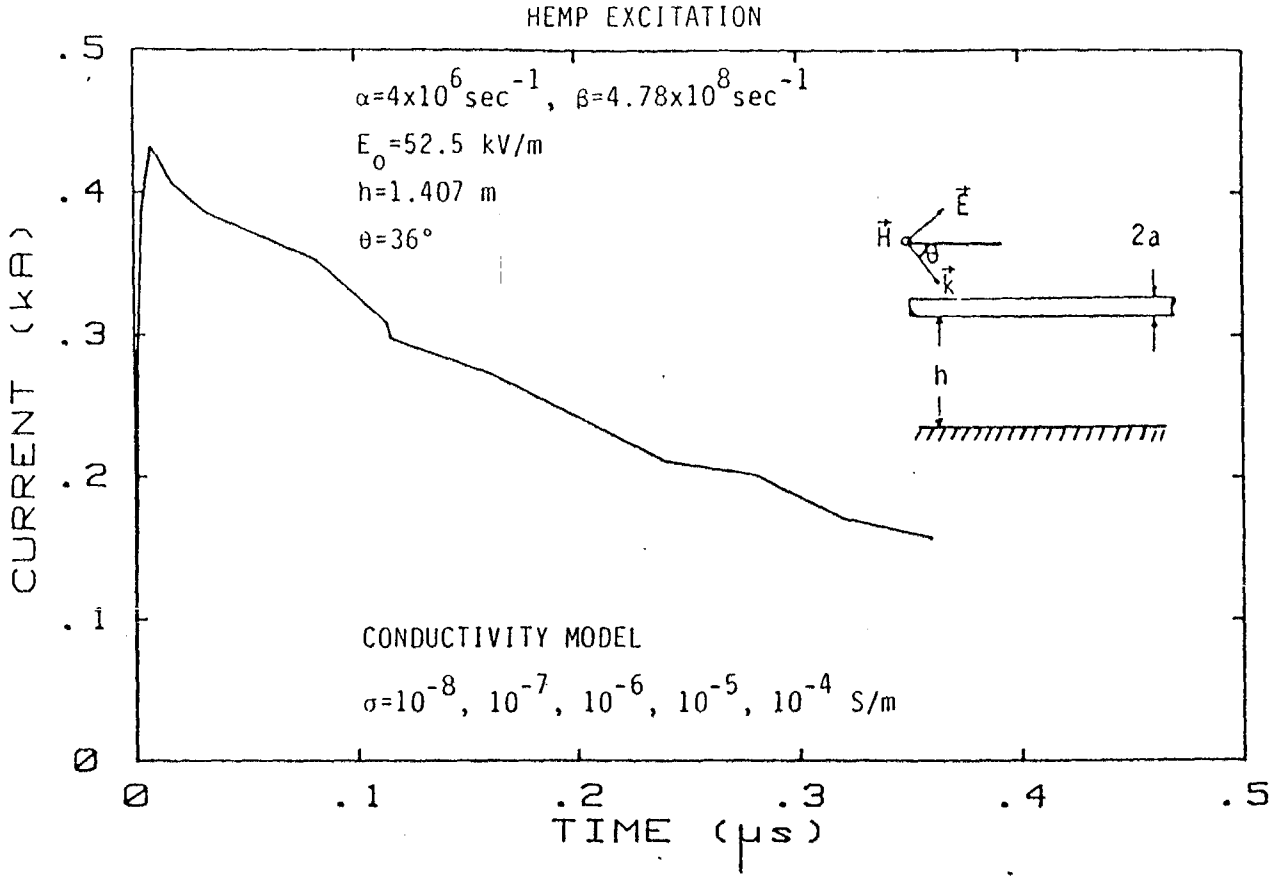

Fig. A18. HEMP-induced current in the wire in the presence of a perfectly conducting ground for elevation angle $\theta = 36°$ and different values of σ in conductivity model for radius a = 1.407 cm and $E_c = 1.5 \times 10^6$ volt m^{-1}.

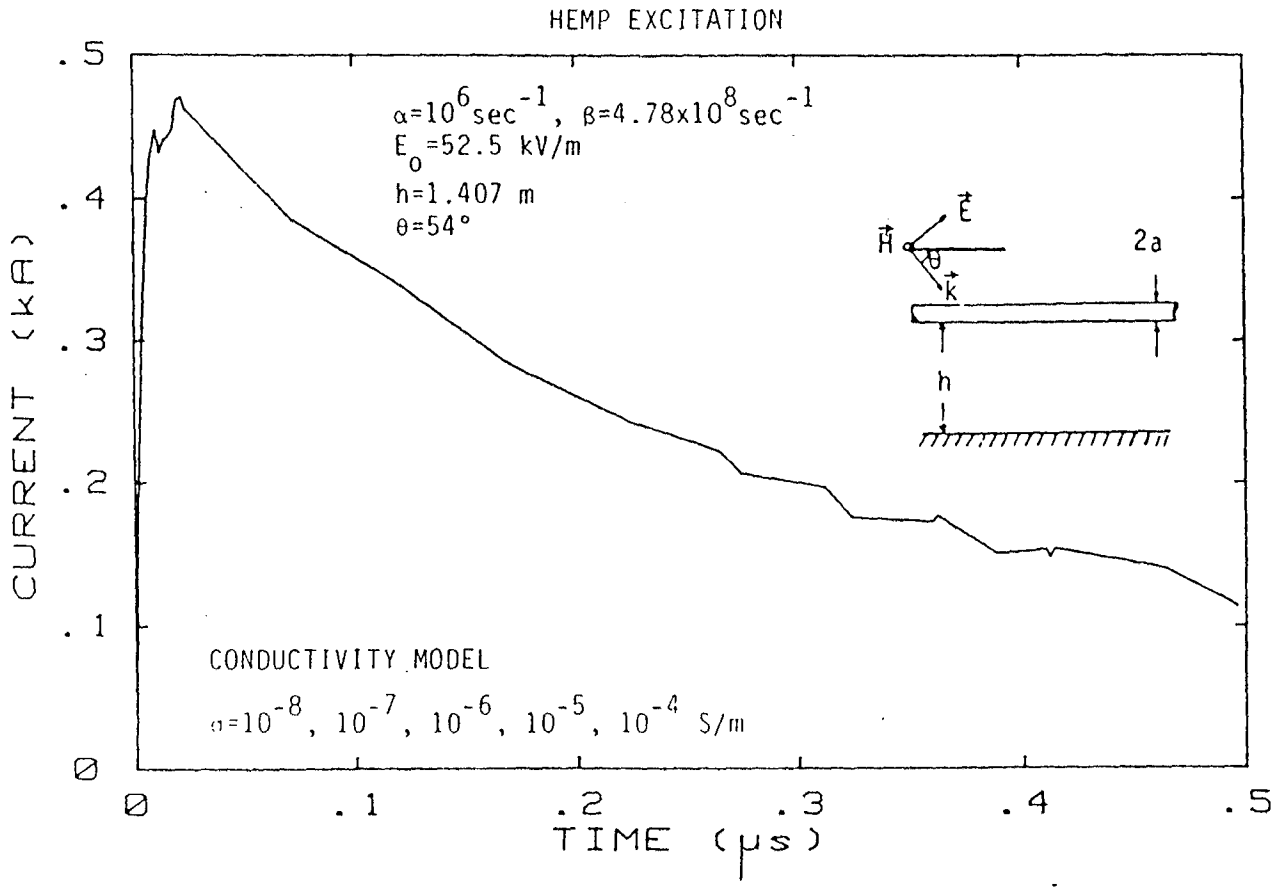

Fig. A19. HEMP-induced current in the wire in the presence of a perfectly conducting ground for elevation angle $\theta = 54°$ and different values of σ in conductivity model for radius a = 1.407 cm and $E_c = 1.5 \times 10^6$ volt m^{-1}.

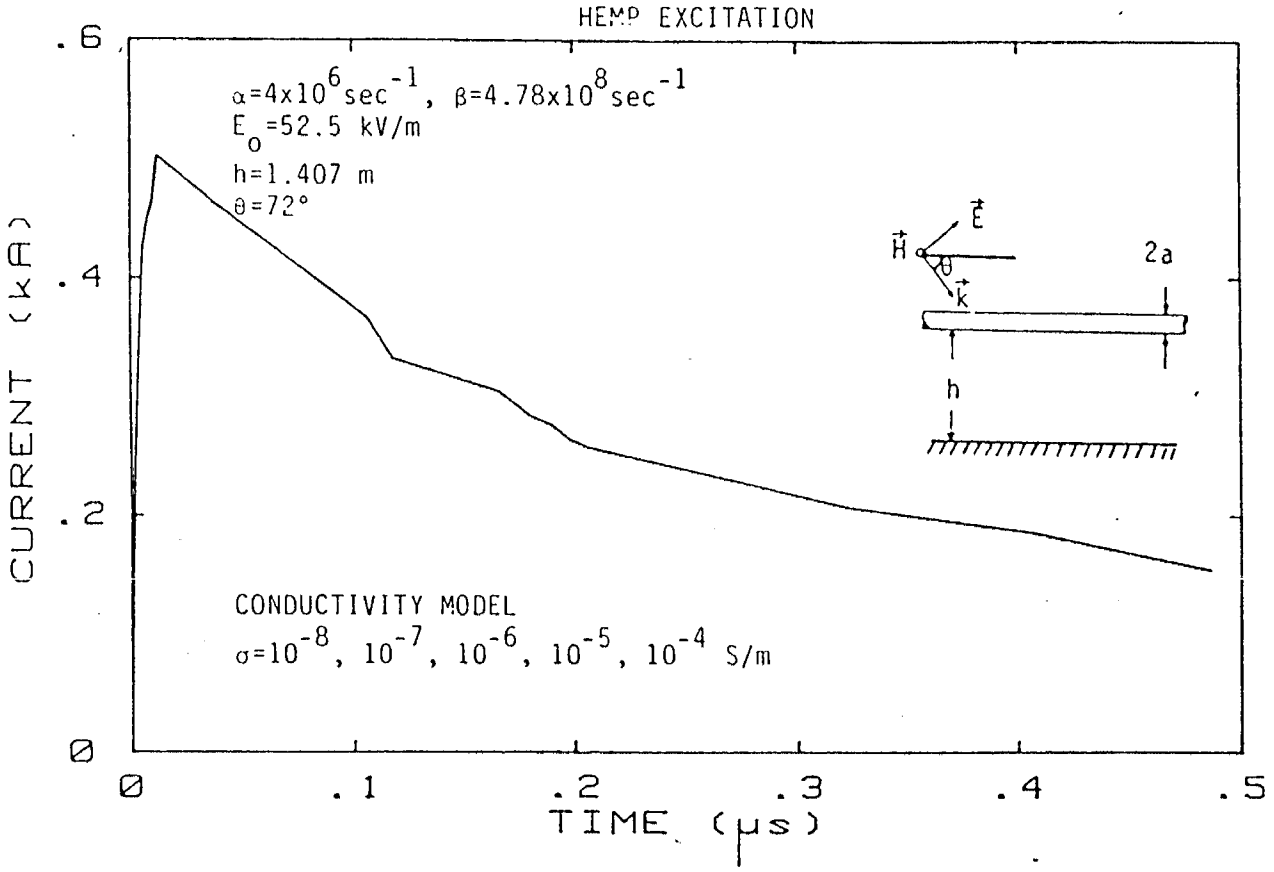

Fig. A20. HEMP-induced current in the wire in the presence of a perfectly conducting ground for elevation angle $\theta = 72°$ and different values of σ in conductivity model for radius a = 1.407 cm and $E_c = 1.5 \times 10^6$ volt m^{-1}.

LOCALIZED VOLTAGE SURGE (TOWNSEND'S MODEL, $\alpha_j = 3.5 \times 10^{-4} \text{volt}^{-1}\text{sec}^{-1}$)

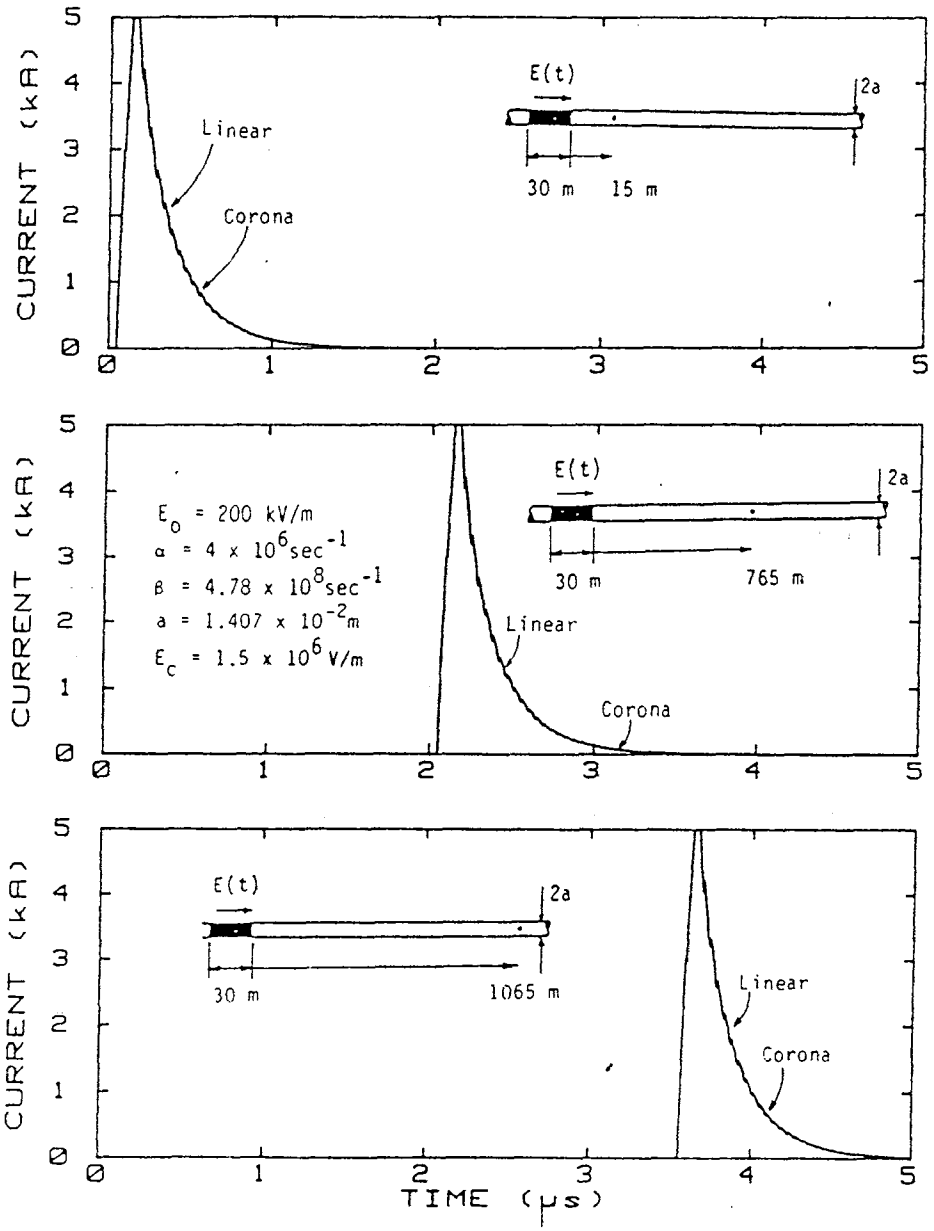

Fig. A21. Voltage surge-induced current in the wire at different distances from the source in Townsend's model for $\alpha_j = 3.5 \times 10^{-4}$ volt^{-1}sec^{-1}.

LOCALIZED VOLTAGE SURGE (TOWNSEND'S MODEL, $\alpha_j = 3.5 \times 10^{-2} \text{volt}^{-1}\text{sec}^{-1}$)

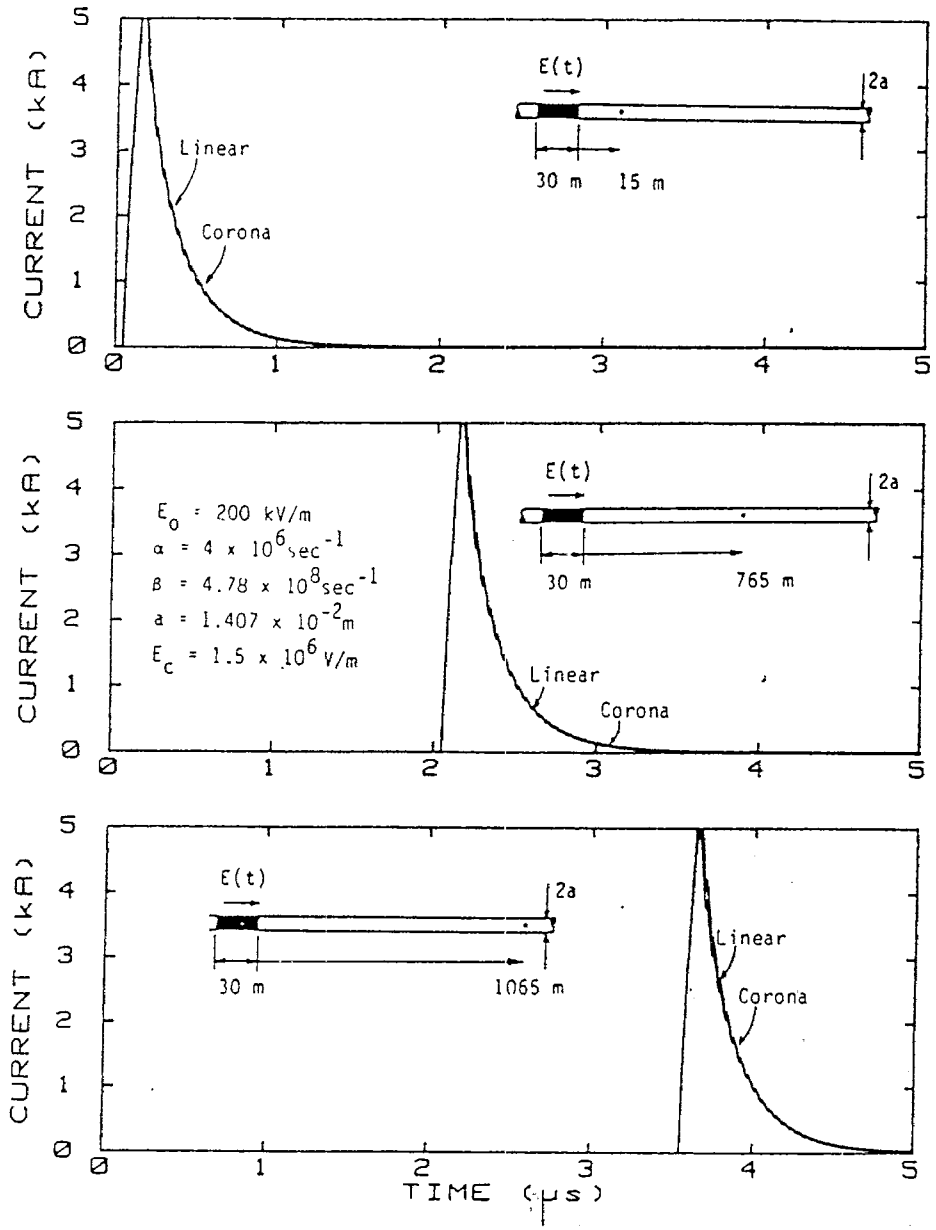

Fig. A22. Voltage surge-induced current in the wire at different distances from surge location in Townsend's model for $\alpha_j = 3.5 \times 10^{-2} \text{volt}^{-1}\text{sec}^{-1}$.

LOCALIZED VOLTAGE SURGE (TOWNSEND'S MODEL, α_j = 3.5 volt^{-1}sec^{-1}.)

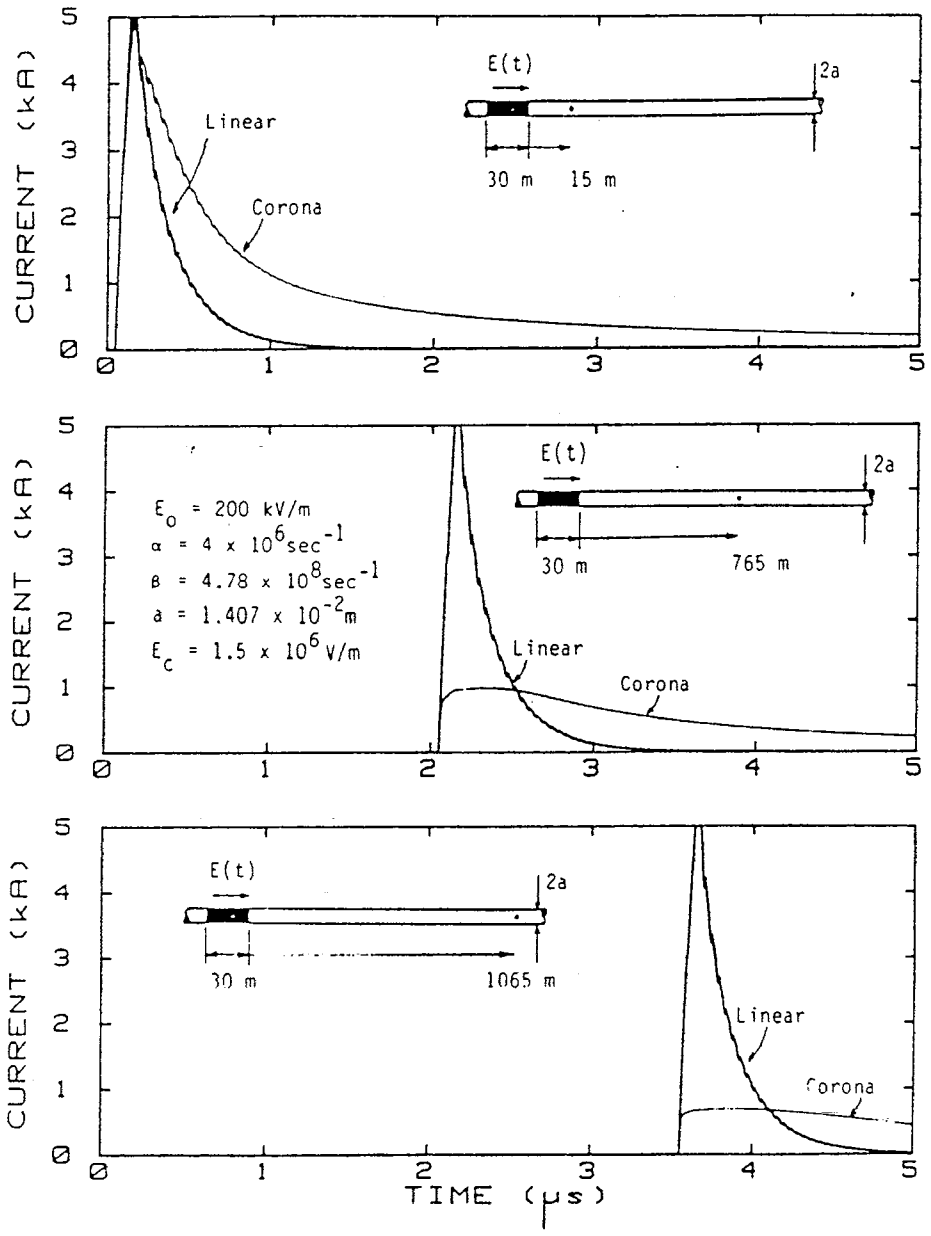

Fig. A23. Voltage surge-induced current in the wire at different distances from surge location in Townsend's model for α_j = 3.5 volt^{-1}sec^{-1}.

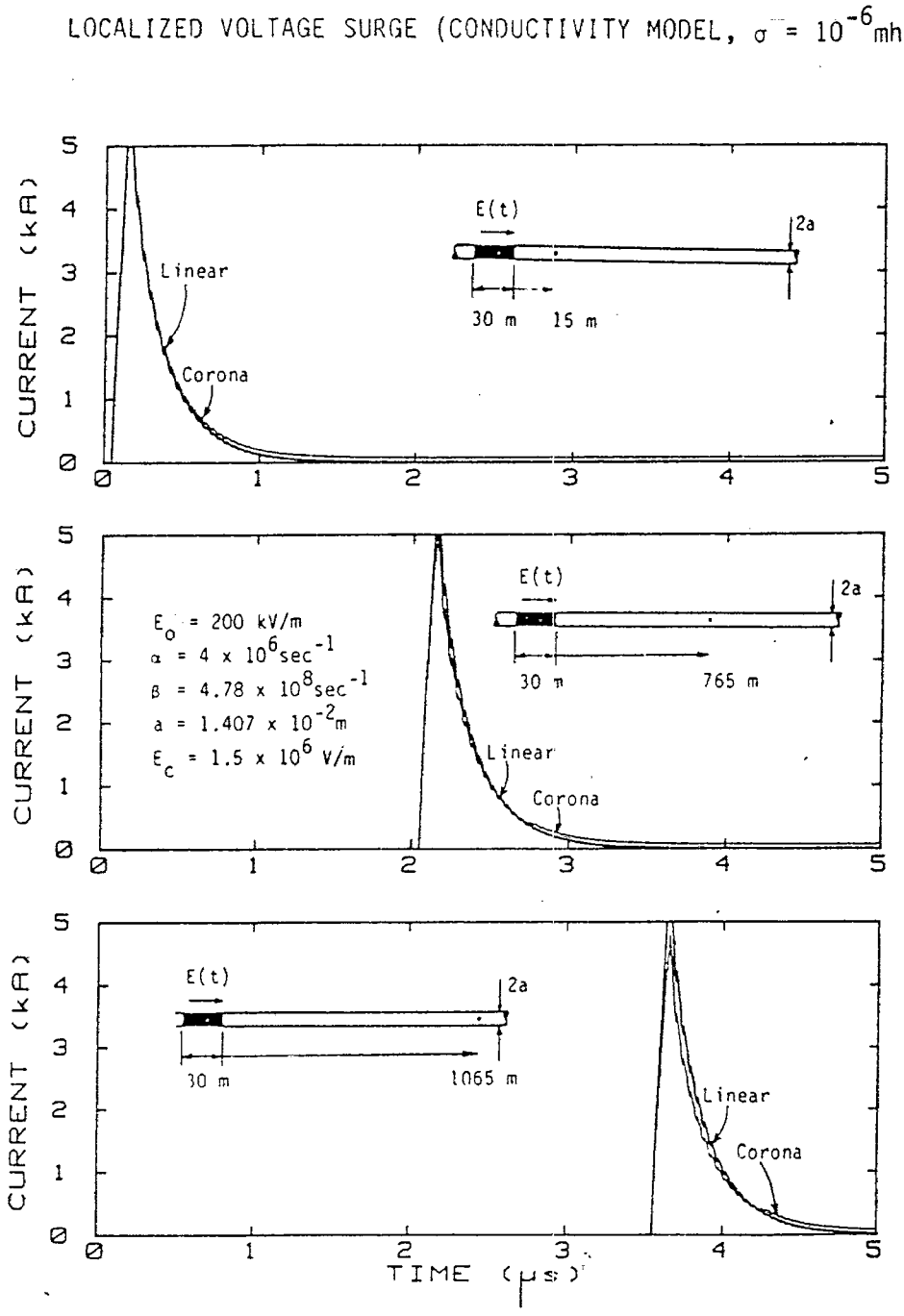

Fig. A24. Voltage surge-induced current in the wire at different distances from surge location in conductivity model for $\sigma = 10^{-6}$ S/m.

LOCALIZED VOLTAGE SURGE (CONDUCTIVITY MODEL, $\sigma = 10^{-4}$ mhos/m)

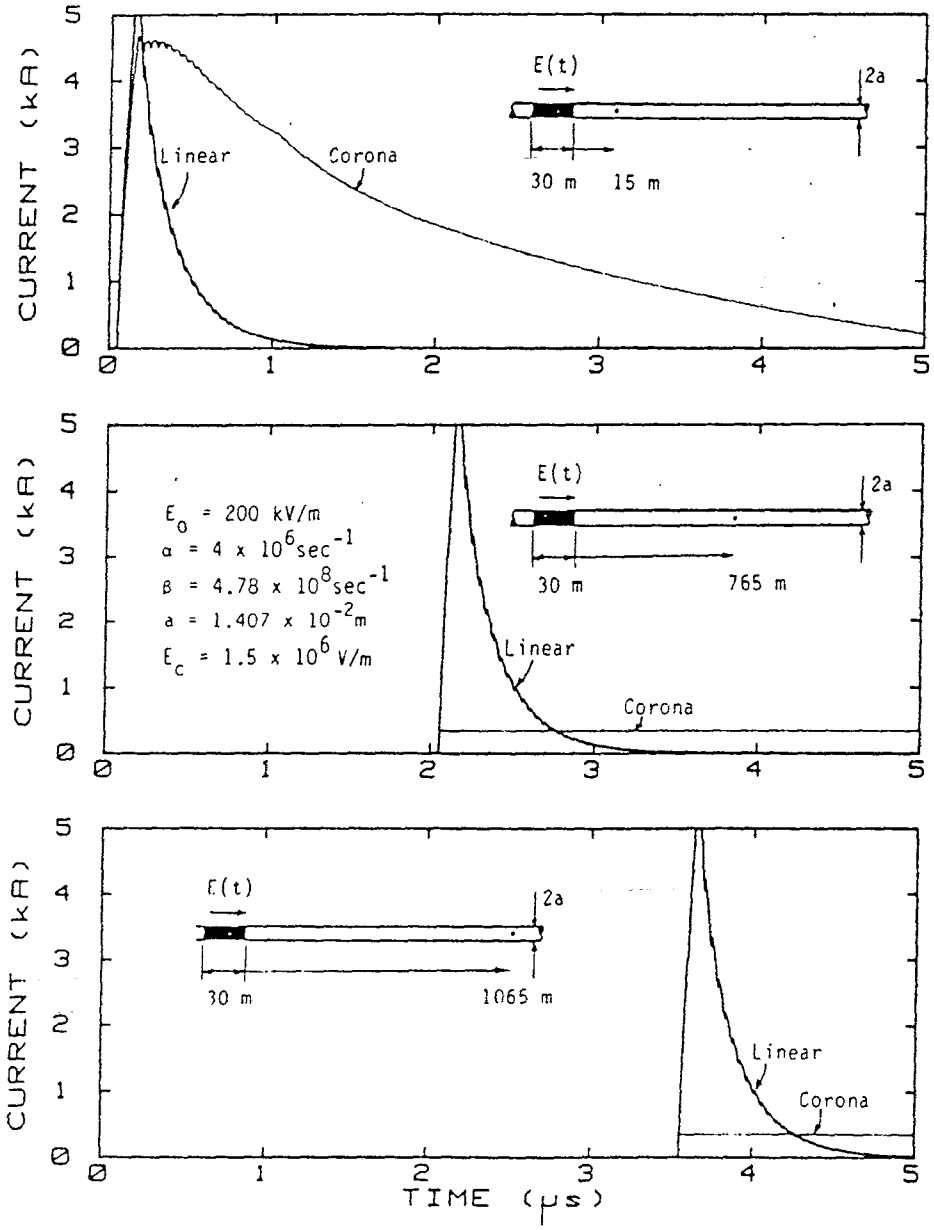

Fig. A25. Voltage surge-induced current in the wire at different distances from surge location in conductivity model $\sigma = 10^{-4}$ S/m.

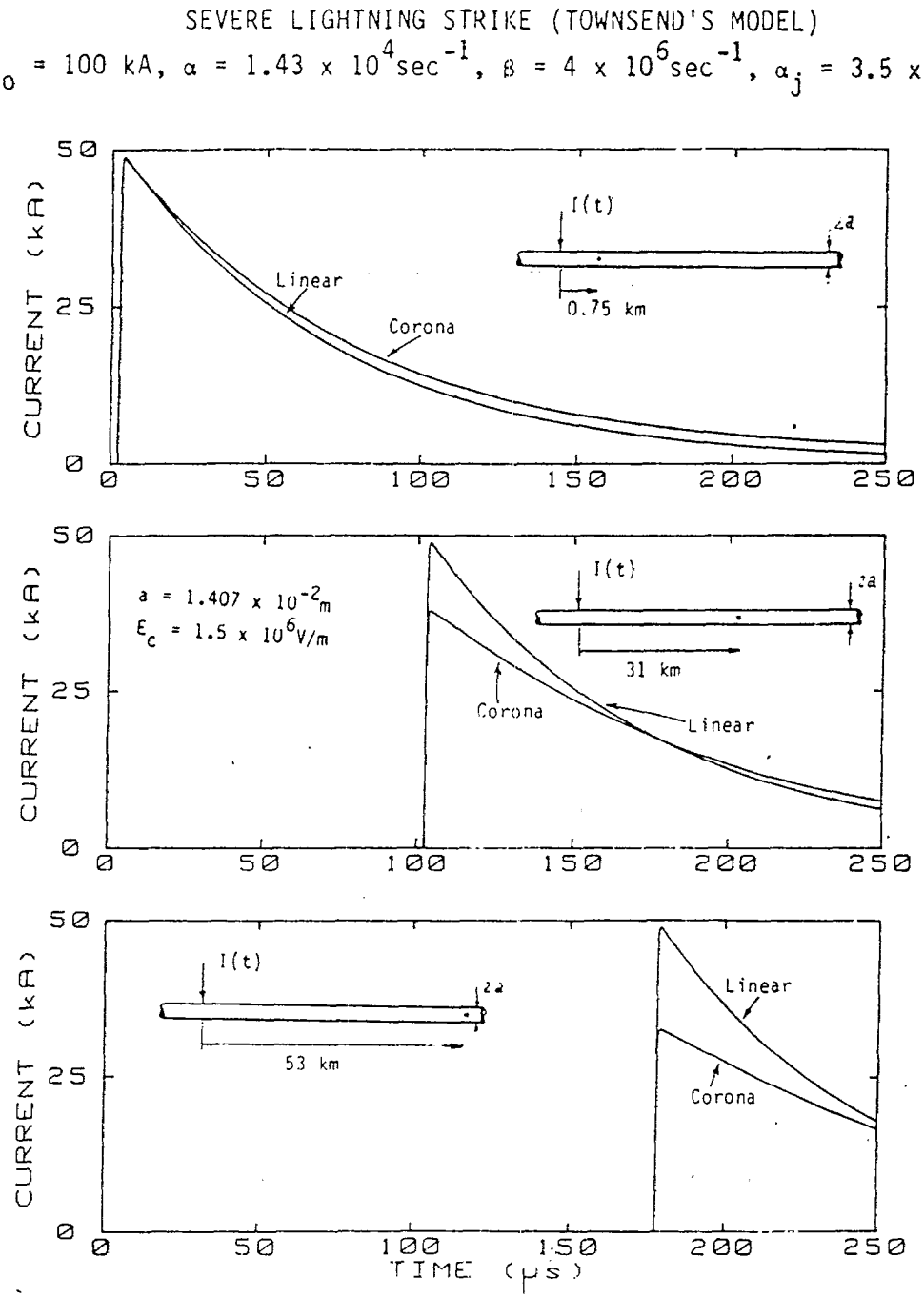

Fig. A26. Lightning strike-induced current in the wire at different distances from strike location in Townsend's model for $\alpha_j = 3.5 \times 10^{-4} volt^{-1} sec^{-1}$.

SEVERE LIGHTNING STRIKE (CONDUCTIVITY MODEL)

(I_0 = 100 kA, α = 1.43 x $10^4 sec^{-1}$, β = 4 x $10^6 sec^{-1}$, σ_0 = 10^{-6} mho m^{-1})

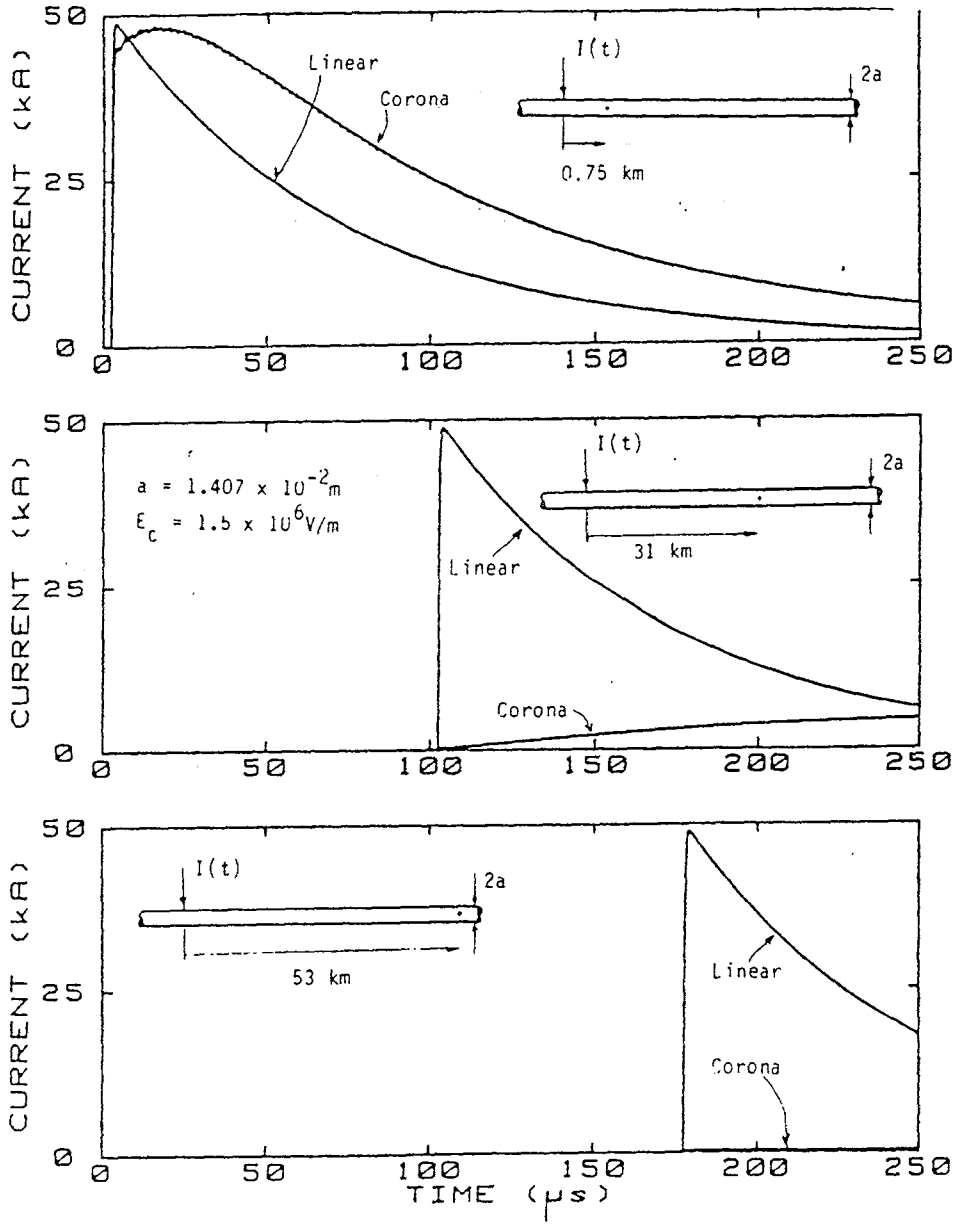

Fig. A27. Lightning strike-induced current in the wire at different distances from strike location in conductivity model for $\sigma = 10^{-6}$ S/m.

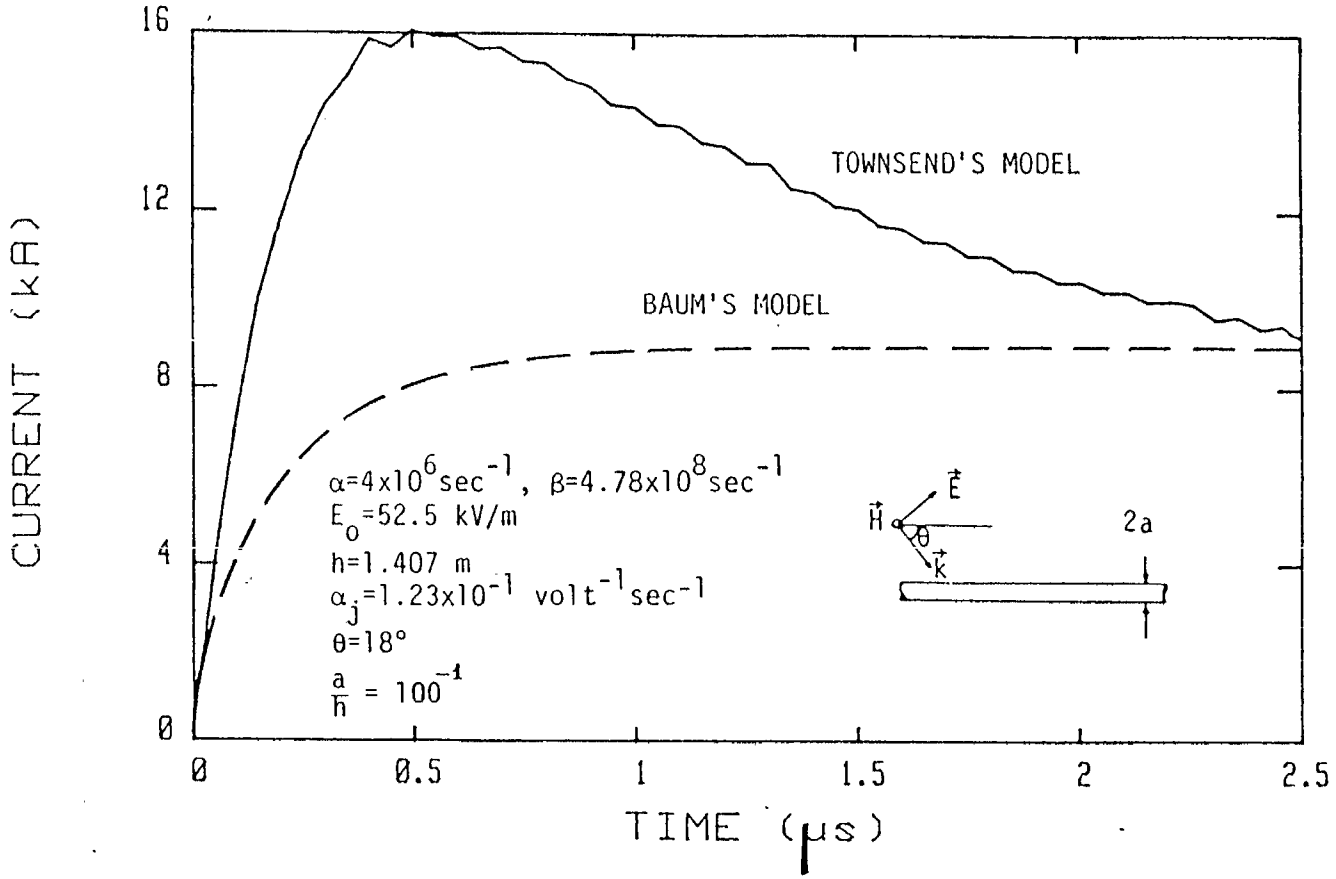

Fig. A28. Comparison of HEMP-induced current using Townsend's model for $\alpha_j = 1.23 \times 10^{-1}$ volt^{-1}sec^{-1} with Baum's model for elevation angle $\theta = 18°$, radius a = 1.407 cm and $E_c = 1.5 \times 10^6$ volt m^{-1}.

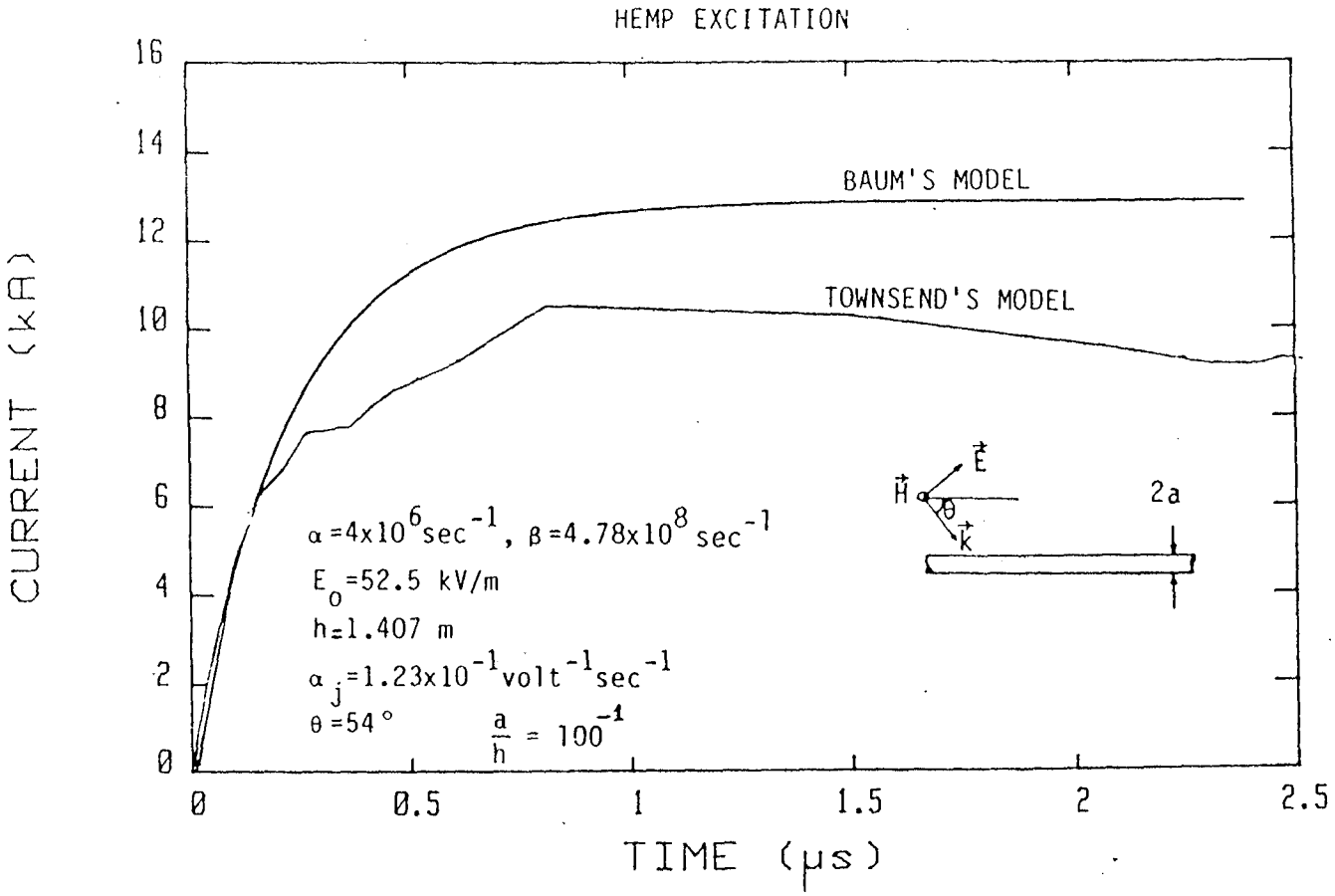

Fig. A29. Comparison of HEMP-induced current using Townsend's model for $\alpha_j = 1.23 \times 10^{-1}$ volt^{-1}sec^{-1} with Baum's model for elevation angle $\theta = 54°$, radius $a = 1.407$ cm and $E_c = 1.5 \times 10^6$ volt m^{-1}.

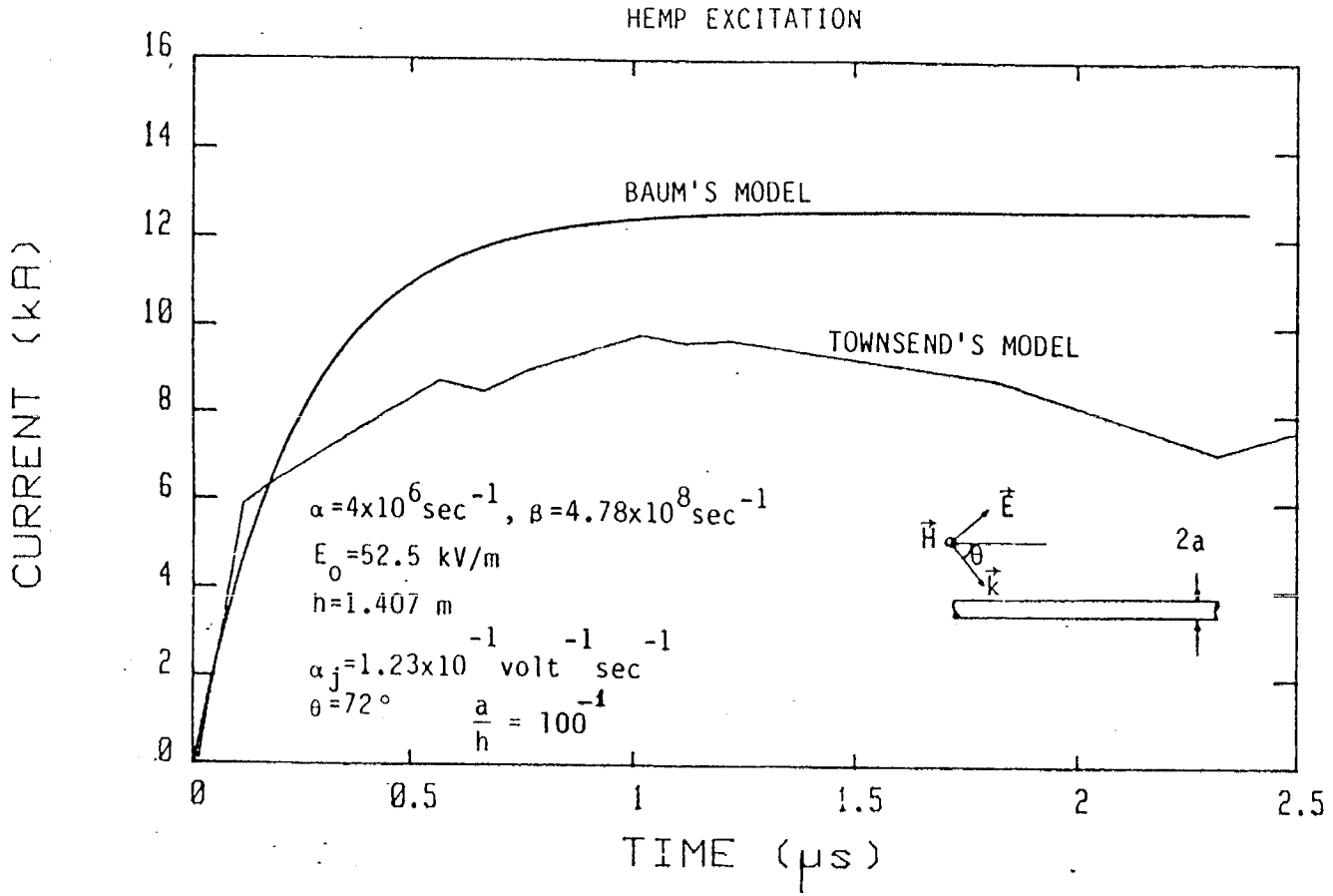

Fig. A30. Comparison of HEMP-induced current using Townsend's model for $\alpha_j = 1.23 \times 10^{-1}$ volt^{-1}sec^{-1} with Baum's model for elevation angle $\theta = 72°$, radius $a = 1.407$ cm and $E_c = 1.5 \times 10^6$ volt m^{-1}.

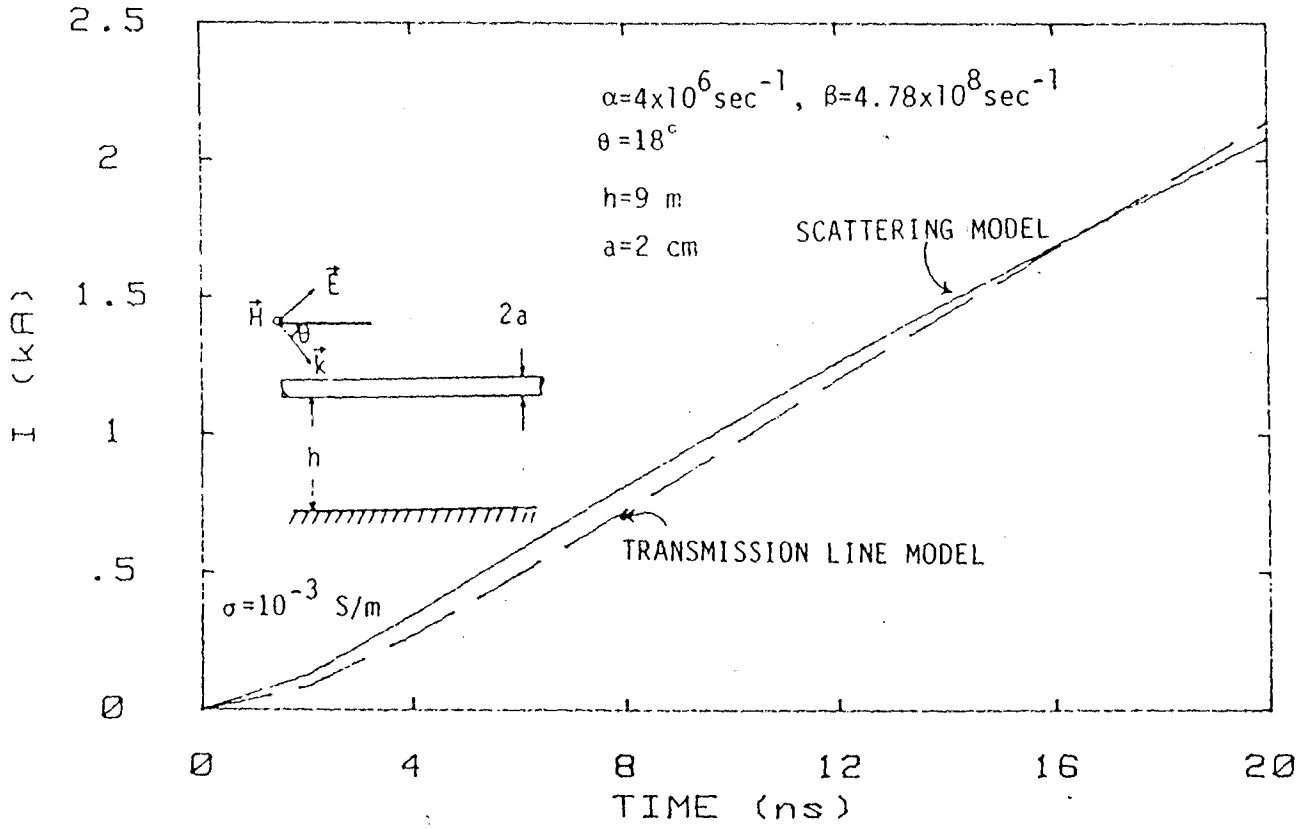

Fig. A31. Comparison of HEMP-induced current using scattering and transmission line models for elevation angle $\theta = 18°$ and ground conductivity $\sigma = 10^{-3}$ S/m.

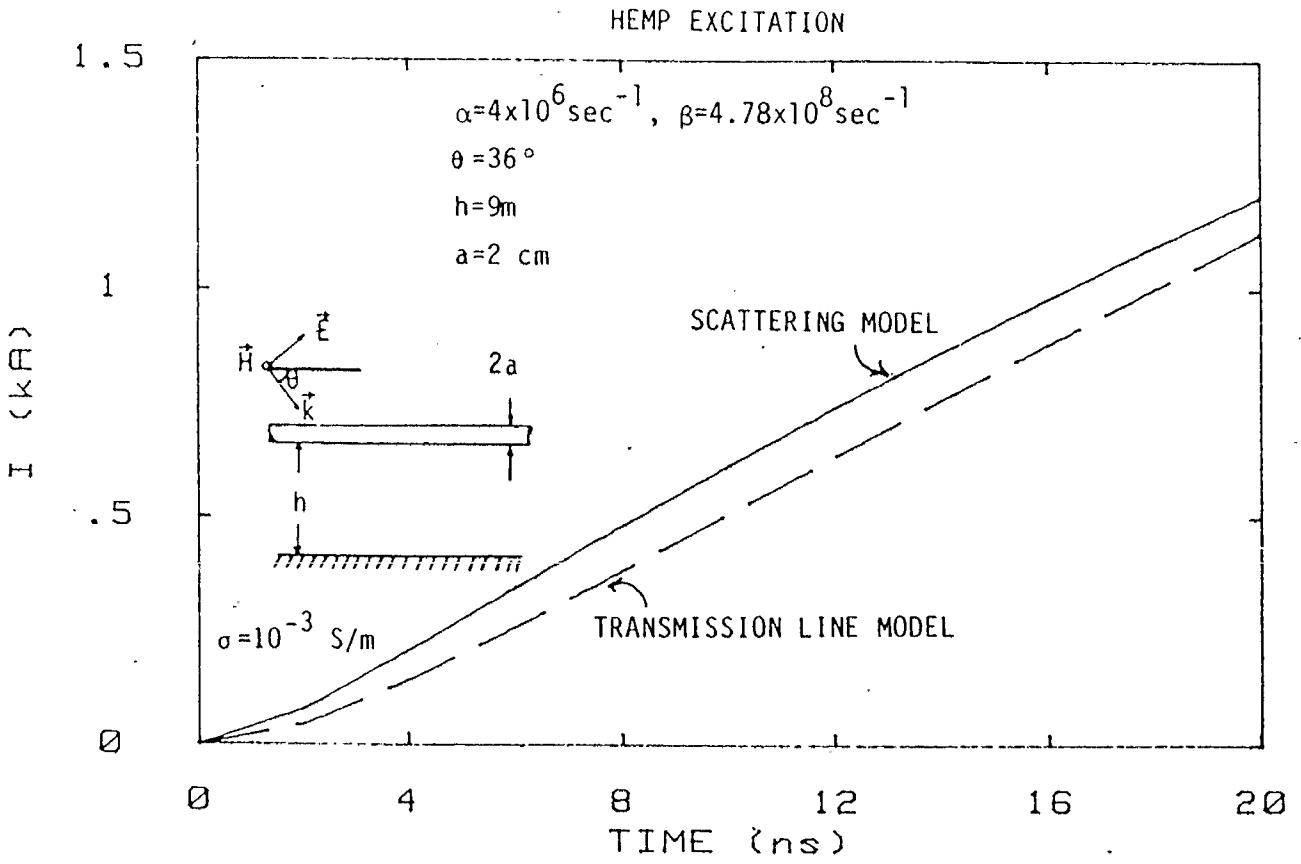

Fig. A32. Comparison of HEMP-induced current using scattering and transmission line models for elevation angle $\theta = 36°$ and ground conductivity $\sigma = 10^{-3}$ S/m.

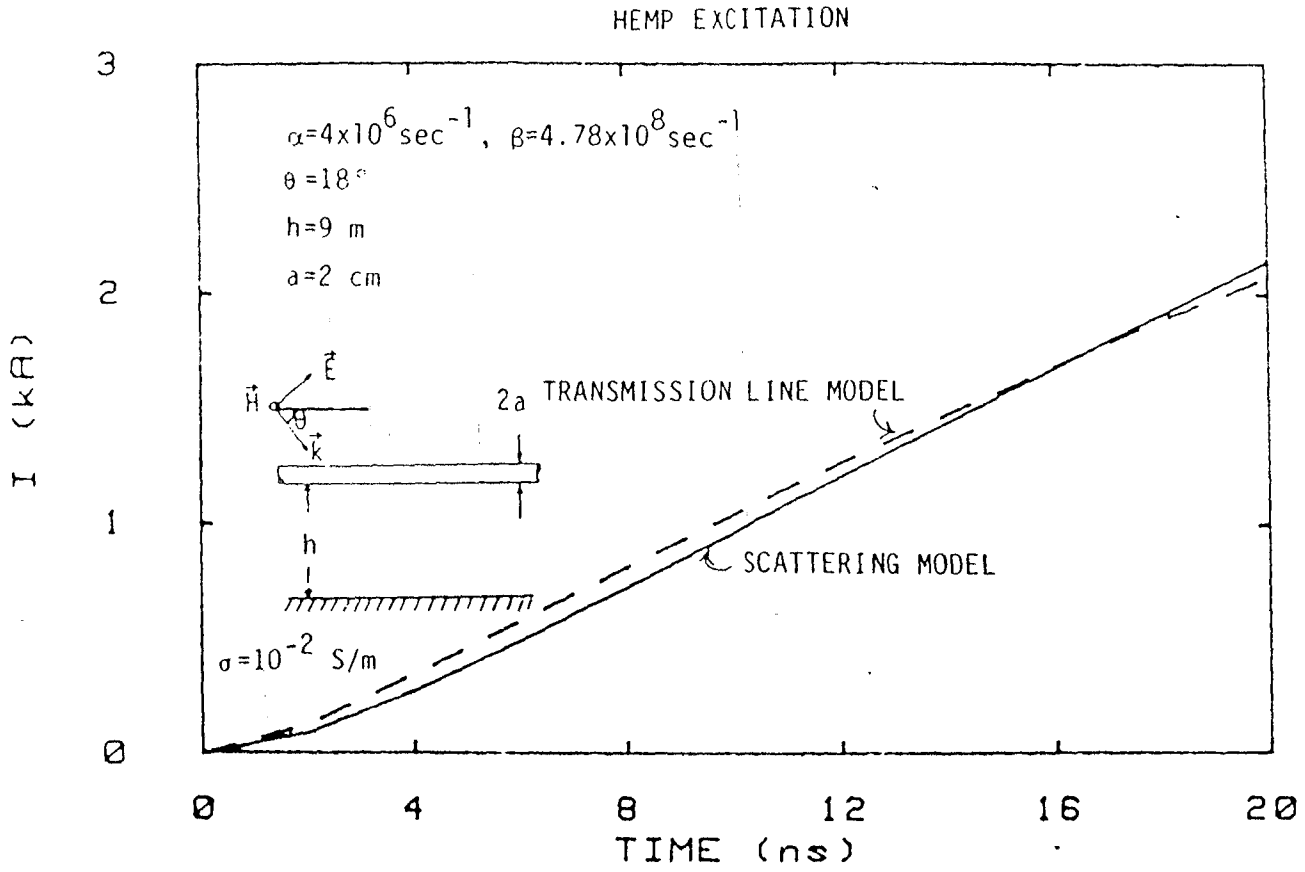

Fig. A33. Comparison of HEMP-induced current using scattering and transmission line models for elevation angle $\theta = 18°$ and ground conductivity $\sigma = 10^{-2}$ S/m.

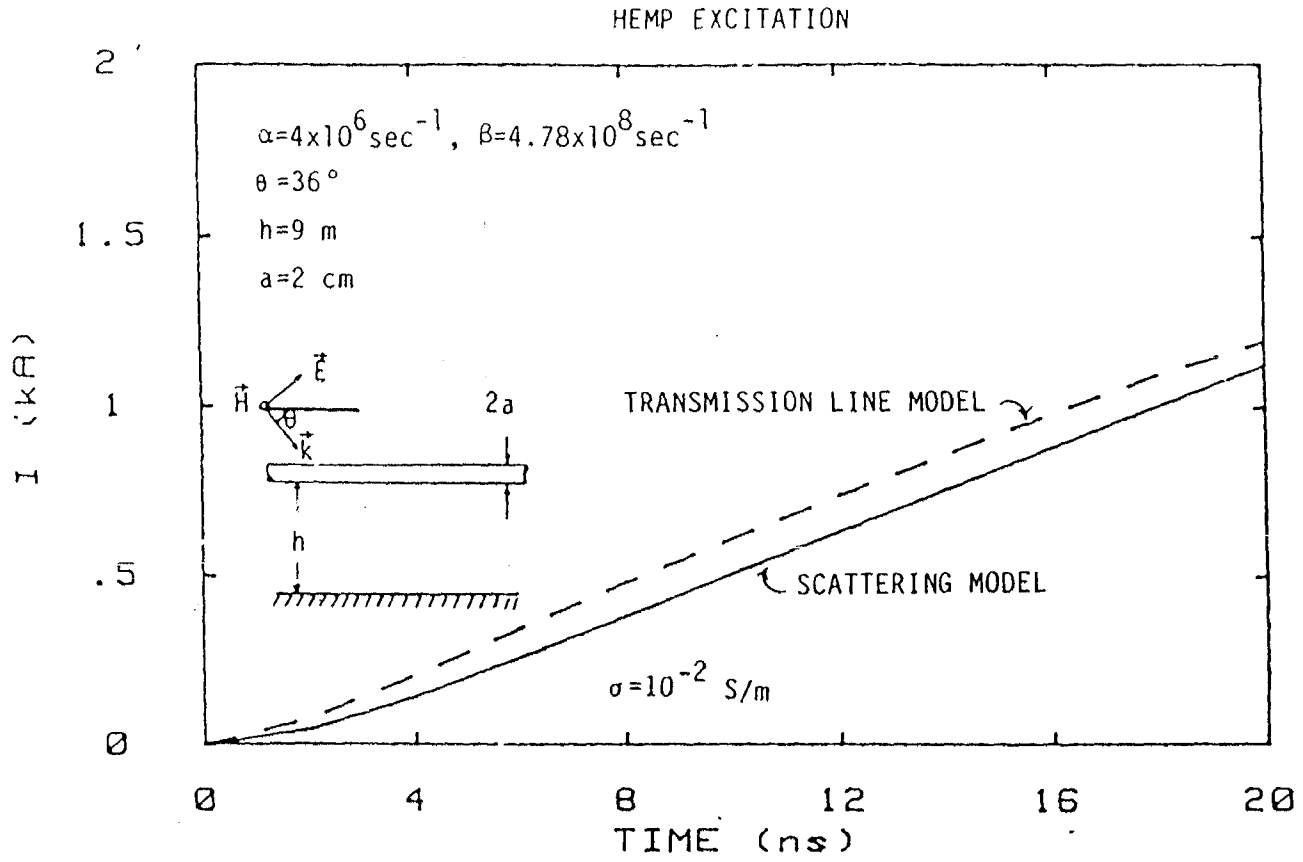

Fig. A34. Comparison of HEMP-induced current using scattering and transmission line models for elevation angle $\theta = 36°$ and ground conductivity $\sigma = 10^{-2}$ S/m.

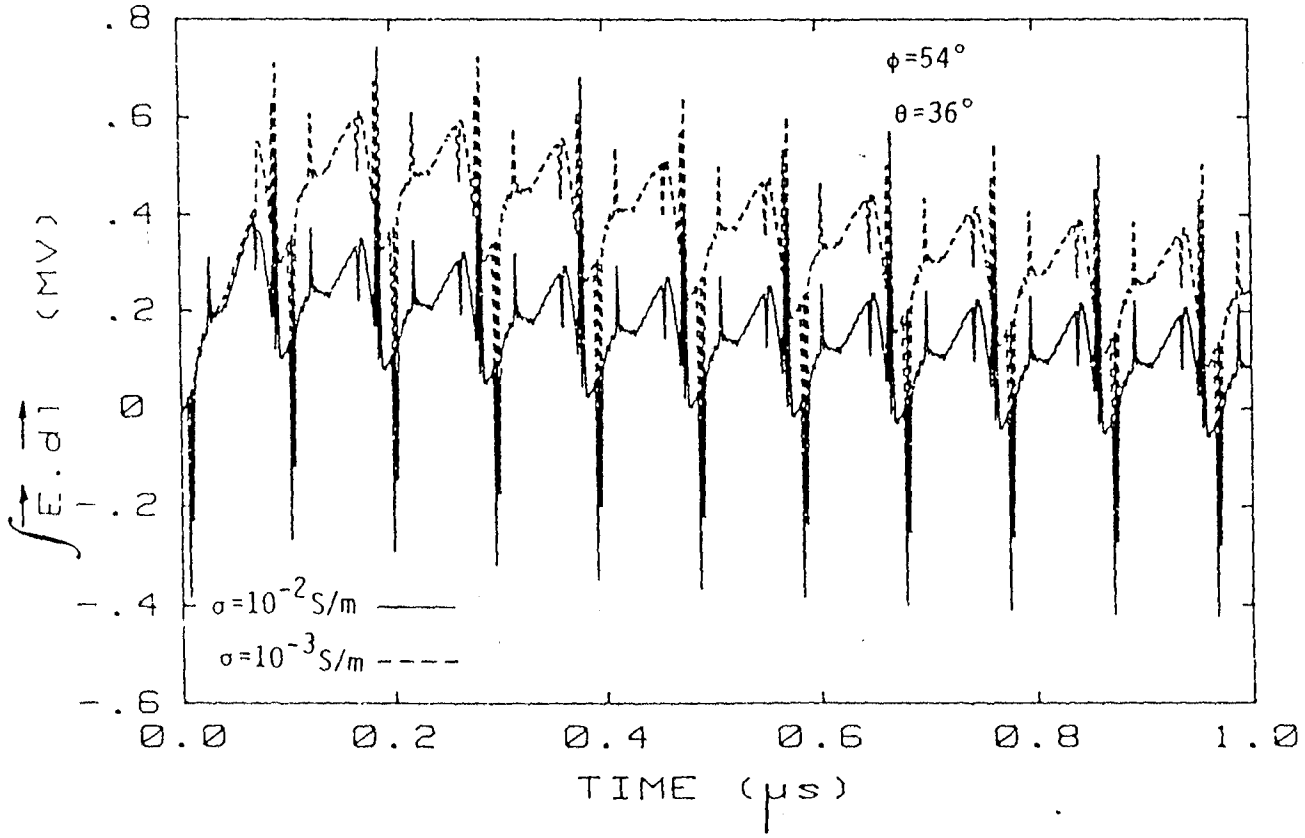

Fig. A35. Calculated HEMP-induced "Potential Difference" between the phase conductor and the horizontal cross arm for azimuthal angle ϕ=54°, elevation angle θ=36°, and for two different values of ground conductivity σ.

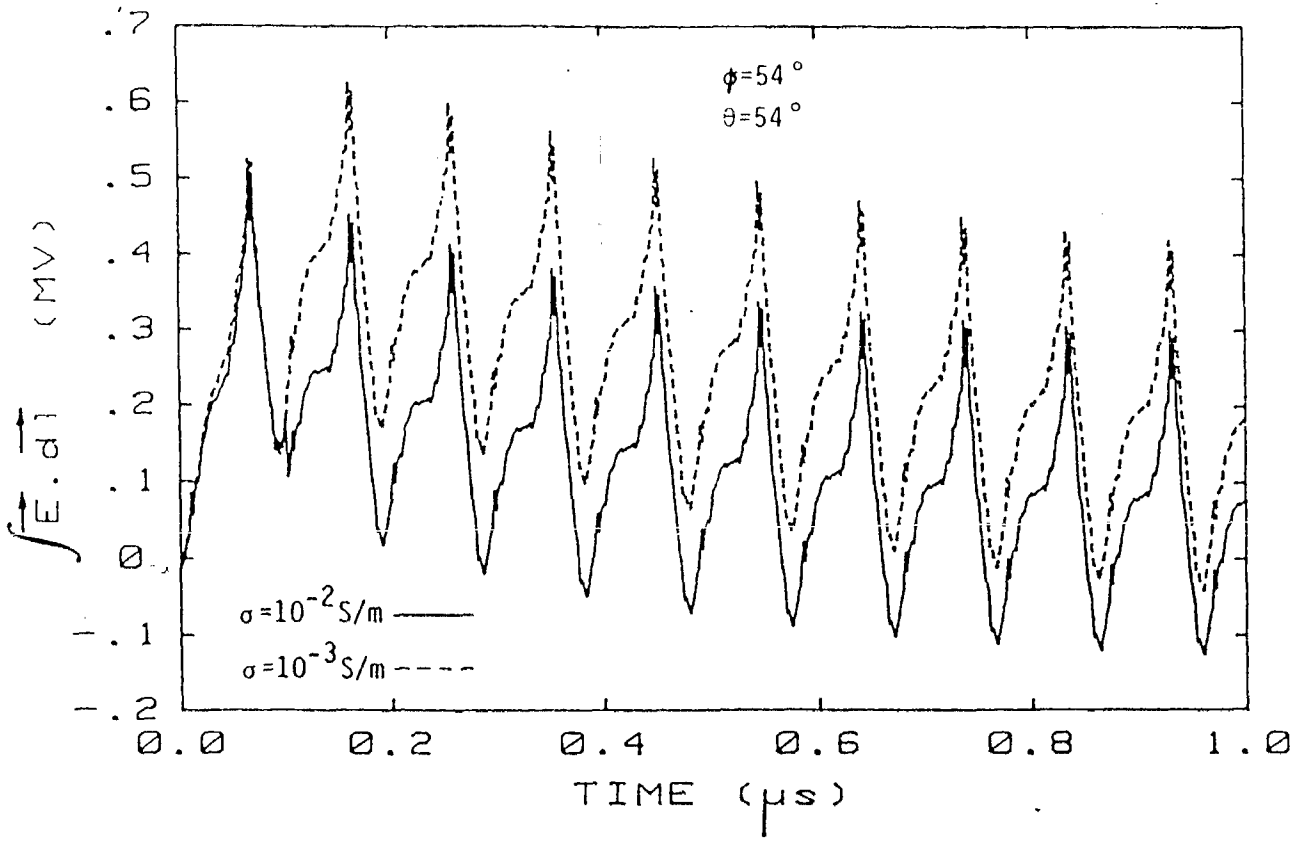

Fig. A36. Calculated HEMP-induced "Potential Difference" between the phase conductor and the horizontal cross arm for azimuthal angle ϕ=54°, elevation angle θ=54°, and for two different values of ground conductivity σ.

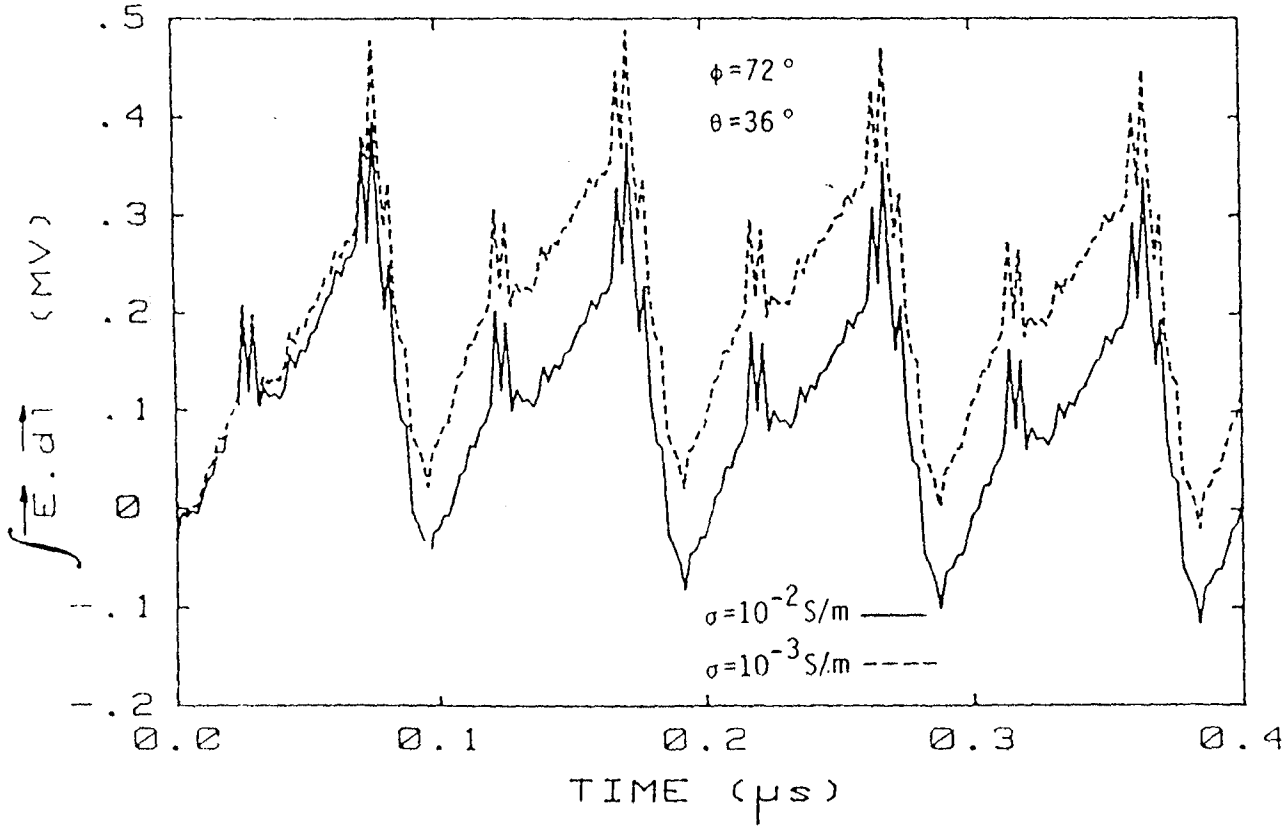

Fig. A37. Calculated HEMP-induced "Potential Difference" between the phase conductor and the horizontal cross arm for azimuthal angle ϕ=72°, elevation angle θ=36°, and for two different values of ground conductivity σ.

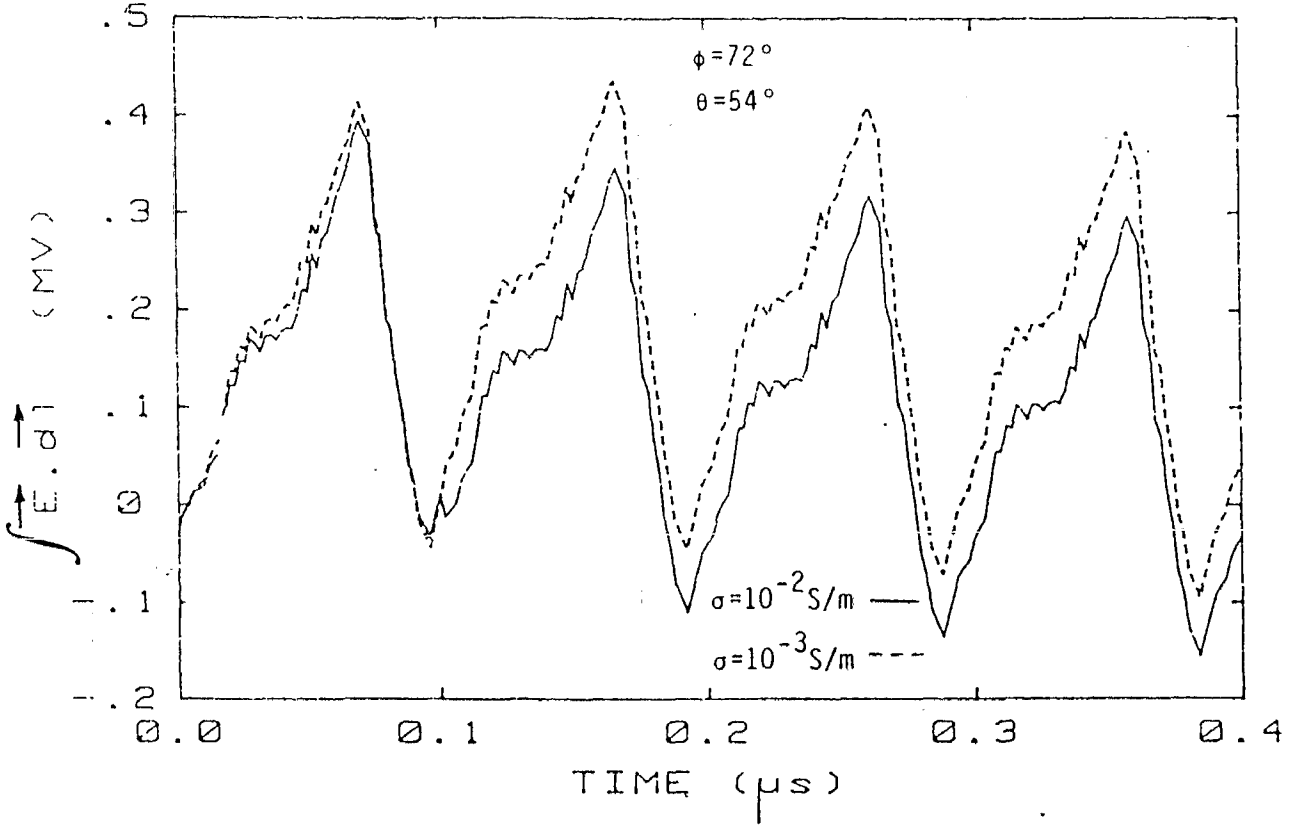

Fig. A38. Calculated HEMP-induced "Potential Difference" between the phase conductor and the horizontal cross arm for azimuthal angle ϕ=72°, elevation angle θ=54°, and for two different values of ground conductivity σ.

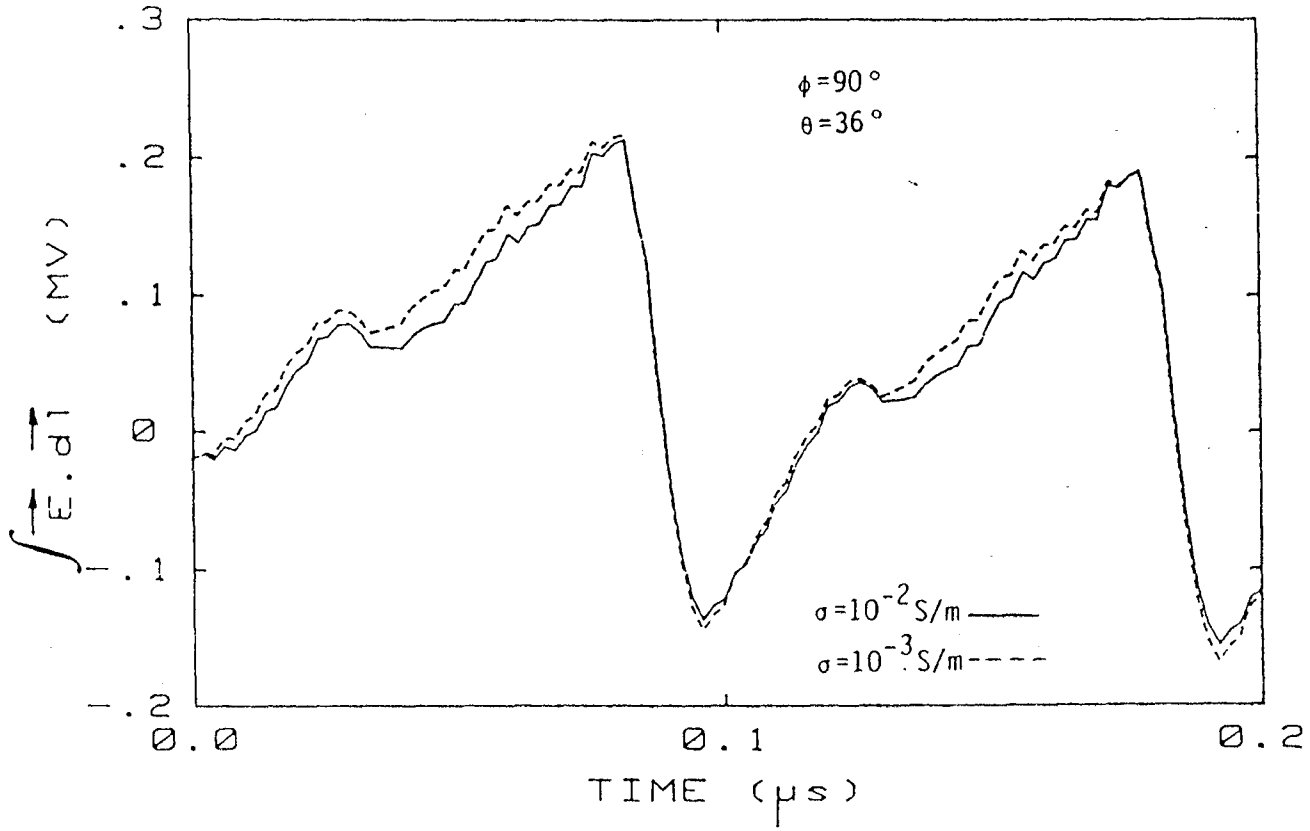

Fig. A39. Calculated HEMP-induced "Potential Difference" between the phase conductor and the horizontal cross arm for azimuthal angle ϕ=90°, elevation angle θ=36°, and for two different values of ground conductivity σ.

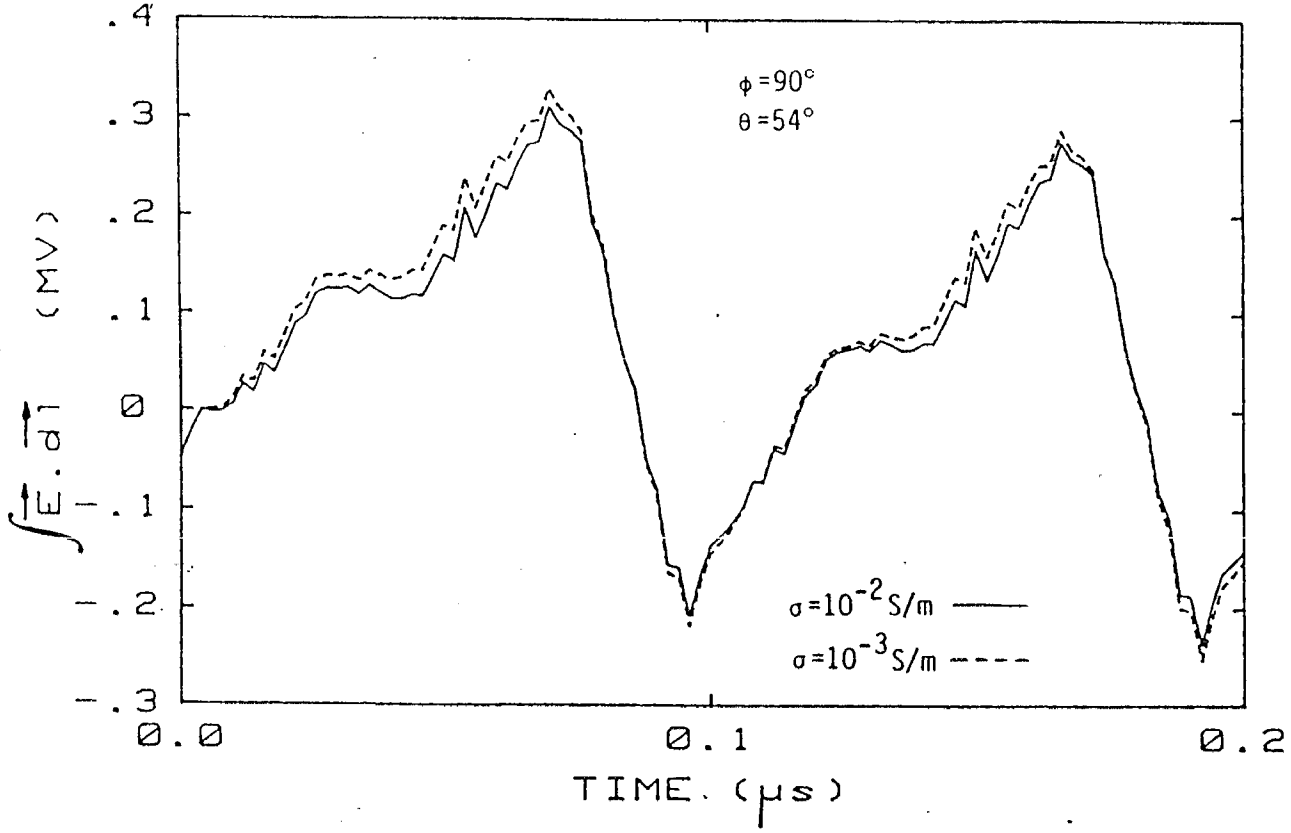

Fig. A40. Calculated HEMP-induced "Potential Difference" between the phase conductor and the horizontal cross arm for azimuthal angle ϕ=90°, elevation angle θ=54°, and for two different values of ground conductivity σ.